

Interactive Physically-based Sound Simulation

Nikunj Raghuvanshi

A dissertation submitted to the faculty of the University of North Carolina at Chapel Hill in partial fulfillment of the requirements for the degree of Doctor of Philosophy in the Department of Computer Science.

Chapel Hill
2010

Approved by:

Ming C. Lin, Advisor

John Snyder, Reader

Dinesh Manocha, Reader

Gary Bishop, Reader

Marc Niethammer, Reader

© 2010
Nikunj Raghuvanshi
ALL RIGHTS RESERVED

Abstract

Nikunj Raghuvanshi: Interactive Physically-based Sound Simulation.
(Under the direction of Ming C. Lin.)

The realization of interactive, immersive virtual worlds requires the ability to present a realistic audio experience that convincingly complements their visual rendering. Physical simulation is a natural way to achieve such realism, enabling deeply immersive virtual worlds. However, physically-based sound simulation is very computationally expensive owing to the high-frequency, transient oscillations underlying audible sounds. The increasing computational power of desktop computers has served to reduce the gap between required and available computation, and it has become possible to bridge this gap further by using a combination of algorithmic improvements that exploit the physical, as well as perceptual properties of audible sounds. My thesis is a step in this direction.

My dissertation concentrates on developing real-time techniques for both sub-problems of sound simulation: synthesis and propagation. Sound synthesis is concerned with generating the sounds produced by objects due to elastic surface vibrations upon interaction with the environment, such as collisions. I present novel techniques that exploit human auditory perception to simulate scenes with hundreds of sounding objects undergoing impact and rolling in real time. Sound propagation is the complementary problem of modeling the high-order scattering and diffraction of sound in an environment as it travels from source to listener. I discuss my work on a novel numerical acoustic simulator (ARD) that is hundred times faster and consumes ten times less memory than a high-accuracy finite-difference technique, allowing acoustic simulations on previously-intractable spaces, such as a cathedral, on a desktop computer.

Lastly, I present my work on interactive sound propagation that leverages my ARD

simulator to render the acoustics of arbitrary static scenes for multiple moving sources and listener in real time, while accounting for scene-dependent effects such as low-pass filtering and smooth attenuation behind obstructions, reverberation, scattering from complex geometry and sound focusing. This is enabled by a novel compact representation that takes a thousand times less memory than a direct scheme, thus reducing memory footprints to fit within available main memory. To the best of my knowledge, this is the only technique and system in existence to demonstrate auralization of physical wave-based effects in real-time on large, complex 3D scenes.

*To my dearest,
Papa, Mummy, Gunjan di, Vandan di and Pritu*

Acknowledgments

When I started my dissertation research many years ago, I had the following in my mind: “do some really useful research, quickly, and graduate.” It took me many years to realize that “quickly” and “useful research” just do not go together in an applied area of research. So, while I can assure you that my former wish wasn’t fulfilled, hopefully, after reading this thesis, you would feel that the latter was. I owe a great deal of gratitude to so many people who have helped me in various ways in my doctoral studies, that I am sure to miss many of them. To all of them, my apologies for the omission, and my sincerest, heartfelt thanks for all of your much-needed help.

I thank Ming C. Lin for being a great advisor and helping me guide my efforts productively through all these years, giving me the freedom to choose my own direction, leaving me on my own when I was trying to dig into my chosen research direction, pushing me when I needed to get publications done and promoting my work tirelessly. And quite importantly, keeping up with my night owl schedule, staying up at nights many times to help me meet deadlines. My sincerest thanks to her.

I am grateful to Dinesh Manocha for his early support when I started as a graduate student and his much-needed help in getting me quickly into hands-down research. He has also been a very helpful committee member. I am especially indebted to Naga Govindaraju, who mentored me in my first year as a graduate student as well as later when I was interning in his group at Microsoft Research. He has been a great manager, mentor and friend. I extend gratitude to Gary Bishop and Marc Niethammer for their valuable feedback as my committee members.

Also, many thanks to the fellow students in the GAMMA group, who were always

there for interesting discussions, research or otherwise, many of whom are good friends, some of whom are collaborators too: Jason Sewall, Nico Galoppo, Brandon Lloyd, Rahul Narain, Sachin Patil, Anish Chandak, Micah Taylor, Abhinav Golas and Sean Curtis. I am very sure I am missing many people in this list.

I thank the Computer Science staff, because of whose presence, I was able to stay careless about so many of those practical details that are quite important. They helped me enjoy the freedom of an irresponsible life a little bit longer. Special thanks goes to Janet Jones, who was always patient and helpful in the face of all such transgressions.

I would like to thank Ritesh Kumar and Shantanu Sharma, who were my roommates for nearly four years, during which we had the time of our lives. I am especially indebted to Ritesh. He is a dear friend and we spent countless hours over coffee discussing everything from religion and government to computer science, which was, and continues to be, a richly rewarding experience.

I worked with John Snyder at Microsoft Research during the last year of my doctoral work and he has provided me with great mentoring, technical help, and objective, balanced criticism for my work. I have learned a lot from his sincere, thorough approach to research and I am certain he has helped me become a better scientist. My sincerest thanks to him. I also thank my collaborators from Microsoft Game Studios: Guy Whitmore and Kristofor Mellroth. As audio directors, they were instrumental in giving my thesis a more grounded approach based on their expert knowledge of the requirements of video games. They have also been key in pushing technology based on my work into real games.

The most I owe is to my parents. What they have done for me extends far beyond just my doctoral studies. I will just humbly note the one lesson they've taught me that has been the most invaluable in my doctoral studies: Be aware of the practical realities of the world, but always follow your own compass. It helped me risk choosing my own topic, and working hard and sincerely on making something useful, even if it meant

having to work harder than just meeting the bar. This has helped shape me into a better person and a better scientist.

Most importantly, I would like to thank my dear wife, Priti. She was there with me all through the toughest part of my PhD: the end. She showed tremendous patience when I was stressed (which was nearly all the time). She was loving when I was careless. And most importantly, she was always there for me , ensconcing my stress-ridden life in her calmness. Thank you, Pritu.

Table of Contents

List of Tables	xiii
List of Figures	xiv
1 Introduction	1
1.1 The Quest for Immersion	11
1.2 Physically-based Simulation of Sound	16
1.3 Thesis Statement	18
1.4 Challenges and Contributions	19
1.4.1 Interactive Sound Synthesis	25
1.4.2 Efficient Numerical Acoustics	27
1.4.3 Interactive Sound Propagation	33
1.5 Thesis Organization	41
2 Previous Work	42
2.1 Interactive Sound Synthesis	45
2.2 Interactive Sound Propagation	49
2.2.1 Acoustic Simulation	52
2.2.2 Auralization	61
3 Interactive Sound Synthesis	66
3.1 Methodology	66
3.1.1 Input Processing	68
3.1.2 Deformation Modeling	68

3.1.3	Handling Impulsive Forces	70
3.2	Real-time Sound Synthesis	71
3.2.1	Mode Compression	73
3.2.2	Mode Truncation	76
3.2.3	Quality Scaling	78
3.2.4	Putting Everything Together	79
3.3	Implementation and Results	81
3.3.1	Rigid Body Simulation	81
3.3.2	Position Dependent Sounds	83
3.3.3	Rolling Sounds	83
3.3.4	Efficiency	85
3.4	Conclusion and Future Work	86
4	Efficient Numerical Acoustics	89
4.1	Mathematical Background	89
4.1.1	Basic Formulation	90
4.1.2	A (2,6) FDTD Scheme	91
4.1.3	Numerical Dispersion in FDTD and Efficiency Considerations	92
4.1.4	Wave Equation on a Rectangular Domain	93
4.2	Technique	96
4.2.1	Adaptive Rectangular Decomposition	98
4.2.2	Interface Handling	99
4.2.3	Domain Decompositon Method and ARD	100
4.2.4	Absorbing Boundary Condition	103
4.2.5	Putting everything together	104
4.2.6	Numerical Errors	104

4.2.7	ARD and FDTD: efficiency comparison	107
4.3	Results	110
4.3.1	Offline Sound Rendering	110
4.3.2	Numerical Dispersion: Anechoic Corridor	114
4.3.3	House Scene	115
4.3.4	Cathedral Scene	116
4.4	Conclusion and Future Work	117
5	Interactive Sound Propagation	121
5.1	Perception in Acoustic Spaces	122
5.1.1	Early Reflections (ER)	123
5.1.2	Late Reverberation (LR)	124
5.2	Acoustic Precomputation	125
5.2.1	Numerical Simulation	126
5.2.2	LR Processing	128
5.2.3	ER Processing	130
5.3	Interactive Auralization Runtime	135
5.3.1	Load-time Computation	135
5.3.2	ERIR Interpolation	136
5.3.3	LRIR Scaling	138
5.3.4	Binaural Processing	139
5.3.5	ERIR Short Fourier Transform	139
5.3.6	Auralization	140
5.4	Implementation and Results	141
5.4.1	Living room	144
5.4.2	Walkway	144

5.4.3	Citadel	145
5.4.4	Train station	146
5.4.5	Error Analysis	146
5.4.6	“Shoebox” Experimental Results	150
5.5	Conclusion, Limitations and Future Work	151
6	Conclusion and Future Work	153
	Bibliography	158

List of Tables

4.1	FLOPS comparison of FDTD vs ARD on a scene of volume $V = 10,000m^3$ with maximum simulation frequency $v_{max} = 1kHz$ for the duration $t = 1$ sec. Theoretically, ARD which uses samples per wavelength, $s = 2.6$, is nearly hundred times efficient than FDTD ($s = 10$) on account of using a much coarser grid. The value of “FLOPS per cell” is defined as the ratio of the total FLOPS and N , the total number of cells.	109
5.1	Performance statistics. Tables (a) and (b) show performance numbers for precomputation and runtime stages, respectively, for the four different scenes used for auralization tests. Abbreviated column headings are as follows. Precomputation: “Dim.” is the scene dimensions. “#ERL” is the simulated number of ER listener probes (before downsampling). “#ERS” is the simulated number of ER source probes. “#R” is the number of rooms in the scene. “ST” is total simulation time, including LR and ER probes. Runtime: “Mem.” is the total memory used for all source and receiver positions, including extracted peaks and frequency trend. T_{ER} is the length of the ER phase, and T_{LR} the LR phase, maximized over all rooms in the scene. “#S” is the number of different sources simulated at run-time. “ABT” is the total time needed to process each audio buffer, summed over all run-time sources.	142

List of Figures

1.1	Diffraction and scattering are closely related wave phenomena and depend critically on the relation of wavelength (λ) and object size (h). Visible light wavelengths are much smaller than object dimensions, lying in the geometric optics range, as shown to the right. Audible sound wavelengths, lying in the range of millimeters to meters span all three cases shown above, diffracting and scattering considerably from everyday objects, allowing us to hear behind visual occluders.	4
1.2	A screenshot from the game Half Life 2: Lost Coast illustrating the visual realism achievable with games today.	12
1.3	Numerous dice fall on a three-octave xylophone in close succession, playing out the song “The Entertainer”. Please go to http://gamma.cs.unc.edu/symphony to see and hear the xylophone playing.	24
1.4	Sound simulation on a Cathedral. The dimensions of this scene are $35m \times 15m \times 26m$. My technique is able to perform numerical sound simulation on this complex scene on a desktop computer and precompute a 1 second long <i>impulse response</i> in about 29 minutes, taking less than 1 GB of memory, while the current state-of-the-art FDTD takes a few days to perform the same simulation, at high-accuracy settings. Please go to http://gamma.cs.unc.edu/propagation to see a video containing auralizations on this scene and other examples.	28
1.5	Train station scene from Valve’s Source™ game engine SDK (http://source.valvesoftware.com). My method performs real-time auralization of sounds from dynamic agents, objects and the player interacting in the scene, while accounting for perceptually important effects such as diffraction, low-pass filtering and reverberation. Please go to http://gamma.cs.unc.edu/PrecompWaveSim to see a video containing auralizations on this scene and other examples.	34
3.1	This diagram gives an overview of my sound-synthesis approach.	67

3.2	This plot shows frequency discrimination in humans as a function of the center frequency. Note that the human capacity to discriminate between frequencies degrades considerably for frequencies in the range 2-22 KHz, which forms a bulk of the human audible range. I use this fact to guarantee that no more than 1000 modes need to be mixed for any object in the worst case, <i>irrespective</i> of its geometric complexity. In most cases the actual number is much smaller, in the range of a few hundreds. The red curve shows the piecewise linear approximation of this curve that my technique uses.	74
3.3	This graph shows the number of modes mixed vs time, for a xylophone bar just after it is struck in the middle. τ is the mode truncation threshold. A higher value of τ leads to more aggressive truncation of modes with low amplitude, leading to savings in terms of the number of modes mixed. In this case, $\tau = 2.0$ results in about 30% gain in efficiency over $\tau = 0.01$ which only truncates modes with near-zero amplitude. The sound quality for both the cases is nearly identical.	77
3.4	A metallic cylinder falls onto a wooden table, in the middle (left) and on the edge (right) and rolls off. The bottom part shows the corresponding frequency spectra for the two cases. Note that for the case on the left, most of the impulse is transferred to the low frequency fundamental mode while for the case on the right, the impulse is mostly transferred to higher frequency modes.	82
3.5	A plot of the impulses on a cylinder versus time for the scene shown on the right in Figure 3.4 and the corresponding audio samples. The peaks correspond to impacts while the numerous low-amplitude impulses correspond to rolling forces.	84
3.6	More than 100 metallic rings fall onto a wooden table. All the rings and the table are sounding. The audio simulation runs at more than 200 FPS, the application frame rate being 100 FPS. Quality Scaling ensures that the perceived sound quality does not degrade, while ensuring steady frame rates (See Figure 3.7)	87
3.7	This graph shows the audio simulation FPS for the scene shown in Figure 3.6 from time 1s to 2s, during which almost all the collisions take place. The bottom-most plot shows the FPS for an implementation using none of the acceleration techniques. The top-most curve shows the FPS with mode compression, mode truncation and quality scaling. Note how the FPS stays near 200 even when the other two curves dip due to numerous collisions during 1.5-2.0s.	88

4.1	Numerical dispersion with a (2,6) FDTD scheme for different mesh resolutions. Increasing the sampling reduces the numerical dispersion errors. Our method suffers from no dispersion errors in the interior of rectangular partitions, while FDTD accumulates errors over each cell a signal propagates across. Reducing these errors with FDTD requires a very fine grid.	93
4.2	Overview of the ARD approach. The scene is first voxelized at a prescribed cell size depending on the highest simulated frequency. A rectangular decomposition is then performed and impulse response calculations then carried out on the resulting partitions. Each step is dominated by DCT and inverse DCT calculations withing partitions, followed by interface handling to communicate sound between partitions.	97
4.3	Measurements of numerical error due to interface handling and PML absorbing boundary conditions. The interface handling errors stays near -40 dB for most of the frequency spectrum, which is not perceptible. The absorption error stays around -25 dB which introduces very small errors in the reflectivity of different materials.	105
4.4	Numerical results on the corridor scene, comparing numerical dispersion errors in FDTD and in our method. The reference FDTD solution has a mesh with $s = 10$ samples per wavelength. Note that only the magnitudes of the Fourier coefficients are plotted. Our method suffers from very little numerical dispersion, reproducing the ideal impulse response very closely, while FDTD suffers from large amounts for numerical dispersion. My technique takes an order of magnitude less memory and nearly two orders of magnitude less computation time to produce results with accuracy comparable to the reference solution.	111
4.5	The House scene demonstrates diffraction of sound around obstacles. All the scene geometry shown was included in the simulation. Our method is able to reproduce the higher diffraction intensity of sound at lower frequencies, while reducing the memory requirements by about an order of magnitude and the computational requirements by more than two orders of magnitude. The reference solution is computed on a mesh with $s = 10$ samples per wavelength.	112
4.6	The voxelization and rectangular decomposition of the Cathedral scene. Varying the absorptivity of the Cathedral walls directly affects the reverberation time. Note that my technique is able to capture all reflections in the scene, including late reverberation. The impulse responses shown above correspond to high order reflections, in the range of 30 reflections, which would be prohibitively expensive to compute accurately for geometric approaches.	118

5.1	Impulse response (IR) and corresponding frequency response (FR) for a simple scene with one reflection.	123
5.2	IR encoding. The late reverberation (LR) filter is stored once per room. The early reflections (ER) filter is represented as a set of peaks and a frequency trend, and stored at each source/listener grid point.	130
5.3	Run-time processing. Operations computed at run-time are colored red. Processing for only one channel (ear) is shown at figure bottom. . .	136
5.4	Scenes used for auralization tests.	138
5.5	Sound scattering and diffusion in the living room scene. The top row shows an empty room while the bottom row is fully-furnished. The left three columns show a 2D slice of the sound field generated by a Gaussian impulse emitted near the room’s center, while the right column shows the entire IR at a single receiver point placed at the source location. Red/blue represents positive/negative pressure in the sound field. Black areas represent solid geometry in the scene. Note the large difference in wave propagation in the two scenes because of scattering and diffraction. Refer to the video (link given in Section 5.4) for comparative auralizations.	143
5.6	Error analysis of my technique in the living room scene, at the source/listener points shown on the left. The top graph isolates errors from IR parametrization (peaks and frequency trend) alone, while the bottom graph accounts for interpolation as well, at a point midway between listener samples (red dots on left). The error between the approximated response with my technique and the reference appears in the top part of each plot. The bottom graph also compares linear interpolation (green curve) against my method (black curve). Linear interpolation produces more error overall and incorrectly attenuates higher frequencies.	145
5.7	Error analysis compared to broadband numerical simulation: listener close to source. My method matches the reference solution very closely, while linear interpolation yields substantial errors.	147
5.8	Error analysis compared to broadband numerical simulation: listener on couch. Compression error stays around 2dB till 1kHz and then increases to 4dB at 4kHz. Linear interpolation produces much more error.	148

5.9	Error analysis compared to broadband numerical simulation: listener outside door. Sound from the source undergoes multiple scattering in the room, then diffracts around the door to arrive at the listener. Such high-order effects are very hard to model convincingly and a challenging case for current systems. Notice the clear low-pass filtering in the frequency response plotted and audible in the demo. Compression error lies between 2 to 4 dB, which is quite low. Spatial interpolation errors are higher, crossing 5 dB, but my technique produces less error over all frequencies than linear interpolation.	149
5.10	Effect of atmospheric attenuation. Results for the Image Source method on a simple “shoebox” geometry shown in the upper-right inset are plotted on the left. Impulse responses were calculated assuming a frequency-independent pressure absorption coefficient of 0.15 at the room walls, but with frequency-dependent atmospheric attenuation using the formulae given in ISO 9613-1 assuming an air temperature of 20°C and relative humidity of 40%. The spectrogram on the right shows strong attenuation of frequencies above 5kHz. In particular, a 10kHz sound component decays by nearly 20 dB after just 200 ms of propagation. In a real scene where frequency-dependent material absorption is also accounted for, the attenuation would be even higher.	150
5.11	Error analysis compared with Image Source method. The left image shows the locations of source and listener in a simple “shoebox” room. A reference 200 ms long IR was generated with the Image Source method. The resulting frequency response is compared with my technique’s result based on a wave simulation bandlimited to 1kHz, and including compression and spatial interpolation errors. The result obtained with my technique (red curve) agrees well with the reference solution. In the top error plot, maximum error is about 5 dB while average error over the full frequency range up to 16kHz is 2-3 dB. Linear interpolation (green curve) yields larger errors and incorrectly attenuates higher frequencies.	151

Chapter 1

Introduction

Humans are gifted with the sense of hearing. We are immersed in sounds every day – talking to each other, enjoying music, the violent sound of thunder on one end, to a bird’s tweeting on the other. Hearing complements sight to provide us with a sense of emotional and physical presence in our environment. Our hearing has many properties that are in sharp contrast to sight. Our brain’s cognitive functions meld this complimentary information magnificently, to the extent that usually we are not aware of their separate roles. Thus, in a certain sense, we don’t really see or hear separately, but rather consume the whole “audio-visual landscape” surrounding us, seemingly at once. Most movie designers are acutely aware of this – good sound is as essential to the final emotional impact of a movie as graphics, but in quite different ways, as I’ll elucidate later. It is similarly quite important for video games to have the sounds synchronized with physical events such as collisions and rolling. Currently, most games can handle the visual aspect of such events well, but not so for audio. A part of my work aims at solving this problem. On the other side, while concert halls are designed primarily for sound and good acoustics is of paramount importance, particular attention is still paid to the lighting, making sure it reinforces the “mood” of the particular music number [60]. So, for interactive applications, it makes sense to discuss sight and hearing in the context of each other. My discussion in this chapter follows this pattern, with the purpose of

illustrating the need for better sound simulation in today's applications and contrasting it with light simulation to clarify the uniqueness of many of the problems encountered when trying to create realistic aural experiences on digital computers. This provides context for the contributions of this thesis.

The differences between sight and hearing begin with our sense organs. We have two frontally-located eyes with limited field of view and two ears located on diametrically opposite sides of the head with an unlimited field of view. Our eyes can be opened or closed at will, but our ears are always "on." While we sleep, we can still be awoken at any moment by a loud noise. While eyes don't differ so drastically in their geometry from person to person, the shape of our external ears varies substantially, along with our head and shoulder geometry. All these factors affect how each individual hears sounds in their environment. We regularly hear things that we can't see and by combining both sight and hearing, our mind ensures cognitive continuity even when there is visual discontinuity. For example, usually we are not startled by people walking around corners, by heeding the sound of their footsteps as they approach.¹ In addition to combining audio-visual data, our brain also checks for consistency in the common information. For example, it is disconcerting to have a person visually located in front of you, while his voice comes from behind. This situation is easily created in a teleconferencing environment with the screen in front and speakers behind you. The brain cross-references the location of the other person using both sight and hearing, finds two different results, leading to cognitive conflict and confusion. Therefore, in order to create a realistic experience for a user in a virtual world (such as a player in a 3D video game), one has to pay very close attention that hearing correctly reinforces sight just like in reality. We will see this pattern reappear many times in this discussion.

The complimentary information that sight and hearing provide to the brain is ul-

¹If you think about it, we do get startled in office corridors when the carpet is soft and muffles the footstep sounds too much.

timately based on physics. Our eyes and ears are designed to receive and process two fundamentally different kinds of physical waves – light and sound, respectively. Therefore, in order to create a convincingly realistic virtual world, both light and sound are crucial and a natural way to obtain perceptual realism is to employ “physically-based modeling” – simulate light and sound using a digital computer by employing well known physical equations governing the two phenomena. The thrust of this thesis is on efficient physical simulation of sound. It turns out that the production and propagation mechanisms for the *perceivable* range of light and sound are vastly different. This underlying difference in physics governs what simulation methods and approximations work best for each. In order to motivate why sound simulation poses its unique set of computational challenges, I discuss below in detail some of the most important physical differences between sound and light and how they affect the perception of each as well as dictate the necessary properties a sound simulator must possess in order to be useful. Since attention is restricted to only the perceivable range of light and sound for the purposes of my work, in the rest of this document, the terms “light” and “sound” will be assumed to mean “visible light” and “audible sound” respectively, unless otherwise stated.

The propagation speed of light and sound are very different. While light consists of electromagnetic waves that can propagate through vacuum, sound consists of extremely tiny (about $2/10,000,000,000$ of an atmosphere) pressure fluctuations in air. At a speed of $300,000,000$ m/s (meters per second) in vacuum, light travels staggeringly fast compared to sound, which travels at a comparatively slow speed of 340 m/s in air at room temperature. This causes major perceptual differences in their behavior – when we switch on a light bulb in a room, the light field reaches steady state in a matter of microseconds; too fast for us to perceive it while it is bouncing off the walls. Consequently, we only perceive the steady state light field. In contrast, when a musical instrument plays in a concert hall, in addition to the sound reaching us directly from the musical instrument, we also hear (modified) copies of the sound coming from different directions

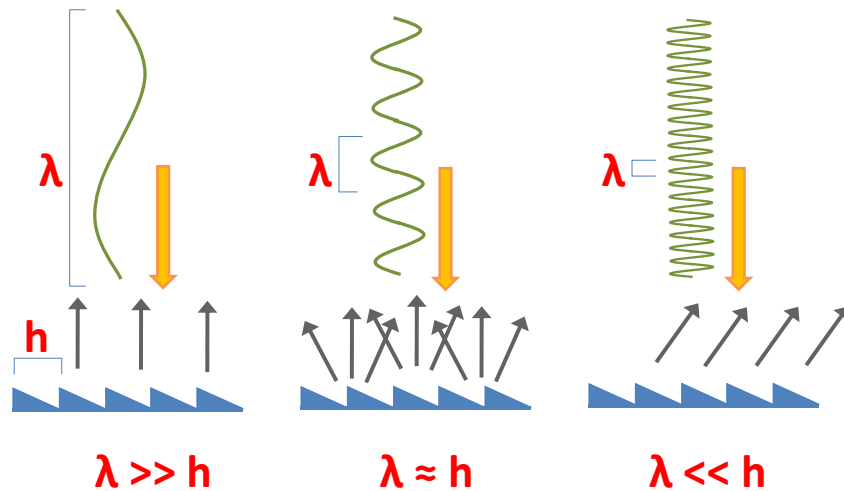


Figure 1.1: Diffraction and scattering are closely related wave phenomena and depend critically on the relation of wavelength (λ) and object size (h). Visible light wavelengths are much smaller than object dimensions, lying in the geometric optics range, as shown to the right. Audible sound wavelengths, lying in the range of millimeters to meters span all three cases shown above, diffracting and scattering considerably from everyday objects, allowing us to hear behind visual occluders.

at different times after bouncing off the walls multiple times. This is perceived as the familiar feeling of “reverberation”. Sound is slow enough that we can hear the separate reflections to some extent and observe the general decay of sound amplitude with time as it propagates in the scene, usually ranging in a few seconds. Although we rarely stop and observe reverberation consciously, we are so accustomed to hearing it that we expect it to always be present. A few seconds of reverberation is present in all concert halls that are generally accepted to have “good” acoustics [27]. Similarly, nearly all digital music that we hear today has had elaborate reverberation filters applied to the “dry” studio recording to make it sound more natural. Walking into an anechoic chamber, which is designed to suppress acoustic reverberation completely, is a very disorienting experience. All sounds seem unnaturally clipped and harsh. Even the most heavily furnished living rooms have a few hundred milliseconds of reverberation. Thus, assuming perceptually convincing reproduction is the final goal, light can be modelled to very good accuracy as a steady-state process, while sound usually requires a time-domain treatment.

The perceivable wavelengths of light and sound differ by many orders of magnitude. Visible light consists of wavelengths in hundreds of nanometers, which is thousands to millions of times smaller than the size of the objects we deal with usually, lying in range of millimeters to meters. This falls entirely in the regime shown on the right side of Figure 1.1 where wave propagation can be safely reduced to the abstraction of infinitely thin rays propagating in straight lines that undergo local interactions with object geometry upon intersection. This is called the “geometric approximation” which underlies techniques such as ray-tracing, and has served quite well for simulating light transport. Because of the minute wavelength of light, we rarely observe its wave-nature with the unaided eye, except in very special circumstances. Such examples are the colored patterns on the surface of a CD or the colored patterns on a bubble’s surface. In both these cases, the geometric feature size, namely the pits on the surface of the CD and the width of the bubble surface, is comparable to visible light wavelengths, thus revealing its wave nature. In complete contrast to light, audible sound has wavelengths in the range of a few millimeters to a few meters, making wave-related effects ubiquitous. One of the most important wave phenomena is *diffraction*, where a wave tends to spread in space as it propagates and thus bends around obstacles. Because sound wavelengths are comparable to the size of spaces we live in, diffraction is a common observation with sound and is integrated in our perception. While we expect sharp visibility events with light, we are not aware of perceiving any sharp “sound shadows” where a sound is abruptly cut off behind an obstacle. Rather, it is common experience that loudness decreases smoothly behind an occluder. As a result, as discussed previously, we can hear footsteps around a corner. The occlusion effect is more pronounced for higher frequency components of the sound since they have a shorter wavelength than the lower frequency components. The net perceptual effect is that, in addition to the the sound getting gradually fainter, its “shrillness” or “brightness” is also reduced behind obstructions. A simple experiment demonstrates this effect. Play a white noise sound on the computer

and then turn off one of the speakers by shifting the balance to completely left or right. This ensures that the sound emanates from only one of the speakers. Now bring a thick obstruction, such as a notepad between yourself and the speaker, making sure that the speaker is not visible. Remove the obstruction, bring it back, and repeat. You will notice that the noise is much more bearable when the source is not visible. This effect is because not only is its loudness reduced but additionally, its overall “shrillness” shifts lower when obstructed. This shift happens because higher frequency components of the noise are attenuated much more in relation to lower frequencies. Stated in the language of signal processing, an obstruction acts like a low-pass filter applied on the source sound signal. In summary, owing to its extremely small wavelength, light diffracts very little around common objects with sizes of a few millimeters or larger. Thus, it carries very precise spatial detail about objects, but on the flip-side, it can be completely stopped by an obstruction, casting a sharp shadow. Sound behaves in the exactly opposite fashion because of its much larger wavelength, not conveying spatial details with the precision of light, but having the ability to propagate and carry useful information into optically occluded regions. Therefore, geometric approximations (eg. rays, beams, photons) work well for light, but perceptually convincing sound simulation requires a full wave-based treatment because of the much larger wavelength of audible sounds. Another important property of sound is interference.

Interference is a physical property of waves. When two propagating waves overlap in a region of space, they add constructively or destructively depending on their respective phases at each point in the region. For example, when a crest and trough overlap at a point, the waves cancel out. We usually do not observe interference effects for light because most light sources are *incoherent*, emitting light with randomized phase. Thus, the total light intensity at any point in space can be described simply as the (phase-agnostic) sum of the intensities of all contributions at that point. In contrast, most sound sources are coherent and interference is quite important for sound. When a

wave undergoes multiple scattering in a domain and interferes with itself, it generates a spatially and temporally varying amplitude pattern called an “interference pattern.” For specific frequencies that are determined by the vibrating entity’s geometry and boundary properties, the interference patterns become time-invariant, forming standing waves. The vibrating entity could be the air column of a flute, the cavity in the wind-pipe of a vocalist, a string of a piano or even the whole air in a room. This is the phenomenon of *resonance*, the effect of which is to selectively amplify specific frequencies, called the resonant modes. The spatial interference patterns for resonant modes are called the mode shapes.

Resonance is the physical mechanism behind nearly all musical instruments – they are designed in such a manner that they resonate at precisely the frequencies of musical notes so that the energy spent by the musician is guaranteed to translate into the desired notes. The act of tuning an instrument is meant to align its resonant frequencies to musical notes. Resonance applies to the whole air in a room as well. Most rooms, especially those with small dimensions, such as recording studios or living rooms, have resonant frequencies of their own because sound will reflect and scatter at the walls and furniture and interfere with itself. The sound emanating from the speakers is thus modified substantially by the room, and to make matters worse, the interference pattern is directly audible at lower frequencies so that at some points there is too much “boom” and at others there is none. Such room resonances create a very inhomogeneous and undesirable listening experience which needs to be mitigated by moving the listener position (couch, for example) and/or placing furniture and other scattering geometry at locations chosen to destroy the standing waves. Thus, while resonance makes life of the musician easy, and makes it equally tough for the room acoustician. This is because the musician relies on resonance to generate select (musical) frequencies, and the room acoustician tries to stop the room from amplifying its own select (resonant) frequencies, in order to ensure that any music played within the room reaches the listener

in essentially the same form as it was radiated from the instrument or loudspeakers. Thus, any simulation approach for sound must be able to capture interference and the resulting resonance effects.

Resonance is very closely related to the mathematical technique of “modal analysis” which has the tremendous advantage of having a direct physical interpretation. Given the computer model of a vibrating entity along with appropriate boundary conditions, modal analysis allows one to find all of its resonant modes and their shapes. These computed resonant modes and shapes correspond directly to their physical counterparts. Mathematically, it is known that an *arbitrary* vibration can be expressed as a linear combination of resonant modes vibrating with different, time-dependent strengths. This offers substantial computational benefits, as I will describe in detail later. To give a quick example, given a guitar string’s length, tension, material etc., it is possible to determine its resonant modes and mode shapes using modal analysis, which is performed beforehand (precomputed). At runtime, given the position and strength of a pluck, one can very quickly evaluate the response of the string and the sound it emits by expressing the pluck strength as well as the resulting vibration as a sum of the resonant mode shapes oscillating *independently* at their corresponding mode frequencies.

The dynamic range² of perceivable frequencies for sound is much larger than light. We can perceive sounds ranging from 20 to 22,000 Hertz, which is a dynamic range of roughly one thousand (three orders of magnitude). The corresponding range for visible light is 400 to 800 Terahertz, the dynamic range being just two. The lowest frequencies of sound propagate very differently from the higher frequencies because of the large difference in wavelength. This means that sound simulation necessarily has to be broadband – simulating within a small frequency range doesn’t work in the general case.

²defined as the ratio of the highest to the lowest values of interest for a physical quantity

Up till now, I have focused on differences in the physical properties of sound and light and how physical properties of sound dictate important aspects of the simulation technique used for computing sounds in a virtual world. In designing such simulation techniques, it is very useful to take into account that such sound will be eventually be played for a human listener and processed by our ears and brain. Therefore, well-known facts from psychoacoustics³ can be used to set error-tolerances, as well as inform the design process for a sound simulator hopefully leading to increases in computational and memory efficiency. This is an important theme in my work and I show that large gains can indeed be obtained by following such a strategy. In the following, I discuss the perceptual aspects of hearing and contrast them with sight.

Pitch and Loudness: Mirroring the physical differences of light and sound, the corresponding human sensory functions are also markedly different from each other. Different frequencies of light are perceived as colors, while different frequencies of sound are perceived as pitch. Pitch is one of the central perceptual aspects of our sensation of hearing and corresponds to the physical frequency of sound. As mentioned previously, our hearing spans an amazing range of three orders of magnitude in frequency, from 20 Hz to 22,000 Hz. Our pitch perception is roughly logarithmic in frequency. In most musical scales, each increase in octave corresponds roughly to a doubling of frequency. Equally astounding is the range of loudness we can perceive. The loudest sound we can hear without damaging our ears has about a **million** times higher pressure amplitude than the faintest sound we can perceive. To give an analogy, this corresponds to a weighing scale that can measure a milligram with precision and works well for a ton! Both pitch and loudness are therefore usually expressed on a logarithmic scale – pitch in octaves, as is common practice in music, and loudness in decibels (dB). The definition

³The scientific area that studies how different sounds are processed by the (human) ears and brain

of the decibel scale is as follows –

$$\text{Loudness (dB)} := 10 * \log_{10} \left(\frac{I}{I_0} \right), \quad (1.1)$$

where I is the intensity of sound, which is proportional to the square of the pressure amplitude. The reference intensity, $I_0 = 10^{-12} \text{ W/m}^2$ corresponds to the lowest audible sound intensity and evaluates to 0 dB. The pitch and loudness scales mirror our perception quite well. Each increase in octave increases the pitch by equal amounts. Similarly, each increase in dB increases the loudness by equal amounts.

Hearing is primarily temporal, sight is spatial: This is the most fundamental difference between how sight and hearing interact with our cognition. The major function of human vision is to provide spatial information carried by the light entering our eyes. Motion is important, but we can resolve temporal events only at roughly 24Hz; intermediate events are fused together to give a smooth feeling of motion. This is exploited by all computer, TV and movie displays by drawing a quick succession of photographs at or above an update rate of 24Hz. In comparison, hearing is a truly continuous and temporal sense. Where sight stops, hearing begins – we hear from 20Hz up to 22,000Hz. What that implies is that we can directly sense vibrations happening with a period less than a millisecond with ease. Moreover, any simulation that needs to capture such vibrations has to have an update rate of at least 44,000Hz. Our sense of hearing is attuned to the overall frequency content of sound and how this composition changes over time. This is fundamental to our perception of all the sounds around us, such as music and speech. Music is almost purely a temporal experience. Using our senses of sight and hearing together, we observe our surroundings at millimeter resolution in space and sub-millisecond resolution in time. However, sounds do provide *approximate* spatial information that can be essential when visual information is not available and can help direct our gaze. When someone calls our name from behind we can “localize

their voice” (that is, find the direction of their voice) to within a few degrees by utilizing the microsecond delay, as well as intensity difference between the sound reaching our ears from the source [10]. However, we cannot deduce the shape of an object from its sound. In fact, it can be proven mathematically that this is impossible to do[35]. Nor can we perceive the geometry of a wall from sound scattered from it, as we can for light. The scattering does produce noticeable differences in the temporal composition of the final sound due frequency-dependent diffraction, reflection and interference, but it does not provide the fine-scale geometric information that light provides.

To summarize, the physical behavior of light and sound are very different, so is the information they provide, so is their perception, and so have to be any techniques that attempt to simulate them on a digital computer. Light simulation techniques can usually use steady state simulations in combination with infinite frequency (geometric optic) approximations that ignore interference, at update rates of 24Hz or higher. In contrast, perceptually convincing sound simulation requires full-wave, broadband, time-domain solutions with update rates of 44,000Hz or higher. Additionally, the simulation techniques must account for interference and diffraction effects correctly.

From this discussion on physical properties of sound and human sensory perception, one can see why simulation techniques for sound have quite different requirements and constraints than light simulation. In the following, I discuss sound simulation in the context of games and virtual environments and enumerate the computational challenges before going on to describe my specific contributions.

1.1 The Quest for Immersion

Ever since digital computers were built, people have striven for building applications that would give an immersive sensory experience to users that would give them the feeling of actually “being there” – a perceptually convincing replication of reality in a



Figure 1.2: A screenshot from the game Half Life 2: Lost Coast illustrating the visual realism achievable with games today.

computer-generated world. This was one of the founding stones of the area of Computer Graphics, a large part of which aims at realistically reproducing our visual perception by simulating matter interaction and light transport in a virtual world.⁴ Although the physical equations governing these phenomena are very well-known from classical physics, performing these tasks efficiently on digital computers is extremely tough. About four decades of research in the area of Computer Graphics has been devoted to finding suitable algorithms and approximations that obtain higher performance while achieving high perceptual quality of the rendered scene. The approximations introduced are typically required to keep the computational time tractable and avoid computing detailed features of physical reality that we are not capable of perceiving. Supplementing this trend in ever more efficient algorithms, the computational power of desktop systems has also increased tremendously over the last few decades. This advance has been further accelerated by Graphics Processing Units (GPUs) designed specifically for performing compute-intensive graphics operations in hardware. With this combination of algorithmic and hardware advancement, computer graphics has now matured as an area and it is possible these days to generate scenes of stunning realism on desktop machines interactively, using a combination of efficient algorithms, perceptual approximations and fast hardware. Figure 1.2 shows a screenshot taken from the game “Half Life 2: Lost Coast” that illustrates the realism achievable today in interactive graphics applications.

Unfortunately, work on providing an immersive **aural** experience, called *auralization*, to complement visualization, has fallen far behind, receiving very little attention in the interactive applications community, in comparison to Graphics. The first well-known publication discussing the integration of sound in interactive applications was nearly two decades ago by Takala and Hahn [100]. Their seminal work was motivated by the observation that accurate auditory display synchronized correctly with the world

⁴Throughout this thesis, I use the terms “virtual world”, “game environment” and “scene” interchangeably, unless otherwise noted.

displayed visually, can augment graphical rendering and enhance the realism of human-computer interaction because in reality we use hearing and sight together, as I discussed previously. There have also been systematic studies showing that realistic auralization systems provide the user with an enhanced spatial sense of presence [26]. The motivation for my thesis is to achieve this goal of producing realistic sound by mimicking reality – use computer simulations of the physical equations governing how sounds are produced and propagate in a scene. By grounding these simulations on the actual models of the interacting objects and propagating the sounds in the same scene shown visually, it is possible to design general techniques and systems that generate realistic sounds in all possible events that might happen in an interactive application, without requiring an artist to foresee all possible circumstances beforehand. Research work in this area has unfortunately been sparse, although finally, the interactive applications community is paying more attention to sound. Commercial applications, like games, reflect the disparity between graphics and sound. Whereas some games today feature close to photo-realistic graphics, game audio engines still rely largely on prerecorded clips and prerecorded acoustic DSP filters, often lacking basic occlusion/obstruction effects. The underlying technology has stayed unchanged in its essential design for nearly two decades, despite its shortcomings. Although I discuss these in more detail in subsequent chapters, I will mention a few of the most important deficiencies here that have guided my work.

Most sounds we hear in games/virtual environments have no real correspondence to the world’s physics, they are prerecorded clips played with perfect timing to give an illusion that the graphics and sound are somehow related. This breaks down in many instances and leads to loss of realism – we are quick to reject sounds that repeat exactly, as artificial. After a few repetitions, we subconsciously classify them as merely indicative rather than informative. The simple reason is that natural sounds simply don’t behave like this, we rarely hear the *exact* repetition of any natural sound and we

respond to slight variations because they often contain useful information. For example, consider a game scene with a cylinder rolling on the floor that is not visible to the player. The rolling sound has a precise correlation with the roughness of the floor, material of both the cylinder and floor, and the speed of rolling. If one uses a prerecorded rolling clip which is insensitive to the above mentioned parameters, the user will respond to the sound with observing subconsciously “A cylinder is rolling”, rather than “A *metal* cylinder is rolling *slowly* on a *wooden* floor.” There is a lot of information contained in this sound – The player might be able to reasonably conclude the room the other player is in, given the wooden floor and type of cylinder. Achieving realistic audio in movie production is comparatively easier, since only particular, known cases have to be handled. After the visual portion of the movie is done, a foley (audio) artist can record a highly realistic clip depending on the exact circumstances shown visually. But the very open-ended nature of interactive applications that makes them so attractive, renders such an approach nearly impossible, requiring huge libraries of prerecorded sounds that cover all possibilities reasonably well – something games are forced to do today. This process turns sound production into a huge asset creation and management problem, while still not producing sounds that are realistic enough for a large number of cases.

In their seminal work [100], Takala and Hahn also discussed the need for adding realistic acoustics in interactive applications. It is well-established that to give a user a sense of presence in a scene, realistic acoustics is an indispensable requirement. Among other things, a major challenge in this regard is the ability to model the effect of occlusions and obstructions for sound. Since diffraction effects are clearly perceivable to us in everyday life, they are added into games using hand-tuned low-pass and gain filters. However, again, the sheer unpredictability of scenarios that will manifest in real time as the sources and listener move, makes such an approach intractable.

1.2 Physically-based Simulation of Sound

The main premise behind my thesis is that if we model the wave physics underlying acoustic phenomena at sufficient accuracy to capture the aurally relevant behavior of the sound-producing objects and their environment using a digital computer, the resulting auralizations should be closely matched to our observation of reality and efficient enough to be executed in real time. This new capability would automatically lead to a higher level of immersion in an interactive environment, since we naturally respond to environments using both visual and aural cues. Computer graphics has shown that this principle can be applied to visualization by simulating light transport using physically-based ray-optic principles and rendering the results to produce a realistic, convincing rendition of the scene. Doing such light simulations efficiently enough for real-time execution has been a major achievement of research in the area of computer graphics.

My thesis work is an application of this same idea for sound simulation – since graphics in interactive applications has reached a high level of believability, to reach the next level of immersion, a realistic rendition of *both* light and sound is the natural next step. Additionally, physically-based simulation of sound seems to be the most promising route to achieve this goal, given the open-ended nature of interactive virtual worlds. However, as discussed earlier, sound simulation and its associated challenges are very different in their essential character from those in graphics. Developing novel approaches to address these challenges is the main contribution of my thesis.

Past work on using physically-based sounds has seen limited success because of two main factors – lack of visual realism and lack of computational power. Even if the user is presented with a highly realistic auralization, unrealistic visualizations lead to immediate sensory rejection. Our visual perception and aural perception are tied together inextricably. It is well-known, for example, that the quality and warmth of the sound in an opera house is affected by the lighting and visual “mood” of the theater. There is no reason the same wouldn’t apply to virtual worlds. Secondly, the computational power

of computers has increased tremendously in recent years, compared to ten years back – something that has enabled many aural tasks cross the limit of interactivity. These days, most of the computation for interactive 3D graphics is done by Graphics Processors (GPUs). This fact, combined with the advent of high performance, multi-core CPUs, is an important factor for the feasibility of many of the approaches I present. Also, as I show in my work on numerical acoustics, GPUs are also very useful for providing the raw computational power necessary for fast off-line numerical simulation, considerably reducing the preprocessing time for acoustic simulation.

Simulating even simple sound-producing systems requires a lot of computation. As discussed earlier, sound simulations required transient, time-domain, simulations while resolving frequencies ranging from 20Hz to 22,000Hz, and spatial scales from millimeters to meters, at update rates surpassing 44,000Hz. From the practical perspective of implementing an interactive auralization system, a central consideration is the continuous nature of sound – *any* temporal incoherence whatsoever will be quickly and clearly perceived. For example, any waveform discontinuity is perceived as a very audible, high frequency “click”, which immediately degrades the audio quality dramatically. Contrast this with visual rendering, where such jittering will only result in a decreased sense of flow in the video. This is a very common experience: While watching a movie, we tolerate momentary degradation in video quality quite easily but degradation in audio quality, such as jittering, is completely unacceptable. Thus, an interactive auralization system must provide very strict performance guarantees and should be able to adapt gracefully to variable time constraints while performing extremely challenging computations.

Because of the computational difficulties outlined above, most real-time systems, including the techniques I present, involve two steps: first, there is a pre-computation step in which physical simulation or other mathematical operation, such as modal analysis, is performed to facilitate fast computations in real time. To improve runtime performance and memory usage, perceptual approximations are used to represent this information

in a compact form that can be utilized efficiently in real time. At runtime, the stored results are used to perform interactive auralization. The main theme of my thesis is to use well-known physical principles to model and simulate the physical aspects of sound, and to develop and improve current computational techniques along with application of relevant perceptual principles to enable and accelerate interactive applications with real-time auralization.

The overall problem of sound simulation can be broken down into mainly two components based naturally on its physics – synthesis (production) and propagation. Think of a cup falling on the ground – after impact, its surface starts undergoing small-scale vibrations which create pressure waves in the surrounding air. After being thus produced, these waves propagate in the scene, undergoing complex interactions with the boundary and reaches our ears after being modified by the scene. Thus, what we hear contains information both about the object creating the sound, as well as the scene in which it propagates. The first part above is the problem of *sound synthesis*: modeling how sound is **produced** by typical objects due to elastic surface vibrations upon such events as collision and rolling. The second part is *sound propagation*: how the sound thus produced **propagates** in an environment, as it reflects and diffracts at the scene boundaries, before reaching the listener’s ears. My work spans both these aspects of sound simulation, with an emphasis on efficiency and real-time execution on today’s desktop machines. This leads me to my thesis statement.

1.3 Thesis Statement

“By exploiting analytical solutions using modal analysis to accelerate numerical simulation and reducing runtime computation to capture only the perceptually important auditory cues, one can design fast algorithms to perform real-time sound synthesis and acoustic wave propagation on complex 3D scenes, enabling realistic, physically-based

auralization.”

By “realistic” in the above statement I mean sounds that, on informal listening, at once seemed consistent with our daily experience. For my work on acoustics, comparisons were performed against simulations with a high-accuracy technique, for the purpose of validation.

1.4 Challenges and Contributions

My contributions can be divided into three main areas: interactive sound synthesis, efficient numerical acoustics, and interactive sound propagation. I will discuss the respective computational challenges and my contributions in each of these areas in the following sub-sections. Here, I describe the relationship between these different components and how they fit in the overall goal of designing an interactive, immersive auralization framework. The connection between sound synthesis and propagation is quite clear from the perspective of an interactive application: the former deals with how sound is produced by objects in an environment and the latter with how it propagates before reaching the listener. It is useful to keep in mind that this classification of sound simulation into synthesis and propagation is only pragmatic nomenclature – in reality, wave propagation underlies both of these problems: the sound of a piano string results from waves propagating back and forth along its length and interfering, while the reverberation in a concert hall results from waves propagating in the volume of the scene, scattering from the walls and interfering. This similarity in physics might motivate us to think that the same simulation technique could work for both cases. Unfortunately, this is not the case because of the drastic differences in the computational cost for sound synthesis and propagation for practical domains. I now describe why this is the case and give the reader some numerical intuition of what makes sound simulation computationally challenging.

Computational Cost: Recall that the speed of a sound wave in a medium, c , is related to its frequency, ν , and wavelength, λ , by –

$$c = \nu\lambda \tag{1.2}$$

The cost of sound simulation on a domain can be measured by its “sound-size”. Given the diameter of a D -dimensional scene, L , and the smallest wavelength to be simulated, λ_{min} , the sound-size, S , of the scene is a dimensionless number defined as –

$$S := \left(\frac{L}{\lambda_{min}} \right)^D \tag{1.3}$$

The smallest simulated wavelength, λ_{min} , is found by considering the highest frequency of interest, ν_{max} , which yields, $\lambda_{min} = c/\nu_{max}$. The highest frequency of interest can be fixed based on perceptual considerations, such as the highest audible frequency (roughly 20,000 Hz), or the highest frequency that can be simulated with feasible computational and memory costs. Intuitively, S corresponds to the number of wavelength-sized cubes that fit in the whole domain and is the main parameter controlling the amount of computation and memory required to do sound simulation. Stated mathematically, after spatial discretization, the domain’s elasticity matrix is sparse with size (number of rows/columns) proportional to S . The technique of modal analysis that was described earlier is the most attractive option to model elastic vibrations in arbitrary domains. This is because once modal analysis is done offline, the results can be used very efficiently in real time to model any vibrations in the domain due to arbitrary excitations. Theoretically, modal analysis applies equally well to sound synthesis and propagation, because both are wave propagation problems and yield a corresponding elasticity matrix on discretization. The problem is that the sound-size for sound propagation problems is many orders of magnitude larger than synthesis problems of practical size.

For sound synthesis, L is much smaller because the dimensions of sound-producing

objects, such as cups, bells, boxes, musical instruments, etc. are necessarily much smaller than the dimensions of acoustic spaces in which they are contained, such as rooms or buildings. Additionally, sound propagates much faster in solids and liquids than in air, which means that audible frequencies have much larger wavelengths in solids than in air. Therefore, for sound synthesis from solids/liquids, λ_{min} is much larger than for propagation in air. Lastly, many sound producing objects can be treated with reduced dimensionality. For example, the string of a piano can be treated as a 1D system, while a drum membrane can be modeled very well as a 2D system. In fact, most thin-shell objects can be approximated as 2D vibrational systems with good accuracy. Sound propagation, on the other hand, almost invariably requires a 3D treatment. Here's a quick numerical comparison of the sound-size of a solid steel box ($c \approx 3000m/s$ for shear waves) versus a concert hall ($c \approx 340m/s$ for sound in air), with $\nu_{max} = 20,000Hz$ for both cases:

$$\begin{aligned}
 L = 1.0m, \lambda_{min} = 0.15m, D = 3 &\implies S_{box} \approx 300 \\
 L = 20m, \lambda_{min} = 0.017m, D = 3 &\implies S_{hall} \approx 1,600,000,000
 \end{aligned} \tag{1.4}$$

Thus, the sound-size, S , for sound propagation is many orders of magnitude larger (million times in the above example) than sound synthesis. The computational cost and memory requirements of modal analysis scale as S^3 and S^2 respectively. It must be clear in context of the above examples why modal analysis works quite well for the purpose of sound synthesis, but is completely infeasible for acoustics on realistically large 3D scenes. On desktop machines today, modal analysis can be performed for S in the range of few thousand while consuming less than 4 GB of memory and taking a few hours of computation time, thus allowing modal analysis for most sound-producing objects. As for propagation, taking the above example, performing a full modal analysis on the orchestra hall would take 10^{18} times the computation time as the steel box and 10^{12}

times the memory. Clearly, a different kind of decomposition of computation into offline and real-time components has to be explored, which is one of the contributions of my dissertation research on interactive sound propagation.

In the first part of my thesis on interactive sound synthesis, modal analysis is used for precomputation as it can be feasibly performed for typical sound-producing objects while staying within the constraints of a few GB of main memory and a few hours of computation. Therefore, in this part of my dissertation, performing the precomputation was not the main challenge and I focused directly on the issues with handling lots of sounding objects in real time. Existing techniques could only handle a few (roughly ten) objects and my key contribution was in designing an perceptual approximations and interactive techniques for handling hundreds of objects in real time while ensuring smooth degradation in perceived quality, as available computation fluctuates in a typical real-time interactive application.

In the second part of my dissertation, I have developed a fast, time-domain numerical acoustic simulation technique. For time-domain acoustic simulation, the current state of the art in room acoustics, as well as in computational acoustics to a large extent, is the Finite Difference Time Domain (FDTD) technique. FDTD is enormously more efficient than modal analysis for performing simulations in the kilohertz range on large 3D scenes and satisfies all the criteria for sound simulation that I discussed earlier, namely, time-domain, broadband simulations that capture all wave properties. Unfortunately, the computational time and memory requirements of accurate, high-order FDTD, even though far superior to modal analysis, were still insufficient for my purpose, even for moderate-sized 3D scenes. Thus, a major portion of my work is devoted to developing a numerical acoustics simulator that exploits suitable physical approximations consistent with room acoustics (mainly that the speed of sound is constant in the domain), to make simulations on acoustically large environments feasible on a desktop computer. I was able to successfully develop such a simulator, that uses an adaptive rectangular decom-

position (ARD) of the scene. The ARD simulator is capable of performing simulations that used to take days with a reference, high-order FDTD, in minutes on a desktop computer.

In the third part of my dissertation on interactive sound propagation, I have used my ARD simulator to perform acoustic precomputation and enable realistic, interactive, acoustics for moving sources and listener, thus “closing the loop,” yielding a system that generates auralizations using wave-based acoustics simulation in real time. Numerical simulations using ARD are utilized to precompute acoustic responses for different source locations in an environment at a dense sampling of listener locations. These results are then stored in a compact representation that allows for very efficient storage and usage at runtime, among other benefits. Thus, it becomes possible to design an interactive system that uses numerical acoustics in real time to perform auralizations that include the effects of physically complex and perceptually important phenomena such as diffuse reflections, reverberation, focusing and occlusion/obstructions.

In totality, these three parts of my dissertation form a solution to the overall problem of interactive physically-based sound simulation. My work contains contributions in both the important aspects of this overall problem, namely, synthesis and propagation. In the following, I separately discuss in technical detail, the specific challenges and my contributions in these three portions of my thesis. There remain many challenges and interesting problems to be addressed in this area that are being addressed in concurrent work, as well as problems that I intend to investigate in the future. This thesis offers a substantial step forward in the design of a comprehensive and consistent set of techniques for performing interactive and immersive physically-based auralization. In future interactive applications, one can imagine the sound being produced as well as propagated in the scene directly from the geometry and material properties of the world and objects contained in it, leading to rich, realistic games and virtual worlds.

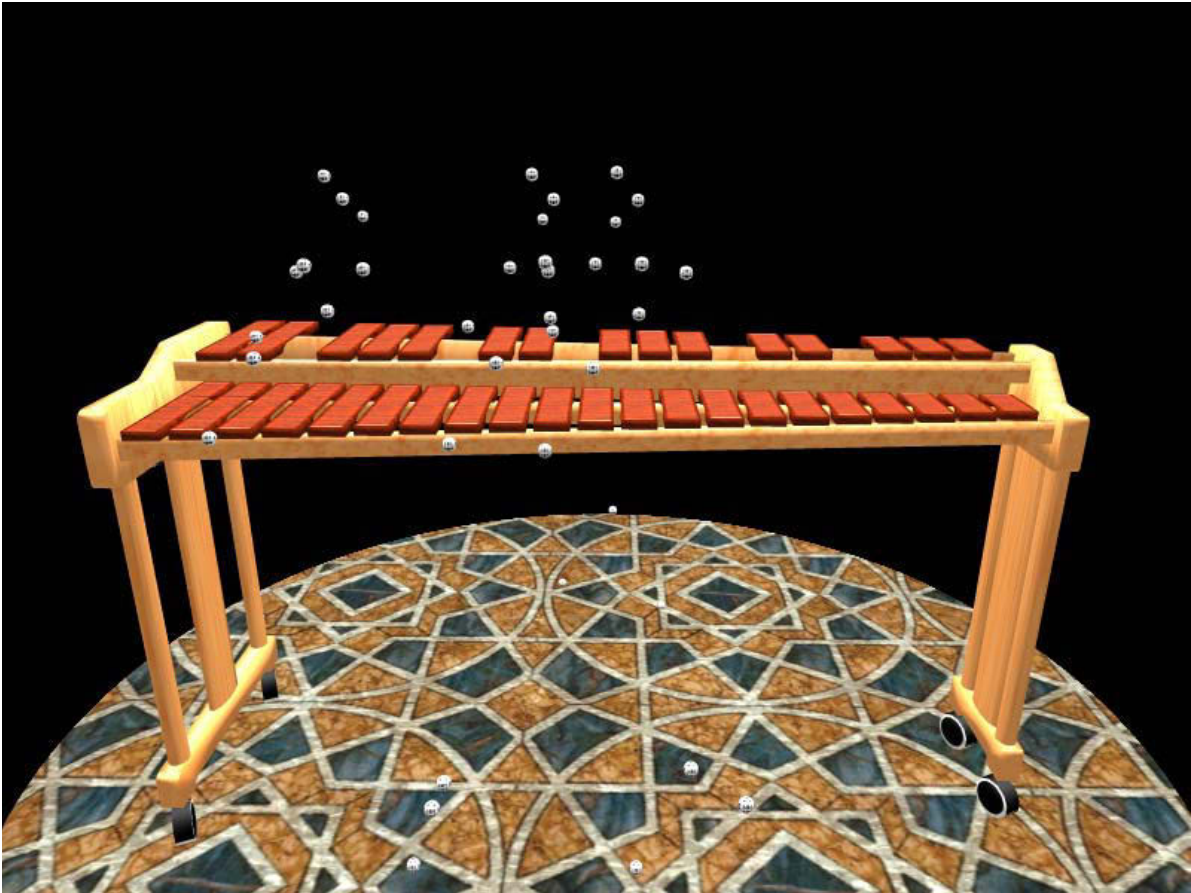


Figure 1.3: Numerous dice fall on a three-octave xylophone in close succession, playing out the song “The Entertainer”. Please go to <http://gamma.cs.unc.edu/symphony> to see and hear the xylophone playing.

1.4.1 Interactive Sound Synthesis

As noted earlier, most interactive applications today employ recorded sound clips for providing sounds corresponding to object interactions in a scene. Although this approach has the advantage that the sounds are realistic and the sound-generation process is quite fast, there are many physical effects which cannot be captured by such a technique. Once such example of a rolling cylinder was given earlier. More generally, in a typical collision between two objects, the loudness and timbre of the sound is determined by the magnitude and location of the impact forces – a plate sounds very differently when struck on the edge compared to when it is struck in the middle. Consequently, if the collision scenario changes slightly, the sound exhibits a corresponding change. Such subtle effects can add substantial realism to a typical scene by avoiding the repetitiveness common to recorded sound clips. However, developing a system which produces sound using physically-based principles in real time poses substantial difficulties. The foremost requirement is the presence of an efficient dynamics engine which informs the sound system of object collisions and the forces involved. Fortunately, many present-day games easily meet this requirement, with physics engines such as NVIDIA PhysX [3] and Havok [2]. Open-source dynamics engines, such as ODE [4], are also available. Given a dynamics simulator, the essential challenge then is to synthesize the sound efficiently enough to play in real time while taking only a small portion of the total running time, which is usually dominated by graphics and rigid-body simulation. As of today, sound engines can typically only afford a few hundred CPU cycles per object per sound sample for many interactive applications.

In this part of my thesis, I present an approach that meets the interactive performance requirements outlined above, while ensuring high realism and fidelity of the sound produced. Given an object’s geometry and a few material parameters, a spring-mass model approximating the object’s surface is constructed. I show that although a spring-mass system is a coarser approximation than FEM models used in prior approaches

[17, 63, 64], it is an adequate model to capture the small-scale surface vibrations that lead to the generation of sound in nature. The advantage of using spring-mass systems is the ease of implementation and ability to easily handle surface meshes designed for visual display. I show how this formulation yields an analytical solution to the equation of motion for the surface of the object which can then be used to find the resonant modes of the object surface using modal analysis. The runtime computation consists of calculating each mode’s contribution which is then suitably mixed to produce the objects’ sound. Modeling only the surface works well for thin-shell objects. For solid objects, it is possible to form spring-mass models of the whole volume, at higher precomputation cost, without changing any other details of the technique I present.

However, a naive implementation of such an approach requires a very high number of modes to be mixed per object and consequently, only a few (less than ten) sounding objects in real time can be handled by prior techniques. I present several perceptually-motivated acceleration techniques to reduce the number of modes being mixed while ensuring minimal perceptual degradation. In addition, the sound quality and the associated computational cost for each object is scaled dynamically in a priority-based scheme which guarantees that the total sound production meets stringent time constraints, while preserving the overall aural experience as far as possible. My approach has the following features –

- It is based on a discretized physically-based representation that offers simplicity of formulation and ease of implementation;
- It makes no assumptions about the input mesh topology – surface meshes used for physics can be used directly for sound synthesis;
- It is capable of yielding both impact and rolling sounds naturally, without any special-case treatment;
- It uses perceptually-motivated approximations enabling rich environments con-

sisting of hundreds of sounding objects, with insignificant reduction in the overall audio quality.

- Its easy to integrate with commonly available physics engines.

To the best of my knowledge, with the possible exception of methods that rely on physical measurements, no work prior to the publication of my work in [71, 72, 70] has been demonstrated to handle complex scenarios (e.g. see Figs. 1.3 and 3.6) in real time. There has been more recent work improving on these techniques, I discuss those in the next section.

1.4.2 Efficient Numerical Acoustics

As explained earlier, the complimentary problem to sound synthesis is that of simulating sound propagation in arbitrary spaces. In this part of my thesis, I have addressed the problem of numerical simulation of acoustic wave propagation, also referred to as computational acoustics. As I discussed previously, due to the physical properties of sound, a fully wave-based, time-domain, broadband simulator is required. Numerical approaches for sound propagation attempt to directly solve the acoustic wave equation, that governs all linear sound propagation phenomena, and are thus capable of performing a full transient solution that correctly accounts for all wave phenomena, including diffraction, elegantly in one framework. Since I use a numerical approach, my implementation inherits all these advantages. This characteristic is also the chief benefit my method offers over geometric techniques, which I will discuss in detail in Chapter 4.

For the purpose of my thesis work, the eventual application for this simulator is real-time auralization, which is discussed in detail in the next sub-section. However, the ideas provided here would be applicable to many other wave propagation problems as well, for example, in electromagnetic wave propagation. The key assumptions underlying my approach are – firstly, the wave propagation is governed by *linear* equations which

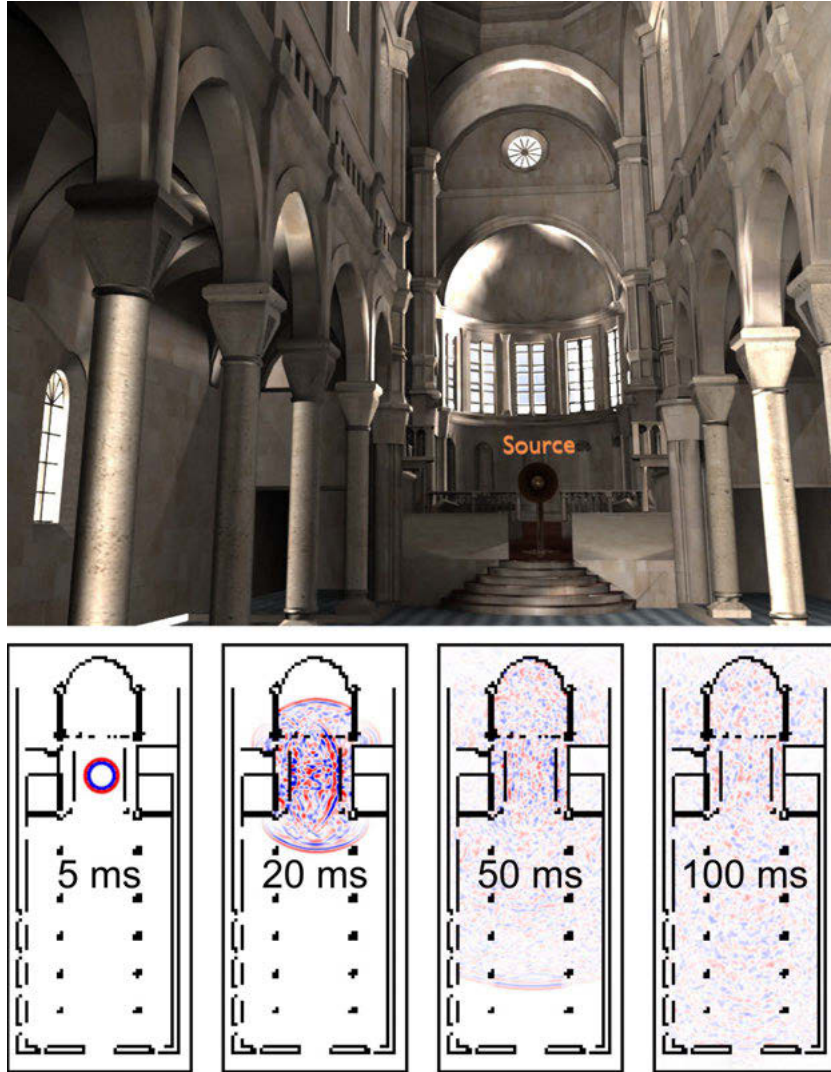


Figure 1.4: Sound simulation on a Cathedral. The dimensions of this scene are $35m \times 15m \times 26m$. My technique is able to perform numerical sound simulation on this complex scene on a desktop computer and precompute a 1 second long *impulse response* in about 29 minutes, taking less than 1 GB of memory, while the current state-of-the-art FDTD takes a few days to perform the same simulation, at high-accuracy settings. Please go to <http://gamma.cs.unc.edu/propagation> to see a video containing auralizations on this scene and other examples.

allows the principle of superposition to be used. Secondly, the speed of wave propagation should be piece-wise constant over the domain of interest. My technique can be applied as long as these two assumptions hold, to yield speeds much faster than is achievable with standard techniques that make more general assumptions.

The input to an acoustic simulator is the geometry of the scene, along with the reflective properties of different parts of the boundary (boundary conditions) and the locations of the sound sources and listener. The final goal in my case is to auralize the source sound – predict the sound the listener would hear. Recall that this process involves complex physical interactions such as diffraction (sound bending around obstructions), reflecting and scattering from the scene geometry, etc. All these interactions are captured succinctly by computing an impulse response (IR) of the scene under consideration that captures its complete response in time for a given source and listener location. Intuitively, the impulse response is the sound received at the listener if an ideal Dirac delta impulse is played at the source. Note that the impulse response varies, depending on both the source and listener locations.

Computational acoustics has a very diverse range of applications, from noise control and underwater acoustics to architectural acoustics and acoustics for virtual environments (VEs) and games. For a general introduction to the whole area of acoustics, I refer to the text by Kinsler [47]. Although each application area has its own unique requirements for the simulation technique, all applications require some level of physical accuracy, although with different error tolerances. For noise control, accuracy translates directly into the loudness of the perceived noise. For architectural acoustics, accuracy has implications on predicting how much an orchestra theater enhances (or degrades) the quality of music. For interactive applications like VEs and games, physical accuracy directly affects the perceived realism and immersion of the scene. This is because we are used to observing many physical wave effects, such as diffraction, in reality and their presence in the scene helps to convince us that the computer-generated environment is

realistic.

For most acoustic simulation techniques, the process of auralization can be broken down into two parts: (a) preprocessing; and (b) sound rendering. During preprocessing, an acoustic simulator does computations on the environment to estimate its acoustical response at different points. These are encoded as impulse responses. The exact precomputation depends on the specific approach being used. For my approach, the preprocessing consists of running a simulation from a source location, which yields the impulse responses on the *whole simulation grid* in the scene in one simulation. The simulation grid is typically quite fine, with a resolution of around 12 cm for a 1kHz band-limited simulation. The rendering at runtime can then be performed by convolving the source signal with the calculated impulse response at the listener’s location. This part of my dissertation deals with the preprocessing phase of acoustic prediction that computes impulse responses. The subsequent real-time auralization is the focus of the next part of my thesis on interactive sound propagation.

I present a novel and fast numerical approach that enables efficient and accurate acoustic simulations on large scenes on a desktop system in minutes, which would have otherwise taken many days of computation on a small cluster. An example of such a scene is the Sibenik cathedral shown in Figure 1.4. This scene would have taken a few days for a 1 second long simulation on a small cluster (due to memory limitations) with the current state-of-the-art in room acoustics, the Finite Difference Time Domain (FDTD) method. With my technique, this same simulation can be completed in about 30 minutes on a desktop computer equipped with a NVIDIA GTX280 GPU.

Most interactive applications today, such as games, use artificial reverberation filters (or equivalently, impulse responses) that are not based on the environment. Instead, they roughly correspond to generic acoustical spaces with different sizes – “Large hall”, “narrow corridor” etc. [5] The filters are assigned to different parts of the world to capture the realism and mood of the scene, and are typically assigned by experience

game audio designers who also have a good intuition of how the artificial reverberator works and what all of its parameters do. In reality, the acoustics of a space exhibits perceptibly large variations depending on its geometry, wall material, and other factors [51]. There is not even a guarantee that the artificial reverberator’s controls provide enough expressiveness to capture all these factors.

A possible alternative to obtain realistic filters for interactive auralization would be to do actual measurements on a scene instead of performing a simulation. This is analogous to using recorded clips instead of synthesizing sounds. Not only is it difficult and time-consuming to do this for real scenes, but for virtual environments and games, one would need to physically construct scale physical prototypes because the scenes don’t exist at all in reality! This is of course, prohibitively expensive, cumbersome and impractical. What if the game artist decides to change the game map to improve gameplay by partially removing a wall? One would need to re-build the scale model and re-measure everything. This is even more impractical considering that most games today encourage users to author their own scenes. Given all these factors, especially the last one, simulation is clearly the best approach since the automatically generated filters would be realistic and correspond to the scene presented visually. If artistic control is desired, these filters could then be modified by an artist. This is not the complete story, as far as games go – one also needs a way to efficiently apply these filters to sounds in real time, and for that a fast and memory-efficient sound rendering system is required, the topic of the next part of my work.

Thus, numerical approaches offer the attractive option to take the scene geometry and automatically provide realistic and immersive acoustics in games and virtual environments which account for all perceptually-important auditory effects, including diffraction. However, this realism comes at a very high computational cost and large memory requirements. In this part of my thesis, I have developed a highly accelerated numerical technique that works on a desktop system and can be used to precompute

high-quality impulse responses for arbitrary scenes without any human intervention.

Another application of this simulator that I have not explored in depth in my work, is in the traditional application of sound simulation to determine the acoustic quality of concert halls. Since my simulator solves for the complete sound field in a scene, an acoustic consultant could give as input the CAD geometry of the hall and actually visualize how the sound wavefronts propagate in the scene over time. This would help him/her make guided decisions about what changes need to be made to the scene to counter any perceived acoustic deficiencies. For example, to identify the portion of a wall that is causing an annoying, strong reflection. Refer to the bottom of Figure 1.4 for an example of such a time-stepped field visualization.

Main Results: My technique takes at least an order of magnitude less memory and two orders of magnitude less computation compared to a standard numerical implementation, while achieving competitive accuracy at the same time. It relies on an *adaptive rectangular decomposition* (ARD) of the free space of the scene. This approach has many advantages:

1. The analytical solution to the wave equation within a rectangular domain is known. This property enables high numerical accuracy, even on grids approaching the Nyquist limit, that are much coarser than those required by most numerical techniques. Exploiting these analytical solutions is one of the key reasons for such a drastic reduction in computation and memory requirements. The main reason such solutions can be employed is the assumption that the speed of sound is constant in the domain, which holds quite well for the purpose of auralization.
2. Owing to the rectangular shape of the domain partitions, the solution in their interior can be expressed in terms of the Discrete Cosine Transform (DCT). It is well-known that DCTs can be efficiently calculated through an FFT. I use a fast implementation of FFT on the GPU [36], that effectively maps the FFT to the

highly parallel architecture of the GPU to gain considerable speedups over CPU-based libraries. This implementation leads to further reduction in the computation time for our overall approach.

3. My technique can handle scene boundaries with arbitrary absorption coefficients. This is achieved by using the Perfectly Matched Layer (PML) absorber. This also allows the modeling of emission-into-infinity, thus allowing the ability to handle outdoor scenes as well as having windows, doors and open ceilings in indoor scenes.
4. The rectangular decomposition can be seamlessly coupled with other simulation techniques running in different parts of the simulation domain, if so required.

In Chapter 4, I demonstrate my algorithm on several scenarios with high complexity and validate the results against FDTD, a standard Finite Difference technique. I show that my ARD approach is able to achieve a similar level of accuracy with at least two orders of magnitude reduction in computation time and an order of magnitude less memory requirements. Consequently, ARD is able to perform accurate numerical acoustic simulation on large scenes in the kilohertz range which, to the best of our knowledge, had not been previously possible on a desktop computer. I wish to emphasize that this technique is the key building-block for the interactive sound propagation system I describe next.

The ARD technique was published in [74] and [73]. An older technique that does not scale as well as ARD but served as a valuable building block, was presented in [69]. This latter technique will not be described in detail in this document since my later work improves upon it.

1.4.3 Interactive Sound Propagation

As discussed in the previous sub-section, interactive auralization can add significant realism to virtual environments and to this end, I have developed a fast simulator that

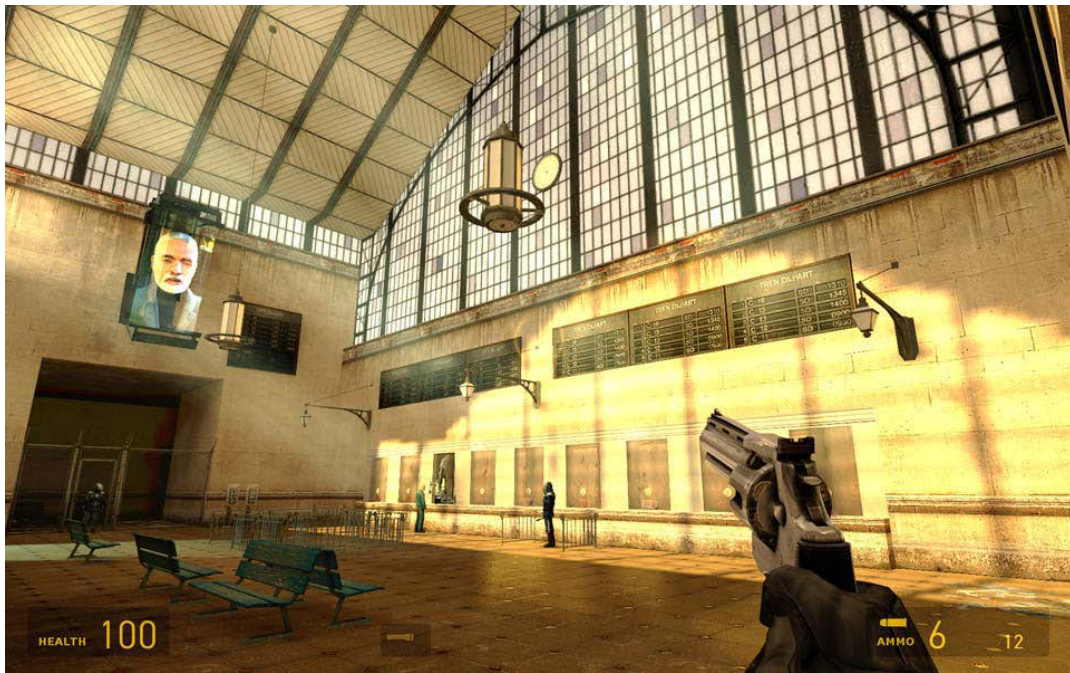


Figure 1.5: Train station scene from Valve's Source™ game engine SDK (<http://source.valvesoftware.com>). My method performs real-time auralization of sounds from dynamic agents, objects and the player interacting in the scene, while accounting for perceptually important effects such as diffraction, low-pass filtering and reverberation. Please go to <http://gamma.cs.unc.edu/PrecompWaveSim> to see a video containing auralizations on this scene and other examples.

allows quick precomputation of acoustic impulse responses using wave propagation. Perceptually realistic simulation of sound propagation must capture two interrelated wave effects: diffraction and scattering since they result in many gross acoustic effects observed in daily life. Smooth reduction in volume as one walks through a doorway or behind a building is due to high-order diffraction. Smooth loudness variation in the sound field of a furnished room results from diffracted scattering off its complex geometry. Neglecting diffraction leads to clicking artifacts and incoherent loudness fluctuation, as well as unnatural termination of sound before it reaches occluded regions.

The input to an interactive sound propagation system is the scene geometry as well as the locations of multiple sources, the sounds they are playing and the location and orientation of the listener. The source sounds may be pre-recorded or synthesized using the techniques I've described earlier. The objective is to auralize the final sound at the listener, assuming the sources as well as the listener may move about. Performing such auralization while capturing all the acoustic effects in real time within a complex 3D environment presents a challenging problem for current approaches. By “complex”, I mean “containing acoustically relevant scene features at length scales down to centimeters” (see Figure 5.4a). Sound frequencies up to 5 kHz scatter diffusely from “rough” surface features at centimeter scales and are mostly unresponsive to finer detail while higher frequencies are more strongly absorbed as they travel through air or scatter off surfaces [51, p. 27]. My method is limited to *static* scene geometry. Fortunately, the static portion of most spaces largely determines the overall acoustics of common architectural/virtual spaces, thus covering a large set of applications. For example, the overall acoustics of a concert hall is not affected drastically by opening or closing a door. Moreover, the local effects of moving geometry could be used to augment the simulation performed on the static portion of the scene in the future. Continuing the previous example, any outside noise entering through the opened door could be added-in at run-time using fast approximations to augment the total sound field.

Existing methods to solve this problem are *geometric*, and trace rays or beams from the source into the scene to collect their contributions near the listener. These methods have the advantage of handling dynamic scenes, but at the cost of high computational requirements at runtime, consuming 8 cores to auralize a single moving source [18]. Most current applications do not invest such computational resources on audio. In contrast, my approach has been explicitly designed to consume a single core while allowing tens of moving sources. In addition, there are many disadvantages of geometric approximations that my work aims to alleviate. Methods based on conservative beam tracing split the beam when it encounters geometric discontinuities, leading to slow performance in complex scenes and exponential scaling in the reflection order [33, 18]. A related problem arises for ray-tracing methods, which must sample a huge number of rays to capture multiple-bounce propagation and avoid missed contributions. In practice, meshes must be simplified and detailed interior objects replaced by simpler proxies to achieve interactive performance, substantially increasing manual effort for producing acoustic geometry. Automatic methods to do this are a nascent area of research [94]. Handling diffraction with geometric approaches is challenging, especially for complex scenes [15]. At long sound wavelengths, current geometric edge-diffraction models either ignore global effects from complex geometry or require too much computation to run interactively.

Even though I have designed a substantially faster acoustics solver than the state of the art, it is still at least 3 orders of magnitude too slow for on-the-fly evaluation. In order to enable real-time wave-based acoustics, my solution is to pre-compute an off-line, wave-based simulation for a given static environment in terms of its 7D spatially-varying acoustic impulse response (IR), $S(t, p_s, p_r)$, where t is time, p_s is source position, and p_r is receiver position. That is, for each possible pair of source and listener locations in 3D, a time-series is stored, which is the impulse response at the listener from the source location. This can be reduced to a 6D problem by restricting the listener to a 2D plane in the scene and leveraging *acoustic reciprocity* which dictates that the impulse response

stays invariant if the source and listener locations are swapped with each other. This dimensionality reduction leads to nearly 10 times reduction in both the runtime memory requirement, as well as the pre-processing time. Even so, the computational and storage requirements are huge. With my ARD technique, simulating a one-second response at a single source position in a scene of volume 12^3m^3 bandlimited to frequencies up to 1kHz requires 30 minutes of computation and generates 24GB of data *for a single source location*. Simulating over many different source locations quickly becomes intractable.

To give the reader a more concrete intuition of the memory and computational requirements of a brute-force approach, lets consider a typical scene with size 12m x 12m x 12m. Additionally, lets assume the length of the required IR to be about 1 second. Assuming a band-limited simulation till 1 kHz, the corresponding grid cell-size is about 12 cm, with an update rate of 6000 Hz. My simulator typically takes about 150 ms (millisecond) per step for a scene with this air volume. Thus, every 1 second long simulation takes $6000 \times 0.15 = 900$ seconds, which is 15 minutes. Now consider the complete 7D space mentioned above, with no sub-sampling and no dimensionality reduction through acoustic reciprocity. The space requirement is about $10^6 \times 10^6 \times 6000 \times 4$ bytes = 24 petabytes and the corresponding pre-processing time is $10^6 \times 15\text{min} = 28$ years! This is obviously completely impractical. By sub-sampling at about 1 meter resolution these numbers are reduced drastically to about 91 gigabytes and 20 days respectively. Using acoustic reciprocity to reduce dimensionality leads to a further reduction to 11 gigabytes and 2 days respectively. Using the techniques I describe next, these numbers can be reduced further to a few hundred megabytes and 2-3 hours respectively.

My technique exploits human auditory perception using the well-known *ER/LR perceptual model* [51, p. 98]. This model temporally decomposes sound propagation in a typical acoustic space into two parts. The first part is the *early reflections* (ER) phase containing sparse, high-energy contributions corresponding to the direct sound and initial reflection/diffraction contributions which are processed separately in the human

brain to some degree. As time progresses, the response smoothly transitions into the second part – the *late reverberation* (LR) phase representing the later arrival of many, nearly simultaneous wavefronts which the human brain fuses and is mainly able to only infer the statistical properties of the sound decay. While the ER exhibits significant perceptual variation within an environment depending on the source and listener location, the LR can be approximated as a property of the room itself, since its statistics don't vary much within a room. Perceptually, the ER conveys a sense of location, for example, occlusion information, while the LR gives a global sense of the scene – its size, level of furnishing and overall absorptivity. For example, in a concert hall, different seats typically have different sound quality because of variation in the ER. However, every concert hall still has a clearly identifiable, “acoustic identity”, which is captured by its LR, which stays largely invariant perceptually over different seats in the hall. Current techniques used in games using artificial reverberation techniques capture the LR, but completely fail to a large degree in capturing the spatial variation in the ER.

The LR is extracted in my technique by performing a 1-2 second simulation from a source placed at the room's centroid and analyzing its impulse response (IR) at a receiver in the same place. This result determines the time length of the ER, as well as the per-room LR filter called the *late reverberation impulse response* (LRIR). ER length is 50-200ms for rooms of typical size. Simulations are then run with the source placed at all sample points on the 2.5D grid described above. For each source position, the resulting *early reflections impulse responses* (ERIRs) are recorded at sample points over the scene's 3D volume. This two-step approach reduces the time duration of expensive ER simulations from 1-2s to 50-100ms, saving at least 10× in precomputation time and runtime storage.

The ERIRs recorded for each source-listener pair are then extracted and compactly encoded using a novel, perceptually-based technique. ERIRs contain distinct pressure peaks in time, corresponding to wavefronts arriving at the listener. My technique then

extracts the highest-energy peaks (yielding roughly 30-40 in most cases) and stores their delay and attenuation in the time domain. Peak data is wide-band information that captures reverberation and interference but ignores diffraction low-pass filtering, so I add a residual *frequency trend* representation which restores these effects and allows them to be plausibly extrapolated to frequencies beyond the ones simulated. Compared to direct storage of simulated ERIRs, this reduces memory use by 10 times while encoding all-frequency information.

A novel run-time system propagates source sounds based on this precomputed data. Spatial interpolation of IRs is required as sources and listener move since these positions are subsampled in my system to about 1m. Straightforward waveform interpolation yields erroneous timbral coloration and “gurgling” artifacts; my technique interpolates in the encoded space of peak times and amplitudes instead, to avoid such artifacts. The ERIR is then *spatialized* to the listener’s left and right ears, the LRIR added, and the source sound convolved in the frequency domain with the final computed impulse responses for each ear.

My thesis is the first to achieve real-time, wave-based sound propagation, including high-order, frequency-dependent sound scattering and diffraction, for moving sources and listener in environments of the complexity and size I demonstrate. I propose a novel decomposition of the computation into three parts: an off-line wave-based simulation on the static scene (which is performed using the ARD technique I have developed), an off-line perceptually-based encoding of the resulting IRs, and a run-time engine. My technique automatically computes from simulation both the ER and LR and separates them based on echo density. My new IR encoding extracts peaks and a residual frequency trend. My key contributions include – (1) computing this information from the bandlimited results of numerical simulation, (2) extrapolating it to higher frequencies in a perceptually plausible manner, (3) employing a grid-based sampling for moving sources and listener along, and (4) using one which exploits acoustic reciprocity. By

using reciprocity, handling ER and LR separately and expressing the ER compactly, I obtain runtime memory usage reduction of 1000 times. This number is even larger if one considers sub-sampling in space. The run-time system then efficiently decodes, interpolates, and convolves source sounds with these encoded IRs in the frequency domain, supporting tens of moving sources and a moving listener in real time.

Main Contributions: My work is the first to achieve real-time, wave-based sound propagation of moving sources and receivers in complex indoor and outdoor environments. The main features of my technique are –

- A novel decomposition of the computation into three parts: an off-line wave-based simulation in the static scene, an off-line perceptually-based encoding of the resulting IRs, and a run-time auralization engine.
- Effective use of Acoustic Reciprocity to reduce runtime memory usage and pre-processing time by a factor of ten;
- Automatically compute both the ER and LR from simulation and separate them based on echo density;
- Representation for Impulse Responses based on ER/LR model, reducing runtime memory usage and pre-processing time further by ten times;
- My new IR encoding extracts peaks and a residual frequency trend yielding a further 10 times reduction in memory usage. Computing this information from the bandlimited results of numerical simulation, extrapolating it in a perceptually plausible manner and employing a grid-based sampling for moving sources and listener are all novel contributions.
- A novel runtime technique for fast interpolation of sampled Early Reflection IRs that preserves important perceptual properties; and

- The first real-time auralization system that captures wave-based effects such as realistic occlusion/obstruction in complex, static indoor and outdoor scenes with tens of moving sound sources and listeners on a desktop computer.

The technique presented in this part of my thesis was published in [75].

1.5 Thesis Organization

The following chapters are organized as follows. In the next chapter, I discuss related work in the areas of sound synthesis and sound propagation. The three subsequent chapters correspond to the three main parts of my thesis work in the same order as discussed here: interactive sound synthesis, efficient numerical acoustics, and interactive sound propagation. I conclude my thesis with a summary of the main contributions, as well as a discussion of future work.

Chapter 2

Previous Work

In the most general case, sound can be defined as elastic waves propagating in a physical medium. One way to organize all applications of sound is based on the phase of the medium of propagation, as there are important physical differences in wave propagation depending on whether the phase of the medium is solid, liquid or gas. In the area of structural and vibrational engineering, one is mainly concerned with solid media and the dynamic behavior of different structures, such as bridges, under time-varying loads. Such problems constitute the area of structural or vibrational engineering. On a smaller scale, the same governing equations also describe a cup's surface vibration upon being hit, or a piano string's vibration after being struck by the hammer, which is related to the problem of interactive sound synthesis. The medium of sound propagation could be liquid, such as water, which is the area of underwater acoustics having wide-ranging applications, such as sonar sensing to image the ocean floor. The medium could be gaseous, such as air, in which case we are concerned with acoustic wave propagation with applications ranging from noise control in an air-plane's cabin to concert hall design. My work on interactive sound propagation is closer in its motivation to the latter application.

One might question in light of the above discussion why there is any need for research on sound simulation in the context of interactive applications, which is the focus

of my thesis, since the governing physical equations are the same as the engineering applications outlined above. Further, computer simulation techniques developed in these engineering disciplines, as well as techniques for modeling wave propagation in related areas, such as electromagnetic simulation, have clear and direct applications to interactive sound synthesis and propagation. But, there are two crucial differences from engineering problems when performing sound simulation for interactive applications –

1. **Real-time, memory-efficient execution:** Interactive applications require that the results of sound simulation be presented in real time. Due to this requirement, the practical limitations of today’s desktop computation power require the computations to be split into precomputation and runtime execution phases, for most cases. The runtime computation should execute in real time and it should also have a small memory footprint. This means that if precomputation is required, it should generate appropriate, compact results that capture all the “necessary” features of the simulated sound. What I mean by necessary is discussed below in the next point. These requirements are made even more stringent because in most interactive applications, there are other components besides audio as well, which typically leave only a small fraction of the available computation power for audio.
2. **Exploiting auditory perception:** The high computation and memory efficiency requirements mentioned above can be met by keeping in mind that very high numerical accuracy is not always a necessary requirement for interactive applications, since the end-consumer is the human auditory system. This aspect can be exploited by avoiding computation of inaudible features of the sound, and/or removing them during the precomputation phase to reduce the memory footprint.

Besides these two differences, from a pragmatic point of view, it is desirable for interactive applications that the precomputation time also be reasonable, in the range of a few hours on a desktop computer. A few minutes would be even more desirable, so

that, for example, a game artist could iteratively try out different scenarios.

Thus, since most engineering techniques are not designed for on-the-fly evaluation, interactive sound simulation presents unique challenges. Additionally, because one can exploit human auditory perception, this immediately opens up many possibilities for acceleration techniques in this area. One might further argue that a few decades of improvement in hardware is going to allow direct application of robust solvers used in engineering applications in real time, making such developments obsolete. The counter-argument is that techniques developed especially for interactive applications that are faster today will be faster tomorrow. This means that a decade from now, much more could be performed in real-time than today – hardware improvements will improve the performance of both kinds of algorithms by similar amounts. Further, it might well turn out that while exploring numerical and perceptual approximations, one comes across useful improvements that apply to some engineering applications as well. I have come up with one such example in my own research described here – The fast wave simulator I have developed (ARD), will be directly applicable to traditional room acoustics applications after adding a few features, most notably, frequency-dependent absorption, and might serve as a valuable room acoustic prediction tool. ARD might even be applicable to electromagnetic scattering, if the interface errors can be reduced from the current -40 dB to -80 dB (which is close to what current FDTD techniques can achieve in this area [99]). This may be achieved by using interface operators that have an order of accuracy higher than six, as employed currently. Additionally, one might explore compact stencils optimized for lowering the frequency-response of the artificial interface. Since ARD is roughly 100 times faster than a high-order FDTD, slowing ARD down by a small factor for achieving this additional accuracy gain will be worthwhile.

My discussion of previous work falls into two parts, both in the context of interactive applications. In the first part, I discuss previous techniques for sound synthesis, focusing on generating sounds from solid objects in real-time. The second part presents a

discussion of simulation methods proposed in the literature for modeling acoustic wave propagation in room acoustic applications and discusses my work on developing a fast numerical acoustics simulator (ARD) in this context. Lastly, I contrast interactive auralization techniques and their room acoustic simulation counterparts with my work on using ARD for interactive auralizations with related work in this area. Most of the work discussed here is based on geometric techniques because there has been very limited work on wave-based simulation for interactive auralization.

2.1 Interactive Sound Synthesis

The following discussion will focus on sound synthesis based on physical deformation modeling of underlying systems. There is a rich history of real-time sound synthesis based on what Perry Cook calls “physically-inspired” sound modeling where the emphasis is on capturing, in simple parametric models, the essential sound-producing mechanism behind any natural sound-producing phenomenon. This is in contrast to my overall “physically-based” approach here which consists of simulating the objects’ actual surface deformation over time. For a great introduction to physically-inspired real-time techniques, as well as a brief discussion of physically-based techniques, the reader is referred to Cook’s book on the subject [21]. A very useful online resource on signal processing for sound synthesis and digital waveguides for musical synthesis is Julius O. Smith’s book available freely online [95].

The concept of modeling the surface vibrations of objects using discretized physical models in real time for generating sounds was first proposed by Florens and Cadoz [30], who used a system of masses and damped springs to model 3D shapes and developed the CORDIS-ANIMA system for physically-based sound synthesis. More recently, numerical integration with a finite element approach was proposed as a more accurate technique for modeling vibrations [17, 63]. These methods had the advantage that the

simulation parameters corresponded directly to physically measurable quantities and the results were more accurate. The main issues were the complexity of formulation and implementation and the low speed of the resulting simulation.

To remedy the performance issue of the above methods, van den Doel and Pai [109, 110] suggested using the analytically computed vibrational modes of an object, instead of numerical integration, leading to considerable speedups and enabling real-time sound synthesis. But, since the solution of PDEs governing the vibration of arbitrary shapes are very complicated, the proposed system could only handle simple systems, such as rectangular or circular plates, for which analytical solutions are known. To handle more complex systems which do not admit direct analytical solution, two approaches have been proposed in literature. The first approach, [113] used physical measurements on a given shape to determine its resonant vibration modes and their dependence on the point of impact. Later, these modes may be appropriately mixed in a real-time application to generate realistic synthetic sounds. But, arbitrary 3D models have to be physically obtained or constructed in order to find their aural properties, which can be a serious limitation in many cases. For example, when the object is created entirely virtually, as is done for computer games. In [64], O'Brien et al. addressed this problem and proposed a method for handling arbitrarily-shaped objects by discretizing them into tetrahedral volume elements. They showed that the corresponding finite element equations can be solved analytically after suitable approximations using modal analysis. Consequently, they were able to model arbitrarily shaped objects and simulate realistic sounds for a few objects at interactive rates.

My work shares some common themes with [64]. Their work used an FEM-based model for the elastic behavior of the object. I propose a simpler system of point-masses and damped springs for modeling the surface vibrations of the object and it also submits to an analytical solution in a similar fashion, while offering much greater simplicity of formulation and ease of implementation. The complexity of scenes demonstrated in [64]

is low, containing less than 10 sounding objects and the interactions captured are mainly due to impacts. My main contribution is a method that scales to handling hundreds of objects in real time using psychoacoustic principles. Also, it is capable of producing realistic *rolling* sounds in addition to impacts.

The main bottleneck at runtime in all techniques that utilize modal analysis is evaluating and mixing all the resonant modes of the object at runtime. Most approaches, including mine, use a time-domain approach for evaluating the modes since they capture the initial transient of an impact sound quite well. There has been very recent work exploring the possibility of evaluating and mixing the modes in frequency-domain instead [11] to obtain significant performance gains, although at some expense in quality for capturing the transients right after impact.

Often, immersive environments are both visually and aurally complex. The problem of scheduling multiple objects for sound synthesis has been addressed before in [31]. They exploited a model of imprecise computation in [20], and proposed a system in which the objects are iteratively assigned time quotas depending on the availability of resources and priorities of the objects. My approach to prioritization and time-quota assignment exploits properties specific to our sound-generation technique, and thus achieves good results using a much simpler scheme. Recently, van den Doel et al. [112] proposed techniques to synthesize sounds in real time for scenes with a few sounding rigid bodies and numerous particles, by exploiting frequency masking. At runtime, they find emitted frequencies which are masked out by other neighboring frequencies with higher amplitude and do not mix the masked frequencies. I use a different perceptual observation presented in [92], which report that humans are incapable of distinguishing frequencies that are very close to each other. I use this observation to prune out frequencies from an object's frequency spectrum as a *pre-processing* step. My technique leads to better performance and much lesser memory consumption at runtime while ensuring little loss in auditory quality.

There has been recent work extending my technique to handling sliding sounds, besides impact and rolling [76]. Sub-millimeter-scale surface geometry is modeled stochastically, intermediate (mesoscopic) scale geometry is obtained from normal-maps used for rendering. The macroscopic geometry is the triangle mesh itself, as in my work. Rolling sounds in my technique are generated directly from the impacts generated by a discretized triangular mesh. There has been work on modeling rolling in a much more detailed fashion that is closer to physical reality [97]. Most work on rigid body sounds, including mine, assumes a linear deformation model for elastic solids. There has been work recently on synthesizing sounds by modeling the non-linear deformation of thin-shell objects [16]. An exciting direction for future research is modeling non-linear *damping* models. Models based on the linear Raleigh damping assumption yield easily to modal analysis and produce great results for metals, but generate considerably artificial sounds for highly-damped materials, such as wood.

There have been a lot of exciting papers recently on synthesizing different categories of sounds than from solid objects. The work presented in [23] focuses on aerodynamic sounds that are produced when, for example, a sword moves fast through the air. A later generalization of the technique also allows it to handle fire sounds [24]. Very recently, there has been work on practically synthesizing sounds based directly on fluid simulation [117]. A more efficient alternative has been proposed more recently [61], which can even execute in real time for certain cases. Both of these formulations rely on a model of bubble sounds that was first utilized for real-time synthesis in [111], in a parametric framework not relying on fluid simulation. Interesting work has also been done on handling sounds due to fracturing objects [118].

2.2 Interactive Sound Propagation

The roots of most simulation techniques for sound propagation in use today can be traced back to the area of room acoustics, which sprung from the need to design musical halls with good music quality by using physical acoustic principles . Sabine [81] was a pioneer in this area, and designed the Boston Symphony Hall based on physically-based statistical rules he had developed, combined with an intuition for acoustic wave propagation and its perceptual effects. It was the first hall to be designed with primary importance given to its physical and perceptual acoustic properties, with the architecture designed to be aesthetically pleasing, as well as fulfilling acoustic requirements. By the application of these principles, Sabine was successful in creating a hall that is still considered to be amongst the very best concert halls in the world. For a history as well as practical design considerations for the room acoustician, refer to the text by Egan [27]. For a general introduction to the area of room acoustics, along with a good discussion of the basic underlying physics and psycho-physics, refer to the classic text by Kuttruff [51]. A very general and quite thorough introduction to the field of acoustics as a whole is presented in the text by Kinsler [47].

With increasing desktop computational power, the rise of Interactive applications such as games and immersive virtual environments, has meant that it is cheaper than ever to design virtual acoustic spaces – all one needs is a desktop computer and a 3D modeling program. A full-featured modeling program, Blender, is even available freely [80]. Advancement in computer technology has also meant that it is possible to predict the complete sound at the listener automatically by explicitly modeling sound propagation in detail based on physical equations, rather than just its statistical properties. After decades of progress, there is a wide selection of such simulation techniques available today for the room acoustician. They broadly fall into two classes – Geometric Acoustics (GA) that uses ray-based approximations for sound propagation, and Numerical Acoustics (NA) that perform a full wave solution based on “first principles”.

Wave-based approaches (NA) are the most desirable since they automatically capture all physical phenomena of interest. More precisely, GA can be derived from NA as an approximation by assuming frequency tending to infinity. However, NA cannot be used for all practical room acoustic problems today because the computational and memory requirements are out of the reach of desktop systems for large 3D scenes with complex shapes that practical problems involve. Moreover, NA scales as the fourth power with increasing frequency for time-domain simulations. This is the underlying reason for the virtually complete dominance of GA in room acoustics.

In all interactive applications and many present-day room acoustic software as well, the process of sound propagation can be broken down into two distinct phases:

1. **Acoustic simulation:** During the simulation phase, acoustic impulse responses are computed based on the source location, listener location, and the scene. Recall that an impulse response is defined as the sound received at the listener, if an ideal Dirac delta impulse is played at the source and captures all the acoustic information for sound propagation from source to listener. Computing this impulse response is the most computationally challenging phase and can be based on any room acoustic simulation technique, geometric or numerical.
2. **Interactive Auralization:** During the auralization phase, the computed impulse response is convolved with the sound playing at the source to yield the final sound at the listener. This sound is then physically delivered through the sound card to speakers or headphones. Binaural processing is done by computing two impulse responses for the left and right ear. Multiple sources are handled by adding their individual contributions computed as above for both ears. It is desired that the sound sources and listener be able to move freely in the environment.

While many geometric techniques can work in real time at the cost of approximating geometric propagation to varying degrees, they face considerable computational and

theoretical challenges in handling diffraction and other wave effects, while ensuring sufficient efficiency. The advantage of these techniques is that since acoustic simulation is also performed in real time, they have the ability to handle dynamic scenes while maintaining a low memory footprint. However, as of today, the computational requirements can still be quite high, consuming all available CPU just for acoustic simulation. Depending on the application, this might or might not be desirable. For instance, games usually allocate roughly 10% CPU for *all* audio computation. On the other hand, while most numerical approaches do not work in real time, they offer the great benefit of capturing all wave phenomena.

My contribution in the area of sound propagation lies in both the parts described above – acoustic simulation and interactive auralization. I propose a novel, fast numerical simulator (ARD), that is much faster than existing techniques. For interactive auralization, I propose a novel scheme in which impulse responses are precomputed using ARD and then utilized in real time. To the best of my knowledge, there is no previous work that has shown a practical algorithm and system based on wave simulation, that can handle large, complex 3D scenes for moving sources and listener on desktop computers today.

The following discussion is organized into two main parts. First, I discuss acoustic simulation techniques, paying special emphasis on numerical techniques and comparing my ARD technique to the state of the art. For a general survey of room acoustic techniques, refer to Lauri Savioja’s thesis [86]. A more recent comparison and classification of techniques can be found in [94]. Second, I discuss my contributions in the context of interactive auralization and existent techniques and systems for handling moving sources and listener in 3D scenes.

2.2.1 Acoustic Simulation

In this sub-section, I describe the state of the art in simulation techniques for room acoustics. Special emphasis is placed on comparing my technique of Adaptive Rectangular Decomposition (ARD) with existing numerical methods in context of the application of the techniques to auralization.

Geometric Acoustics: GA assumes rectilinear propagation of sound waves, a valid approximation only if the wavelength is much smaller than the local feature size. Extensive research over the last few decades has resulted in techniques, as well as commercial software, apply geometric methods to room acoustic prediction. Historically, the first GA approaches that were investigated were Ray Tracing [50] and the Image Source Method [6]. Most room acoustics software for offline processing use a combination of these techniques to this day [78].

Beam tracing [33, 7] bundles rays into continuous beams, to compute their interaction with scene geometry. For *fixed* sources, a beam-tree is built for the scene in an offline processing step, and then used at run-time to render acoustic propagation paths to a moving listener. The method handles low-order specular reflections, scaling exponentially in the order of reflection, thus being infeasible for computing late reverberation. Diffraction can also be included, via the *geometric theory of diffraction* [108], but is applicable only for edges much larger than the wavelength. Motivated from Photon Mapping, there has been work on Phonon Tracing [8, 29] in acoustics. Also, researchers have proposed applying hierarchical radiosity to acoustical energy transfer [105, 42].

More recent work [18] on “Adaptive Frustum Tracing” supports moving sources in real-time without guaranteeing exact visibility, while allowing dynamic geometry with minimal precomputation. This method is quite compute-intensive, taking eight cores for performing its computation. Diffraction is disregarded, which was later added [101] by using the Biot-Tolstoy-Medwin (BTM) theory of diffraction [15]. BTM utilizes a

Huygens-Fresnel approach by expressing the diffracted field from an edge as a superimposition of elementary wavelets emitted all along the edge. For the purpose of computer simulation, diffraction edges are discretized, and the contribution integrated from each discrete edge element. Second-order diffraction must consider all pairs of elements and quickly becomes intractable for high-order diffraction where sound diffracts from multiple edges in sequence. Even finding all potential diffraction edges is computationally challenging in complex scenes.

Adding perceptually plausible diffraction is a significant challenge for all geometric approaches. Since geometric techniques are infinite-frequency approximations of the wave equation, they lead often to clicking or incoherent loudness fluctuation artifacts behind obstructions, as well as missing physical effects such as smooth lowering in volume on occlusions, unless diffraction is explicitly and carefully added. Diffraction effects are especially crucial at lower frequencies that have large wavelengths in the range of meters. Such diffraction-augmentation is an active area of research within geometric techniques and remains challenging, especially for complex scenes such as a furnished living room. Although BTM offers accurate solutions, it doesn't scale well for such complex scenes [15]. Older techniques, such as the Uniform/Geometric Theory of Diffraction have limited utility when edge sizes are similar to the wavelength [108], which is a very common occurrence in common room acoustic scenarios. One of the chief advantages of wave simulation over geometric methods is the ability to handle diffraction in such complex scenes with conceptual elegance, as well as without much degradation in efficiency – an empty room and a furnished room take nearly the same amount of computation with numerical approaches. Moreover, numerical approaches are *completely insensitive* to the order of scattering or diffraction being modeled.

Most interactive acoustic techniques explored to date are based on GA. This is mainly because although numerical approaches typically achieve better quality results, the computational demands have traditionally been out of the reach of most desktop

systems. With improving computational capabilities, improving techniques, and an increasing understanding of trade-offs on accuracy versus efficiency for numerical acoustic simulation, this situation is changing.

Numerical Acoustics: Numerical approaches solve the wave equation on a discrete representation of space and time. For example, in the Finite Difference Time Domain (FDTD) method to be discussed shortly, space is decomposed into cubical cells and the continuous pressure field approximated as the set of values at the centers of the cells¹. The discrete pressure field is stepped through time by turning the governing differential equation into a discrete time-stepping rule that relates the new values at all cell-centers in terms of the past values at all cell-centers. The errors are due to both spatial and temporal discretization. Spatial errors depend on the cell size, as well as the details of how the spatial derivative are expressed in terms of the values at the cell centers. Temporal error similarly depends on the time-step size, as well as how the temporal derivative operator is approximated.

Numerical approaches are insensitive to the shape complexity and polygon count of a scene and instead scale mainly with the following physical parameters – the scene volume, surface area, maximum simulated frequency and time-duration of simulation. The advantage of numerical approaches is that, given enough computation and memory, all wave phenomena can be captured, including diffraction and scattering in complex scenes.

Based on the particulars of how the discretization of a differential equation is performed and the resulting discrete equations solved, numerical approaches for acous-

¹This is an application of the method of *collocation* and is only one of many possible alternatives for expressing a continuous field as a set of discrete values. For example, one is not confined to sampling at the cell centers. A more general approach, used by most FEM (Finite Element Method) implementations, is to choose a finite-dimensional basis within the elements/cells and express the field as a linear combination of the basis vectors. The set of basis coefficients is the discrete set of values approximating the continuous field. I discuss the collocation approach described here solely for the purpose of conveying the basic idea of numerical approaches.

tics may be roughly classified into: Finite Element Method (FEM), Boundary Element Method (BEM), Digital Waveguide Mesh (DWM), Finite Difference Time Domain (FDTD) and Functional Transform Method (FTM). In the following, I briefly review each of these methods in turn. Many of these techniques, specifically FDTD, FEM and BEM, have evolved from solving partial differential equations in areas other than acoustics. All of them can be considered as general numerical techniques today. When applied to room acoustics, specific considerations arise, which will be the focus of the discussion in this section.

FEM and BEM have traditionally been employed mainly for the steady-state frequency domain response, as opposed to a full time-domain solution, with FEM applied mainly to interior and BEM to exterior scattering problems [48]. Interactive auralization requires a time-domain solution, which has been dominated almost completely by the FDTD method. The DWM method can be formally shown to be a subset of FDTD [45]. We still discuss DWM separately from FDTD because their historical roots are quite different.

For an extensive survey of FEM techniques for frequency-domain acoustics refer to [102]. FEM, in its usual formulation, works on a tetrahedral mesh. Generating skinny tetrahedra can cause instabilities for time-domain solutions and thus, generating a valid mesh is usually the most difficult part, reducing the usefulness of the fully automatic simulation that follows this step. Finite difference methods, in contrast, are usually implemented on a regular Cartesian mesh, making mesh-generation quite easy for arbitrary 3D structures and quite easy to ensure stability for a time-domain solution. When solving in frequency domain, instability problems are largely avoided by seeking a steady-state solution, rather the accuracy of the solution is degraded. Auralization requires time-domain impulse responses. Generating time-domain results from frequency-domain simulations requires solving a large number of problems corresponding to different frequencies. Although the overall asymptotic complexity in using such

an approach is the same as the FDTD method, the constant tends to be much larger. In summary, although there are no difficulties in principle in using FEM for time-domain acoustics, FDTD has seen far wider adoption for time-domain acoustics because of its relative ease of conceptual formulation and mesh generation, ensuring stability robustly.

BEM, in contrast to all other methods discussed here, only requires a discretization of the surface of the domain, and not its interior. This offers a great advantage for modeling the simulation domain with good accuracy. For a mathematical as well as historical treatment of BEM, refer to [19]. However, the ease of mesh generation comes at the cost of very adverse performance scaling because the resulting matrices are dense. The memory and performance scaling is at least the fourth power of the scene diameter, compared to third power as with FEM/FDTD approaches because the latter lead to sparse matrices for the volume of the scene. Intuitively, this is because all surface elements interact strongly with all others, for wave propagation. Moreover, when implemented for time-domain acoustics, BEM faces stability problems due to the use of retarded potentials, although there has been some promising work to address this problem recently [79]. The problem of adverse scaling for time-domain BEM still remains, though. Recent work on the fast multipole accelerated BEM (BEM-FMM) [38, 39] has shown very promising initial results showing that an asymptotic performance gain can be achieved for frequency domain solution of acoustic problems, yielding performance that scales linearly with the surface area of the scene (square of diameter), instead of its volume (cube of diameter), as is obtained with FEM/FDTD, which require a discretization of the volume of the scene. This is a very attractive option since it would allow handling structures much larger than possible with all other current approaches, at least beyond size large enough to hide the large constant of current BEM-FMM approaches [38]. Significant challenges remain for BEM-FMM because firstly, current implementations are quite complex, requiring separate treatment of low and high frequencies [39]. Secondly, it still remains to be shown that this technique can indeed give useful results on practical acoustic

scenes that tend to have complex shapes, and the actual performance of BEM-FMM depends considerably on how the parameters are chosen depending on the shape of the scene [38]. Assuming that all these problems can be addressed, applying this method for time-domain acoustics still requires a large number of frequency-domain simulations. While asymptotically better, a more practical approach is bound to be a re-formulation of the solution technique directly in time-domain. To the best of my knowledge, no such investigations have been undertaken yet. In summary, more research is required to make BEM-FMM method useful for 3D, frequency-domain room acoustics. Beyond that, time-domain formulations of BEM-FMM would conceivably need to be developed.

DWM (Digital Waveguide Mesh) approaches [114, 87, 86, 45, 62], on the other hand, are specific to the Wave Equation and have their roots in musical synthesis, specifically, digital waveguides. Digital waveguides are used to model essentially 1D domains that support wave propagation, such as a string of a guitar. The wave equation can be solved analytically (D'Alembert's solution) in such cases and consists of propagating solutions in opposite directions along the length of the waveguide. This formulation can be implemented very efficiently, allowing for digital sound synthesis of musical instruments at very high computational speeds. Digital waveguide meshes are a generalization of digital waveguides to 3D. The domain is expressed as a mesh of discrete waveguides that carry waves along their length. Multiple waveguides connect at nodes called *scattering junctions*. Application of conservation laws at the scattering junctions ensures correct propagation of waves along the waveguide mesh as the mesh resolution is increased without bound. One of the main problems of this method is direction and frequency-dependent dispersion, which means that sound does not propagate with the same numerical speed for all frequencies and for all directions. So, for instance, a pulse radiated by a point source will not be spherical spatially, and additionally, the temporal signal received at a point will no longer have the same shape as at the source because different constituent frequencies in the signal did not travel with the same speed. Sig-

nificant improvements have been made by using a combination of interpolation and frequency warping [89]. For a recent survey of DWM techniques, refer to [62]. For a discussion of DWM as a general numerical method, refer to the book by Bilbao [9]. In [45], it is shown that DWM is equivalent to the well-known finite difference method, which I describe next.

The FDTD method, owing to its simplicity and versatility, has been an active area of research in room acoustics for more than a decade [88, 12, 13]. Originally proposed for electromagnetic simulations [116], FDTD works on a uniform grid and solves for the field values at each cell over time. It is a well-established technique in electromagnetic propagation. Taflove’s work [99] is a good textbook and reference and discusses the vast range of electromagnetic applications FDTD has seen over the last few decades. For a dated but thorough review of FDTD’s rise, refer to [93]. Initial investigations into FDTD for acoustics were hampered by the lack of computational power and memory, limiting its application to mostly small scenes in 2D. It is only recently that the possibility of applying FDTD to medium sized scenes in 3D has been explored [84, 82, 85]. Even then, the computational and memory requirements for FDTD are beyond the capability of most desktop systems today [82], requiring days of computation on a small cluster for medium-sized 3D scenes for simulating frequencies up to 1 kHz. I have been able to reduce this number to minutes with the ARD (Adaptive Rectangle Decomposition) technique I have developed.

In some very recent work, Savioja [90] has shown that by using the Interpolated WideBand (IWB) FDTD scheme mentioned in [49] and parallelizing it efficiently on modern Graphics Processing Units (GPUs), one can obtain real time performance for numerical simulation on 3D scenes with dimensions similar to a concert hall for frequencies till nearly 500 Hz. However, the numerical dispersion error tolerance is kept quite high and it is still under investigation whether good quality auralizations can be achieved on complex scenes with this technique. Also, the technique as described au-

realizes sounds directly from source to listener without computing impulse responses as an intermediate step. The advantage of such a strategy is that an effectively unlimited number of (moving) sources can be handled without much impact on efficiency, since no digital signal processing is required. The disadvantage is that if the source sound signal changes, the whole computation has to be repeated. Thus, for larger scenes and/or higher frequencies where such a technique won't be real-time and computing impulse responses is thus the most viable alternative, this technique might not be applicable, as useful impulse responses are hard to compute due to the presence of significant numerical dispersion. The ARD technique I have proposed in my work avoids dispersion errors to a large extent, and has been demonstrated to generate useful impulse responses on complex 3D scenes that can be used in an interactive auralization system for all-frequency auralizations and thus seems to be the best alternative for such cases. With proper optimizations, ARD might even be extensible to become real-time for smaller scenes and frequencies near 500 Hz.

In summary, at present, real-time FDTD as proposed in [90] solves a different set of practical problems than ARD that I have proposed. ARD is more applicable for large scenes at kilohertz frequencies, for which impulse responses need to be computed. Of course, both approaches are applicable, in principle, in each other's domain. Detailed listening tests while carefully varying error tolerances need to be performed to address the question of the error tolerances required in [90] to yield useful auralizations.

Domain Decomposition Method (DDM): It is typical in numerical methods to partition the simulation domain into many partitions to gain performance by parallelizing over multiple cores, processors, or machines. Such approaches are called Domain Decomposition Methods (DDM) and have widespread applications in all areas where numerical solution to partial differential equations is required. DDM has interesting parallels to my work on ARD, which I discuss in detail in Section 4.2.3. For a brief history of DDM and its applications, I refer the reader to the survey [22]. For an in-depth

discussion of DDM, the reader is referred to the books [67, 104]. Also, the website [1] has many references to current work in the area.

Functional Transform Method (FTM): Another method which is related to my work, although in a different mathematical framework, is the Functional Transform Method (FTM) [65, 68], which takes a signal-processing based approach for modeling sound propagation in spaces.

Pseudo-spectral techniques are a class of very high order numerical schemes in which the global field is expressed in terms of global basis functions. Typically, the basis set is chosen to be the Fourier or Chebyshev polynomials [14] as fast, memory efficient transforms are available to transform to these bases from physical space and vice versa by using the Fast Fourier Transform (FFT). My ARD method may also be regarded, to some degree, as a pseudo-spectral technique, although there is an important difference which will be discussed shortly. The closest pseudo-spectral technique to ARD is the Fourier Pseudo-Spectral Time Domain (PSTD) method proposed by Liu [54]. PSTD is generally considered to be a viable alternative to FDTD to control its numerical dispersion artifacts [99, chapter 17]. PSTD uses a coarse spatial sampling of the field, uses an FFT to project the sampled values at all points into spectral domain, differentiates in Fourier space analytically, and then performs an inverse FFT to project the differentiated field back to the spatial domain. Assuming proper treatment at the boundaries, infinite-order accuracy can be achieved. This approach allows meshes with points per wavelength approaching two, the Nyquist limit, while still controlling numerical dispersion to a large degree. My ARD technique is quite similar to PSTD in that it allows spectral accuracy and thus, a similarly coarse mesh, while calculating the spatial derivatives. The crucial difference lies in how temporal derivatives are handled. PSTD uses a second-order accurate explicit time-stepping scheme. This means that numerical dispersion error is reduced compared to a standard FDTD scheme, but still present. With ARD, by assuming rectangular shape for the partitions with sound-hard walls,

the temporal derivative errors can be reduced substantially by using the known analytical solution to the wave equation for propagation within the rectangular partitions. Thus, numerical dispersion is absent with ARD for propagation within each rectangular partition. Some dispersive error is still introduced for waves propagating across partition interfaces, but this error is much smaller than with FDTD or PSTD, where waves accumulate dispersive errors of similar magnitude at each cell.

2.2.2 Auralization

The process of interactive auralization usually has two important components: acoustic simulation for computing impulse responses, and convolution of impulse responses with the input sound signal at the source to generate the sound to be delivered to the user's ears (eg., using headphones). There are many real-time auralization techniques and systems in existence, but they use geometric techniques almost exclusively. For most such systems, the acoustic simulation to compute the impulse responses is also performed at runtime. My technique uses an offline, wave-based acoustic simulation. The focus of the discussion here will be on prior auralization systems and related techniques.

A thorough overview of the complete problem of auralization is given in [91]. For an overview of interactive auralization for virtual environments, please refer to the text by Vorlander [115]. A discussion on a recent auralization system with emphasis on integration of all required components of an auralization system – room acoustic modeling, moving sources, listener and delivering binaural audio using dynamic cross-talk cancellation over speakers, is discussed in the work by Lentz et. al. [52].

A real-time auralization system, called DIVA, based on image sources was first introduced by Savioja [86] and later improved by Lokki [55]. It can handle moving sources and listener, and uses an image-source technique for auralizing early reflections. Late reverberation is generated statistically and matched to the early reflections to ensure a realistic impulse response. Image source methods face considerable difficulty in the

presence of complex geometry. Moreover, handling higher order reflections with image source methods results in an exponential scaling in computational requirements. A combination of these two cases (high-order reflections in a complex scene) leads to an explosive, unmanageable growth of the number of image sources. Furthermore, integrating diffraction with image source methods causes further difficulties, although attempts have been made in literature which work for simple geometries [103]. The DIVA system can be very useful and efficient when the scene geometry is simple and the early reflections consist mainly of very low order interactions.

The beam tracing system developed by Funkhouser, Tsingos, and colleagues [33] can handle static sound sources and moving listener in densely occluded architectural environments with simple, flat-walled geometry. Given the current position of the listener, corresponding ray paths that reach from the source to listener can be quickly evaluated using the precomputed beam tree. As the listener moves, correct interpolation of impulse responses is obtained naturally by re-evaluating the ray paths and their corresponding strengths and delays.

A very recent fast ray-tracing based framework developed by Chandak and Taylor et. al. [18, 101] allows for practical interactive auralization on complex environments. It improves upon the beam tracing work by allowing both moving sources and listener, and also allowing dynamic geometry in 3D scenes with complex geometry, along with diffuse reflections and diffraction based on the recent Biot-Tolstoy-Medwin (BTM) theory of diffraction [15]. Thus, in terms of the number of acoustically important physical phenomena captured, this system is one of the most complete geometric auralization systems known. Current work is ongoing to incorporate all features robustly and automatically, while ensuring that diffraction and diffusion approximations are performed so that real-time execution is maintained, while ensuring plausibly realistic auralization.

A few systems have been proposed that, although not complete auralization systems, offer interesting parallels to my work. For these applications, the wave equation

in frequency domain is employed, known as the Helmholtz equation. A technique was proposed in [43] that has been designed to capture the frequency-dependent directional distribution of sound emitted by an object in real time. This technique relies on a full BEM-based numerical simulation which is performed offline at the object’s modal frequencies, and is then used in real time for generating sounds at the listener, depending on his relative direction to the object. Thus, the basic theme of offline numerical simulation combined with real-time auralization is similar to my work, although the application is quite different – rendering sounds at select frequencies from an impulsively struck, precomputed sounding object. In contrast to propagating arbitrary, broadband sounds between moving sources and a receiver inside a precomputed 3D scene. My approach assumes sources are monopole (point sources), but it could easily be extended to handle multiple monopole and dipole sources, thus allowing for an integration with this technique.

The problem of sound emission from complex-shaped objects is closely related to the problem of scattering of sound from surfaces. A real-time technique for sound scattering was proposed by Tsingos et. al. in [107], where it was shown that by using the Kirchoff Approximation combined with a boundary-element formulation, real-time performance can be obtained on modern Graphics Processing Units (GPUs). However, this work is useful only for first-order scattering effects, while neglecting intra-object diffraction and time-domain effects such as propagation delay. In general, solutions based on the Helmholtz equation are efficient for simulating at one or a few frequencies, but become much less efficient than time-domain solvers for capturing transient, broadband information, as is required for full room acoustics.

Precomputed methods for interactive auralization I now specifically focus and discuss methods in literature that have offered a combination of offline precomputation of impulse responses, followed by real-time auralization, as in my thesis work.

In [66], Pope et. al. propose sampling impulse responses on a dense grid which are later utilized for convolution and auralization. However they do not describe how moving sources might be handled, nor how to represent or interpolate impulse responses for handling the moving listener. Thus, although similar in the basic idea, their work doesn't cover all the important aspects that are required to make such a scheme feasible, such as, in addition to the above factors, the ability to express the impulse responses compactly.

In [106], Tsingos et. al. use an approximate image-source based method for providing rough correspondence to the actual acoustics in game environments. The user manually specifies rooms in the scene and a few salient source locations per room. Image source locations and their gradients with respect to motion of the actual source, are computed and stored. Since image-source method is employed, the scene can't have complex geometry. Diffraction is ignored. Spatial variation in the impulse responses are captured by the location gradients of the image sources. At runtime, the early reflection component is approximated using globally computed image sources from the sampled locations. The overall approach is well-suited for scenes with large, specular reflectors but insufficient for handling spatially detailed acoustic effects that I target, such as diffracted shadowing behind walls or focusing/diffraction/scattering effects off complex geometry.

ER/LR separation In my technique, a separation of early reflections (ER) and late reverberation (LR) is performed based on echo density. Other approaches have also proposed similar ideas. LR effects are typically specified through *artificial reverberation*, based on IIR (Infinite Impulse Response) filters whose parameters (e.g. exponential decay time and peak density) are hand-tuned to match scene geometry. Based on a well-known idea presented in [34], earlier work presented in [58] separate the ER and LR using echo density as my technique also does, but handle the LR with artificial

reverberation. Recent geometric techniques use ray-tracing to explicitly compute the LR from geometry [96, 106]. However, the former does not account for the ER at all while the latter segments based on a user-specified number of initial wavefronts arriving at the receiver. My approach automatically computes and segments both the ER and LR using a wave-based simulation on the scene geometry – the LR is sampled sparsely, while the ER is sampled densely in space.

Peak detection Peak detection is proposed in [28] to encode a single acoustic response with the goal of accelerating run-time convolution of input signals during playback of MPEG streams. Neither spatial interpolation nor compactness is a concern. My method for impulse response encoding also employs peak detection but it differs substantially: it resolves peaks possibly merged by the bandlimited simulation to recover individual peaks; [28] segments the input impulse response into a sparse (~ 10) set of coalesced “peaks” and computes detailed spectral properties for each in 64 frequency sub-bands. This method requires at least $10\times$ more memory than my approach.

Impulse response interpolation Dynamic Time Warping (DTW) [56] finds correlations between two signals of lengths N and M in $O(NM)$ time and could be used to interpolate simulated acoustic responses in my approach. However, my representation is based on sparse peaks which can be correlated and interpolated much more efficiently while being at least an order of magnitude faster than DTW.

In summary, I have developed a novel numerical simulator (ARD) as well as a novel wave-based interactive auralization system that is capable of auralizing moving sources and listener in large, complex 3D scenes. To the best of my knowledge, no known auralization systems can generate auralizations based on kilohertz-range wave simulation on 3D scenes of sizes and shape complexity that I demonstrate, and capture the realistic acoustic effects that I discuss in Chapter 5, in a single, integrated system and corresponding set of techniques.

Chapter 3

Interactive Sound Synthesis

In this chapter, I discuss my work on designing a real-time system and associated perceptual acceleration techniques that allows for an interactive simulation of hundreds of sounding objects undergoing impacts and rolling, while producing realistic sounds. The rest of this chapter is organized as follows – In the next section I describe the overall methodology and the underlying mathematical framework of my approach. After that, I discuss the novel perceptually-based acceleration methods I have designed that allow for this system to deliver high performance, while gracefully adapting to variable time constraints in an interactive system. Following this, I discuss the results obtained with my approach and conclude with a summary of my contributions and a discussion of future work in the area of sound synthesis.

3.1 Methodology

Sound is produced by surface vibrations of an elastic object under an external impulse. These vibrations disturb the surrounding medium to result in a pressure wave which travels outwards from the object. If the frequency of this pressure wave is within the range 20 to 22000 Hz, it is sensed by the ear to give us the subjective perception of sound. The most accurate method for modeling these surface vibrations is to directly apply classical mechanics to the problem, while treating the object as a continuous

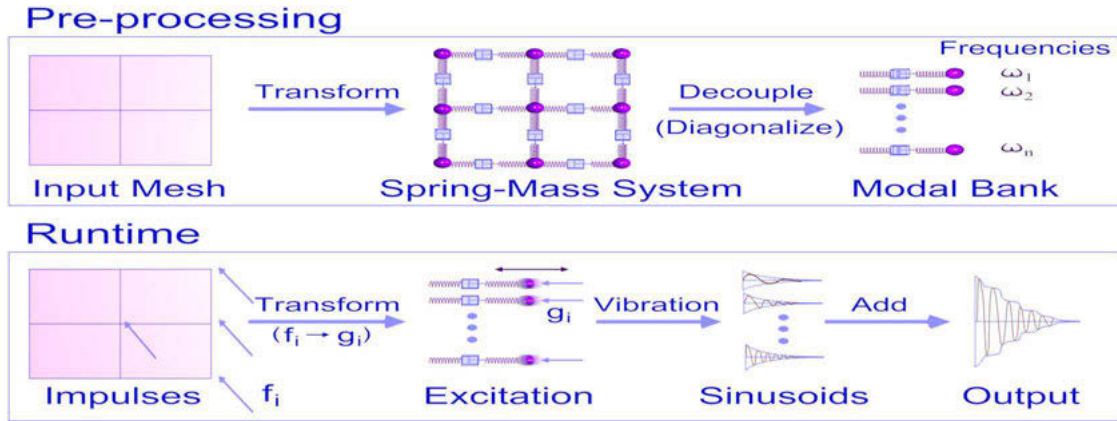


Figure 3.1: This diagram gives an overview of my sound-synthesis approach.

(as opposed to discrete) entity. This results in PDEs for which analytical solutions are not known for arbitrary shapes. Thus, the only avenue left is to make suitable discrete approximations of the problem to reduce the PDEs to ODEs, which are more amenable to analysis. In this section, I show how a spring-mass system corresponding to a physical object may be constructed to model its surface deformation and how it may be analyzed to extract the object's modes of vibration. For ease of illustration, I assume a homogeneous object; inhomogeneous objects may be handled by a simple extension of the approach presented here. Further, I assume that the input object is in the form of a thin shell and is hollow inside. This assumption is motivated by practical concerns since most of the geometry today is modeled for rendering and is invariably only a surface representation with no guarantees on surface connectivity. If a volumetric model is available, the approach outlined here applies with minor modifications. Figure 3.1 gives an overview of our approach. In the pre-processing step, each input surface mesh is converted to a spring-mass system by replacing the mesh vertices with point masses and the edges with springs, and the force matrices are diagonalized to yield its characteristic mode frequencies and damping parameters. At runtime, the rigid-body simulator reports the force impulses f_i on a collision event. These are transformed into the mode gains, g_i with which the corresponding modes are excited. These yield damped

sinusoids which are suitably combined to yield the output sound signal.

3.1.1 Input Processing

Given an input mesh consisting of vertices and edges, an equivalent spring-mass system is constructed by replacing the mesh vertices with point masses and the edges with damped springs. I now discuss how to assign the spring constants and masses based on the material properties of the object so that the discrete system closely approximates the physical object. The spring constant, k and the particle masses, m_i are given by:

$$\begin{aligned}k &= Yt \\ m_i &= \rho t a_i\end{aligned}\tag{3.1}$$

where Y is the Young's Modulus of elasticity for the material, t is the thickness of the object surface, ρ is the material density and a_i is the area "covered" by a particle, which is calculated by dividing the area of each mesh face equally amongst all its constituent vertices and summing all the face contributions for the vertex corresponding to the mass in consideration. Note that I did not discuss fixing the spring damping parameters above, which I will return to shortly.

3.1.2 Deformation Modeling

Once the particle system has been constructed as above, we need to solve its equation of motion in order to generate the corresponding sound. Unfortunately, the resulting system of equations is still mathematically complex because the interaction forces between the masses are non-linear in their positions. However, by making the reasonable assumption that the deformation is small and linearizing about the rest positions, this

problem can be cast in the form of a coupled linear system of ODEs:

$$M \frac{d^2 r}{dt^2} + (\gamma M + \eta K) \frac{dr}{dt} + Kr = f \quad (3.2)$$

where M is the mass matrix, K is the elastic force matrix, γ and η are the fluid and viscoelastic damping constants for the material respectively. The matrix M is diagonal with entries on the diagonal corresponding to the particle masses, m_i . The elastic force matrix K is real symmetric, with entries relating two particles if and only if they are connected by a spring. The variable r is the displacement vector of the particles with respect to their rest position and f is the force vector. Intuitively, the terms in the above equation correspond to inertia, damping, elasticity and external force respectively. The specific form of damping used above, which expresses the overall damping matrix as a linear combination of K and M is known as Raleigh damping and works well in practice. For a system with N particles in three dimensional space, the dimensions of all the matrices above is $3N \times 3N$.

This formulation of the problem is well known and is similar to the one presented in [64]. The main difference in our approach is that the force and inertia matrices are assembled from a spring-mass system which makes the formulation much simpler. The solution to Equation (3.2) can be obtained by diagonalizing K so that:

$$K = GDG^{-1} \quad (3.3)$$

where G is a real matrix consisting of the eigenvectors of K and D is a diagonal matrix containing the eigenvalues. For reasons I will explain later, I will henceforth call G the “gain matrix”. Plugging the above expression for K into Equation (3.2) and multiplying by G^{-1} throughout, we obtain:

$$G^{-1}M \frac{d^2 r}{dt^2} + (\gamma G^{-1}M + \eta DG^{-1}) \frac{dr}{dt} + DG^{-1}r = f \quad (3.4)$$

Observing that since M is diagonal, $G^{-1}M = MG^{-1}$ and defining $z = G^{-1}r$ equation(3.4) may be expressed as:

$$M \frac{d^2 z}{dt^2} + (\gamma M + \eta D) \frac{dz}{dt} + Dz = G^{-1} f \quad (3.5)$$

Since both M and D in the above equation are diagonal, Equation (3.2) has been decoupled into a set of unrelated differential equations in the variables z_i , which correspond to individual modes of vibration of the object. The equation for each mode is the standard equation of a damped oscillator and has the following solution for the i 'th mode:

$$\begin{aligned} z_i(t) &= c_i e^{\omega_i^+ t} + \bar{c}_i e^{\omega_i^- t} \\ \omega_i^\pm &= \frac{-(\gamma \lambda_i + \eta) \pm \sqrt{(\gamma \lambda_i + \eta)^2 - 4 \lambda_i}}{2} \end{aligned} \quad (3.6)$$

where the constant c_i , called the gain for the mode, is found by considering the impulses applied as I will discuss shortly. I use \bar{c}_i to denote the complex conjugate of c_i . The constant λ_i is the i 'th eigenvalue in the diagonal matrix, D . The real part of ω_i^\pm gives the damping coefficient for the mode, while the imaginary part, if any, gives the angular frequency of the mode.

3.1.3 Handling Impulsive Forces

Once an input mesh has been processed as above and the corresponding modes extracted as outlined in Equations (3.2)-(3.6), we have all the information needed regarding the aural properties of the object. The sound produced by an object is governed by the magnitude and location of impulsive force on its surface. Short-duration impulsive contacts are modeled by dirac-delta functions. Given an impulse vector f containing the impulses applied to each vertex of an object, we compute the transformed impulse, $g = G^{-1}f$ in order to evaluate the right-hand side of Equation (3.5). Once this is done,

the equation for the i 'th mode is given by:

$$m_i \frac{d^2 z_i}{dt^2} + (\gamma m_i + \eta \lambda_i) \frac{dz_i}{dt} + \lambda_i z_i = g_i \delta(t - t_0) \quad (3.7)$$

where t_0 is the time of collision and $\delta()$ is the dirac delta function. Integrating the above equation from a time just before t_0 to a time just after t_0 and noting that $\int_{t_0^-}^{t_0^+} \delta(t - t_0) dt = 1$, we obtain:

$$m_i \Delta \left(\frac{dz_i}{dt} \right) + (\gamma m_i + \eta \lambda_i) \Delta z_i + z_i \Delta t = g_i \quad (3.8)$$

Assuming that Δt is very small, and using the fact that the deformation is small compared to the change in velocities, one can neglect the last two terms on the left-hand side to obtain:

$$\Delta \left(\frac{dz_i}{dt} \right) = \frac{g_i}{m_i} \quad (3.9)$$

The above gives a very simple rule which relates the change in the time derivative of the mode to the transformed impulse. Referring to Equation (3.6) and requiring that z_i should stay the same just before and after the collision while $\frac{dz_i}{dt}$ should increase as in Equation (3.9), the update rule for the mode gain c_i can be shown to be:

$$c_i \leftarrow c_i + \frac{g_i}{m_i (\omega_i^+ - \omega_i^-) e^{\omega_i^+ t_0}} \quad (3.10)$$

Initially, c_i is set to 0 for all modes.

3.2 Real-time Sound Synthesis

In this section, I describe how the mathematical formulation presented in the previous section is utilized to efficiently generate sound in real time. First, I describe a naive implementation and then discuss techniques to increase its efficiency.

Assume that there exists a rigid-body simulator which can handle all the dynamics. During a collision event, the sound system is informed of the object that undergoes

the impact and the magnitude and location of impact. This impact is processed as described in Section 3.1.3 to result in the gains for the different modes of vibration of the object, where the gain for the i 'th mode being c_i . The equation for a mode from the time of collision onwards is given by (3.6). The amplitude contribution of a mode at any moment is proportional¹ to its *velocity* (and not position). This is because the pressure contribution of a particle is determined by its velocity and the mode velocities are linearly related to the physical velocities of the particles. The mode velocity is found by taking a differential of Equation (3.6) with respect to time:

$$v_i = \frac{dz_i}{dt} = c_i \omega_i^+ e^{\omega_i^+ t} + \bar{c}_i \omega_i^- e^{\omega_i^- t} \quad (3.11)$$

For generating each audio sample, we need to evaluate the above equation for all vibration modes of the object, which is quite inefficient. As mentioned in [64], the simple observation that $e^{i\omega(t+\Delta t)} = e^{i\omega t} e^{i\omega \Delta t}$ offers some gain in performance since generating a new audio sample just requires a single complex multiply with the previous value. However, the efficiency is still not sufficient to handle a large number of objects in real time. We may estimate the running time of the system as follows: A simple spring-mass system with N particles has $3N$ modes, and the above operation needs to be repeated for each mode for each audio sample. Assuming a sampling rate of 44100 Hz, the number of floating-point operations (FLOPS) needed for this calculation for generating audio samples worth t seconds is:

$$T = 3N \times 4 \times 44100t \text{ FLOPS} . \quad (3.12)$$

Considering that the typical value of N is about 5000 or higher, producing sound worth

¹The constant of proportionality is determined based on the geometry of the object and takes the fact into account that vibrations in the direction of the surface normal contribute more to the resulting pressure wave than vibrations perpendicular to the normal. I do not describe it in detail here as it is not critical to the approach being presented.

1 second would take 2646 MFLOPS. Since today’s fastest desktop processors operate at a few thousand MFLOPS [25], the above processing would take about a second. Given that this estimated amount of time is for just one object and a typical scene may contain many such objects, such an approach is clearly not fast enough for interactive applications. Furthermore, for many real-time environments such as games and virtual environments, only a very small fraction of the actual time can be allocated for sound production. Thus, in the rest of this section, I will discuss techniques to increase the efficiency of the proposed base system to enhance its capability in handling scenarios with a large number of sounding objects at interactive rates.

From Equation (3.12), it is clear that the running time is proportional to the number of modes being mixed and the number of objects. Next, I present acceleration techniques for sound simulation by reducing the number of modes per object: “Mode Compression” and “Mode Truncation”, and by scaling the audio quality of different objects dynamically with little degradation in perceived sound quality.

3.2.1 Mode Compression

Humans have a limited range of frequency perception, ranging from 20 to 22000 Hz. It immediately follows that modes with frequencies lying outside this range can be clipped out and need not be mixed. However, there is another important fact which can lead to large reductions in the number of modes to be mixed. A perceptual study described in [92] shows that humans have a limited capacity to discriminate between nearby frequencies. Note that this is different from frequency masking [119] in which one of two *simultaneously* played frequencies masks out the other. Rather, this result reports that even if two “close enough” frequencies are played in succession, the listener is unable to tell whether they were two different frequencies or the same frequency played out twice. The authors call the length of the interval of frequencies around a center frequency which sound the same, the “Difference Limens to Change” (DLC).

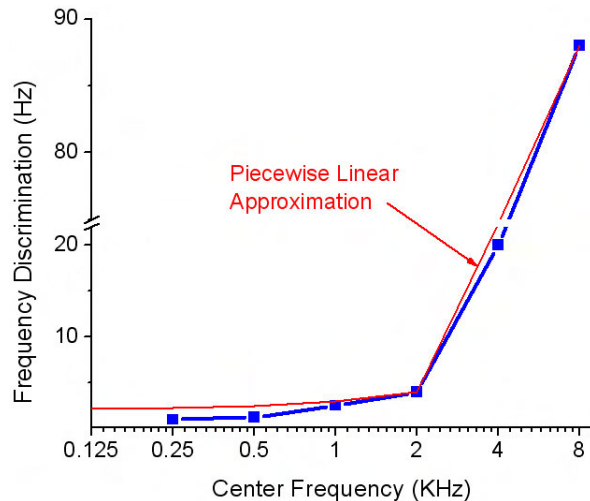


Figure 3.2: This plot shows frequency discrimination in humans as a function of the center frequency. Note that the human capacity to discriminate between frequencies degrades considerably for frequencies in the range 2-22 KHz, which forms a bulk of the human audible range. I use this fact to guarantee that no more than 1000 modes need to be mixed for any object in the worst case, *irrespective* of its geometric complexity. In most cases the actual number is much smaller, in the range of a few hundreds. The red curve shows the piecewise linear approximation of this curve that my technique uses.

Figure 3.2 shows a plot of the DLC against center frequencies ranging from .25 to 8 KHz. Interestingly, the DLC shows a large variation over the audible frequency range, getting very large as the center frequency goes beyond 2 KHz. Even at 2 KHz, the DLC is more than 1 Hz. That is, a human subject cannot tell apart 1999 Hz from 2000 Hz.

I exploit the above fact to drastically reduce the number of modes that are mixed for an object. The DLC curve is approximated with a piecewise linear curve shown as the red line in Figure 3.2. The approximation has two segments: one from 20 Hz to 2 KHz and another from 2 KHz to 22 KHz. As I show in the figure, the DLC is slightly overestimated. This increases the performance further and I have observed minimal loss in quality in all the cases I have tested. The main idea behind our compression scheme is to group together all the modes with perceptually indistinguishable frequencies. It can be easily shown that if the above mentioned linear approximation to the DLC curve is used and indistinguishable modes clustered at the corresponding frequency centers,

the maximum number of modes that need to be mixed is less than 1000. It is important to note that this is just the worst case scenario and it happens only when the frequency spectrum of the object consists of all frequencies from 20 to 22,000 Hz, which is very rare. For most objects, the frequency spectrum is discrete and consequently, the number of modes after mode compression is much smaller than 1000, typically in the range of a few hundreds.

I now describe the details of my technique. Recall the gain matrix from Equation (3.3), G . The gain matrix has a very simple physical interpretation: Rows of the matrix correspond to vertices of the object and columns correspond to the different modes of vibration (with their corresponding frequencies). Each row of G lists the gains for the various modes of vibration of the object, when a unit impulse is applied on the corresponding vertex. It is clear from the above discussion that all the mode gains within a row of G which correspond to modes with close frequencies need to be clustered together. This is achieved by replacing the gain entries for all such modes by a single entry with gain equal to the sum of the constituent gains. Since a mode corresponds to a whole column, this reduces to summing together columns element-wise based on their frequencies. The complete procedure is as follows:

- Sort the columns of G with the corresponding mode frequencies as the key. ²
- Traverse the modes in increasing order of frequency. Estimate the DLC, Δ at the current frequency using the piecewise linear curve shown in Figure 3.2. If the current frequency and next frequency are within Δ of each other the two mode frequencies are indistinguishable, replace the two columns by their element-wise sum.

Below, I enumerate the main advantages of this scheme:

²This step is usually not needed as most linear algebra packages output the eigenvector matrix sorted on the eigenvalues

1. The running time is constant instead of linear in the number of vertices in the object. For example, if the input mesh is complex with 5,000 vertices, the number of modes mixed is bounded by 1000 instead of the earlier $3N = 15,000$ which is a substantial performance gain.
2. Since this scheme requires just the frequencies of the different modes, the whole processing can be done as a pre-process without requiring any extra runtime CPU cycles.
3. From the above mentioned procedure, it is clear that the number of columns in the matrix G , which is the same as the number of modes, is now bounded by 1000 instead of the earlier value of $3N$. Since this matrix needs to be present in memory at runtime for transforming impulses to mode gains, its memory consumption is an important issue. Using this technique, for an object with 5000 vertices, the memory requirement has been reduced from 225 MB to less than 15 MB, by more than a factor of 15.
4. Most objects have a discrete frequency spectrum with possibly many degenerate frequencies. Due to numerical inaccuracies while diagonalizing the elastic force matrix and the approximations introduced by the spring-mass discretization, these degenerate frequencies may appear as spurious distinct modes with near-equal frequencies. Obviously, it is wasteful to treat these as distinct modes. It is our observation that most of the times these modes' frequencies are close enough so that they are naturally summed together in this scheme.

3.2.2 Mode Truncation

The sound of a typical object on being struck consists of a transient response composed of a blend of high frequencies, followed by a set of lower frequencies with low amplitude.

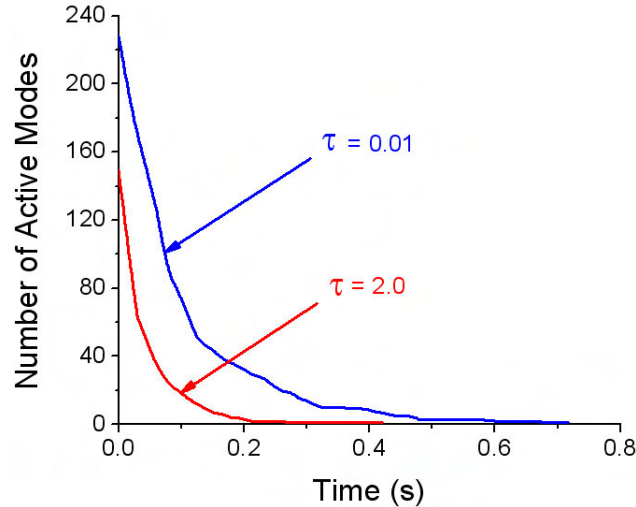


Figure 3.3: This graph shows the number of modes mixed vs time, for a xylophone bar just after it is struck in the middle. τ is the mode truncation threshold. A higher value of τ leads to more aggressive truncation of modes with low amplitude, leading to savings in terms of the number of modes mixed. In this case, $\tau = 2.0$ results in about 30% gain in efficiency over $\tau = 0.01$ which only truncates modes with near-zero amplitude. The sound quality for both the cases is nearly identical.

The transient attack is essential to the quality of sound as it is perceived as the characteristic “timbre” of the object. The idea behind mode truncation is to stop mixing a mode as soon as its contribution to the total sound falls below a certain preset threshold, τ . Since mode truncation preserves the initial transient response of the object when τ is suitably set, the resulting degradation in quality is minimal. Figure 3.3 shows a plot of the number of active modes with respect to time for a xylophone bar struck in the middle for two different values of τ : .01 and 2. These values are normalized with respect to the maximum sample value which is 65536 for 16-bit audio. The first case with $\tau = .01$ performs essentially no truncation, only deactivating those modes which have near-zero amplitude. Note that with $\tau = 2$ the number of modes mixed is reduced by more than 30%. Also, the number of active modes floors off much earlier (.2 secs compared to .6 secs). It is important to note that this results in little perceptible loss in quality.

The details of the technique are as follows: Assume that an object has just un-

dergone a collision and the resulting mode gains c_i have been calculated as given by Equation (3.10). From this time onwards until the object undergoes another collision, Equation (3.11) gives a closed-form expression for the mode’s contribution to the sound of the object. This can be used to predict exactly when the mode’s contribution drops below the threshold τ . The required “cutoff time”, t_i^c is such that for all times $t > t_i^c$:

$$c_i \omega_i^+ e^{\omega_i^+ t} + \bar{c}_i \omega_i^- e^{\omega_i^- t} < \tau \quad (3.13)$$

Using the fact that for any two complex numbers x and y , $|x + y| \leq |x| + |y|$ it can be shown that,

$$t_i^c \leq \frac{1}{-Re(\omega_i^+)} \ln \left(\frac{2 |c_i| |\omega_i^+|}{\tau} \right) \quad (3.14)$$

Using the above inequality, the cutoff times are calculated for all the modes just after a collision happens. While generating the sound samples from a mode, only one floating point comparison is needed to test if the current time exceeds the cutoff time for the mode. In case it does, the mode’s contribution lies below τ and consequently, it is not evaluated.

3.2.3 Quality Scaling

The two techniques discussed above are aimed at increasing the efficiency of sound synthesis for a single object. However, when the number of sounding objects in a scene grows beyond a few tens, this approach is not efficient enough to work in real time and it is not possible to output the sound for all the objects at the highest quality. It is critical in most interactive applications that the sound system have a graceful way of varying quality in response to variable time constraints. My technique achieves this flexibility by scaling the sound quality for the objects. The sound quality of an object is changed by controlling the number of modes being mixed for synthesizing its sound. In most cases of scenes with many sounding objects, the user’s attention is on the objects

in the “foreground”, that is, the objects which contribute the most to the total sound in terms of amplitude. Therefore, if it is ensured that the foreground sounds are mixed at high quality while the background sounds are mixed at a relatively lower quality, the resulting degradation in perceived aural quality should be reduced.

I use a simple scheme to ensure higher quality for the foreground sounds. At the end of each video frame, the sum of the vibrational amplitudes of all modes for each object are stored, which serve to determine the object’s priority. At the next video frame, all objects are sorted in decreasing order based on their priority and the total time-quota for sound-generation divided among the objects as a linearly decreasing ramp with a preset slope, S . After this, all objects are processed in their priority order. For each object, its quality is first scaled so that it can finish within its assigned time-quota and then the required modes are mixed for the given time period. If an object finishes before its time-quota has expired, the surplus is consumed greedily by the next higher priority object. The slope, S of the ramp decides the degree to which the foreground sound quality is favored over a degradation in background sound quality. The case with $S = 0$ corresponds to no priority scheduling at all, with the time-quota being divided equally among all objects. The converse case with $S = \infty$ corresponds to greedy consumption of the time-quota. That is, the whole time-quota is assigned to the highest priority object. After the object is done, the remaining time, if any, is assigned to the next highest priority object and so on.

3.2.4 Putting Everything Together

To illustrate how all the techniques described above are integrated, I present a summary of my approach.

Pre-processing

- Construct a spring-mass system corresponding to the input mesh. (Section [3.1.1](#))

- Process the spring-mass system to extract the gain matrix, G and the (complex) angular frequencies of the object's modes of vibration: ω_i^+ and ω_i^- . (Section 3.1.2, Eqns. (3.3) and (3.6))
- **Mode Compression:**
Aggregate columns of G based on frequencies of the corresponding modes, as described in Section 3.2.1.
- Store the resulting gain matrix along with the (complex) constants ω_i^+ and ω_i^- for modes correspond to the columns of G after compression. Note that ω_i^- need not be stored in case ω_i^+ has a non-zero imaginary part since in that case $\omega_i^- = \overline{\omega_i^+}$.

Runtime Processing

- Load the gain matrix and mode data for each object.
- Begin simulation loop:
 1. Run rigid-body simulation
 2. For each object, O :
 - **Collision Handling:**
If the rigid-body simulator reports that O undergoes a collision event, update its gain coefficients as per Equation (3.10) using the collision impulse and its location. (Section 3.1.3)
 - **Mode Truncation:**
Compute cutoff times t_j^c for each mode based on the mode truncation threshold, τ . (Section 3.2.2, Equation (3.14))
 3. **Quality Scaling:**
Sort objects based on amplitude contribution, assign time-quotas and compute the number of modes to be mixed for each object. (Section 3.2.3)

4. Sound Synthesis:

For each timestep at time t and for each object, O :

- Consider all modes permitted by the current quality setting which satisfy $t_j^c > t$. Sample and summate all these modes as described at the beginning of this section. This is O 's contribution to the sound.
- Output the sum of all objects' sample contribution as the sound sample for time t .

End simulation loop

3.3 Implementation and Results

In this section I present results to demonstrate the efficiency and realism achievable with our approach.

3.3.1 Rigid Body Simulation

I have implemented the algorithm and acceleration techniques presented in this chapter using C++ and OpenGL. The rigid-body simulator extends the technique presented by Guendelman et al. [37] to incorporate DEEP [46] for fast and more accurate penetration depth estimation, instead of sample-based estimation using distance fields. It also uses a more complex friction model presented by Mirtich and Canny [59], which results in more robust contact resolution. More recently, I have also integrated this system with the Open Dynamics Engine (ODE), as well as the NVIDIA PhysX engine, showing that the sound system doesn't put any special requirements on the physics engine and works with present-day game technology.

A video containing synthesized sounds for all the tests described below can be found at the website: <http://gamma.cs.unc.edu/symphony>.

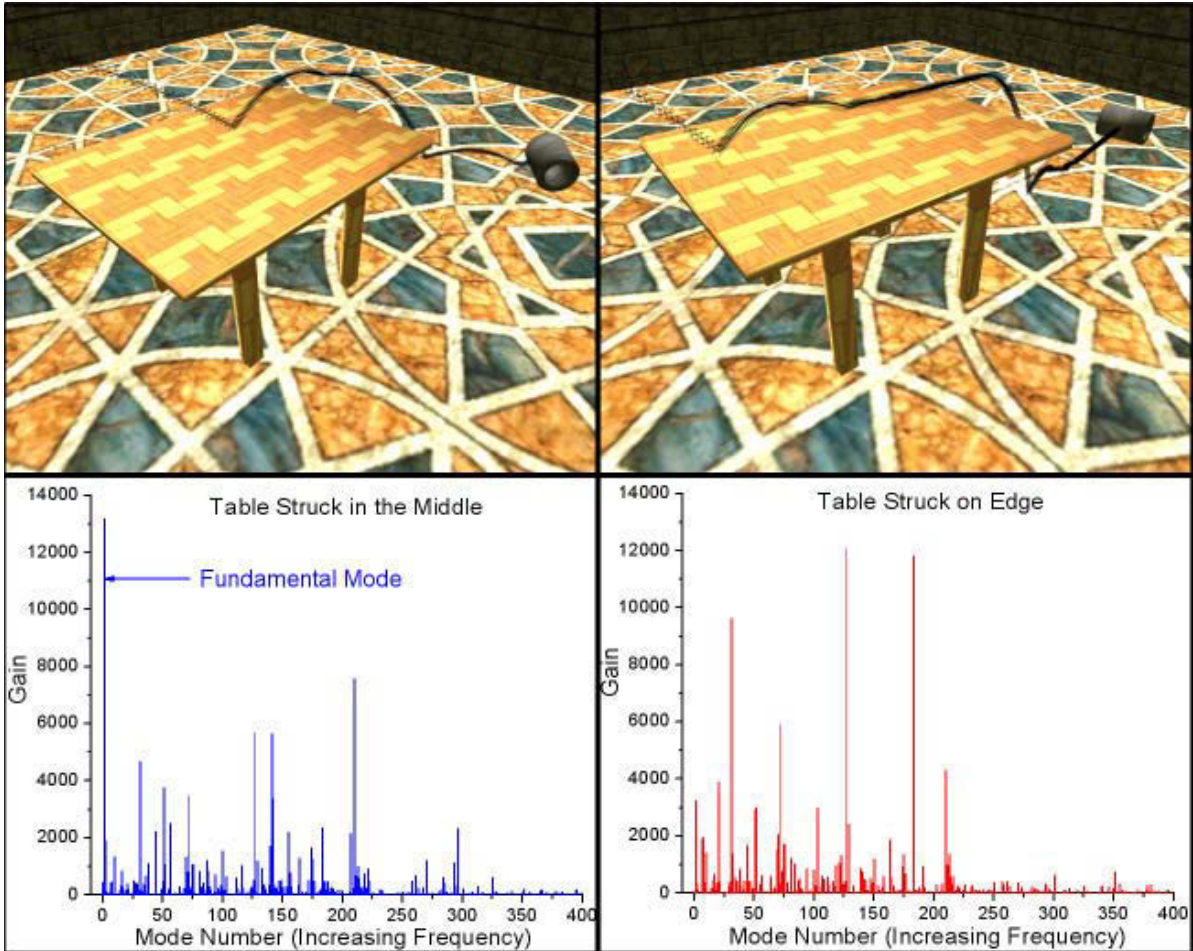


Figure 3.4: A metallic cylinder falls onto a wooden table, in the middle (left) and on the edge (right) and rolls off. The bottom part shows the corresponding frequency spectra for the two cases. Note that for the case on the left, most of the impulse is transferred to the low frequency fundamental mode while for the case on the right, the impulse is mostly transferred to higher frequency modes.

3.3.2 Position Dependent Sounds

As discussed earlier, the main advantage of using physically-based sounds over recorded audio is the ability to capture effects such as the magnitude of impacts between objects and more importantly, the subtle shift in sounds on striking an object at different points. Figure 3.4 shows a scene with a metallic cylinder tossed onto a wooden table. Both the table and cylinder are sounding. The figure contrasts two cases: the first case, shown on the left, depicts the cylinder striking the table near the middle and rolling off, while in the second case it strikes the table near the edge. I discuss the rolling sound in the next subsection, and will focus on the impact sound here. Since the table-top is in the form of a plate, one would expect that striking it on the edge would transfer a larger fraction of the impulse to higher frequencies, while striking it in the middle should transfer most part of the impulse to the fundamental mode of vibration, leading to a deeper sound. To verify this, I plotted the frequency spectra for the two cases just after the cylinder makes first impact with the table. The corresponding plots for the two cases are shown in the lower part of the figure. The case on the left shows a marked peak near the fundamental mode while the peak is completely missing in the second case. Conversely, the second case shows many peaks at higher frequencies which are missing in the first one. This difference clearly demonstrates that the sound for the two cases is markedly different, with the same qualitative characteristics as expected. Another important point to note is that this technique does not require the meshes to be highly tessellated to capture these effects. The table consists of just 600 vertices and the cylinder 128 vertices.

3.3.3 Rolling Sounds

In addition to handling impact sounds, my technique is able to simulate realistic rolling sounds without requiring any special-case treatment for sound synthesis. This is in part made possible because of the rigid-body simulator I have used, which is able to handle contacts in a more graceful manner than most impulse-based simulators. Figure 3.5

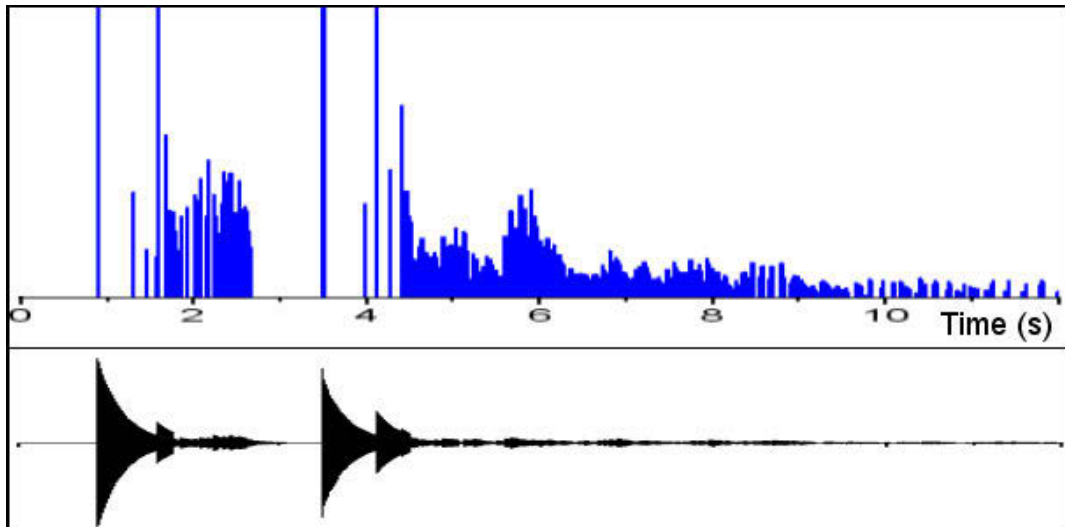


Figure 3.5: A plot of the impulses on a cylinder versus time for the scene shown on the right in Figure 3.4 and the corresponding audio samples. The peaks correspond to impacts while the numerous low-amplitude impulses correspond to rolling forces.

shows the impulses on the cylinder and the corresponding audio for the case shown in the right side of Figure 3.4. The cylinder rolls on the table after impact, falls to the ground and rolls on the floor for sometime. The initial rolling sound, when the cylinder is on the table, has a much richer quality. The sound of the table as the cylinder rolls over it conveys a sense of the cylinder’s heaviness, which is only partly conveyed by the sound of the impact. The cylinder, although uniformly tessellated, is very coarse, with only 32 circumferential subdivisions. Figure 3.5 shows the impulses applied on the cylinder against time. The peaks correspond to impacts: when the cylinder falls on the table, and when it falls to the ground from the table. Note that the audio waveform shows the corresponding peaks correctly. The period of time stretching from 6 to 8 seconds consists of the cylinder rolling on the floor and is characterized by many closely-spaced small-magnitude impulses on the cylinder as it strikes the floor again and again due to its tessellation. To test how important the periodicity of these impulses was for the realism of rolling sounds, the mean and standard deviation of the interval between these impulses were computed from the data presented in Figure 3.5. The mean time between

the impulses was 17 ms with a standard deviation of 10 ms. The fact that the standard deviation is more than 50% of the mean demonstrates that the impulses show very little periodicity. This seems to suggest that the periodicity of collisions is not critical for the perceived realism of rolling sounds.

3.3.4 Efficiency

My technique is able to perform sound synthesis for complex scenes in real time. Figure 3.6 shows a scene with 100 metallic rings falling simultaneously onto a wooden table and undergoing elastic collision. All the rings and the table are sounding. Each ring is treated as a separate object with separate aural properties. The rings consist of 200 vertices each. Figure 3.7 shows the audio FPS³ for this simulation against time for the one second interval during which almost *all* the collisions take place. The application frame rate is 100 FPS. Note that this is not the raw data but a moving average so that the short-range fluctuations are absorbed. The plot on the bottom is the base timing without using any of the acceleration techniques described in Section 4. The audio in this case is very choppy since the audio generation is not able to keep up with the speed of rendering and rigid-body simulation. With mode truncation and mode compression, the performance shows significant improvement. However, after initially starting at about 200 FPS, the frame rate drops in the latter part where the maximum number of collisions happen. With quality scaling in addition to mode compression and truncation (shown by the top-most curve), the frame rate exhibits no such drop, continuing to be around 200 FPS. This is because quality scaling gives priority to sound generation for those rings which just underwent collision, while lowering the quality for other rings which may have collided earlier and are contributing less to the overall sound. This illustrates the importance of quality scaling for scenarios with multiple collisions. It is

³An audio frame is defined as the amount of sound data sufficient to play for a duration equal to the duration of one video frame.

important to note that although this example sufficiently demonstrates the capability of the system to maintain steady frame rates, it is improbable in a real application, since there are about 100 collisions within a second. This is the reason why the CPU utilization is high (50%). A more common scenario would be as shown in Figure 1.3, which has a much lower CPU utilization (10%).

To illustrate the realistic sounds achievable with my approach, I designed a three-octave xylophone shown in Figure 1.3. The image shows many dice falling onto the keys of the xylophone to produce the corresponding musical notes. The audio simulation for this scene runs in the range of 500-700 FPS, depending on the frequency of collisions. The dice have been scripted to fall onto the xylophone keys at precise moments in time to play out any set of musical notes. Because of the efficiency of the sound generation process, the overall system is easily able to maintain a steady frame rate of 100 FPS. Also, there are situations in which many dice fall on different keys within a few milliseconds of each other, but the sound quality exhibits no perceptible degradation. Although the xylophone keys were tuned to match the fundamental note, they were not tuned to match the exact frequency spectrum of a real xylophone. The resulting sound is realistic and captures the essential timbre of the instrument. The material parameters for the xylophone were taken from [17].

3.4 Conclusion and Future Work

I have presented a physically-based sound synthesis algorithm with several acceleration techniques for rendering large-scale scenes consisting of hundreds of interacting objects in real time, with little loss in perceived sound quality. This approach requires no special mesh structure, and is simple to implement. This framework can be extended in the future for the auditory display of sliding sounds, explosion noises, breaking sounds, and other more complex audio effects that are difficult to simulate today at interactive rates.

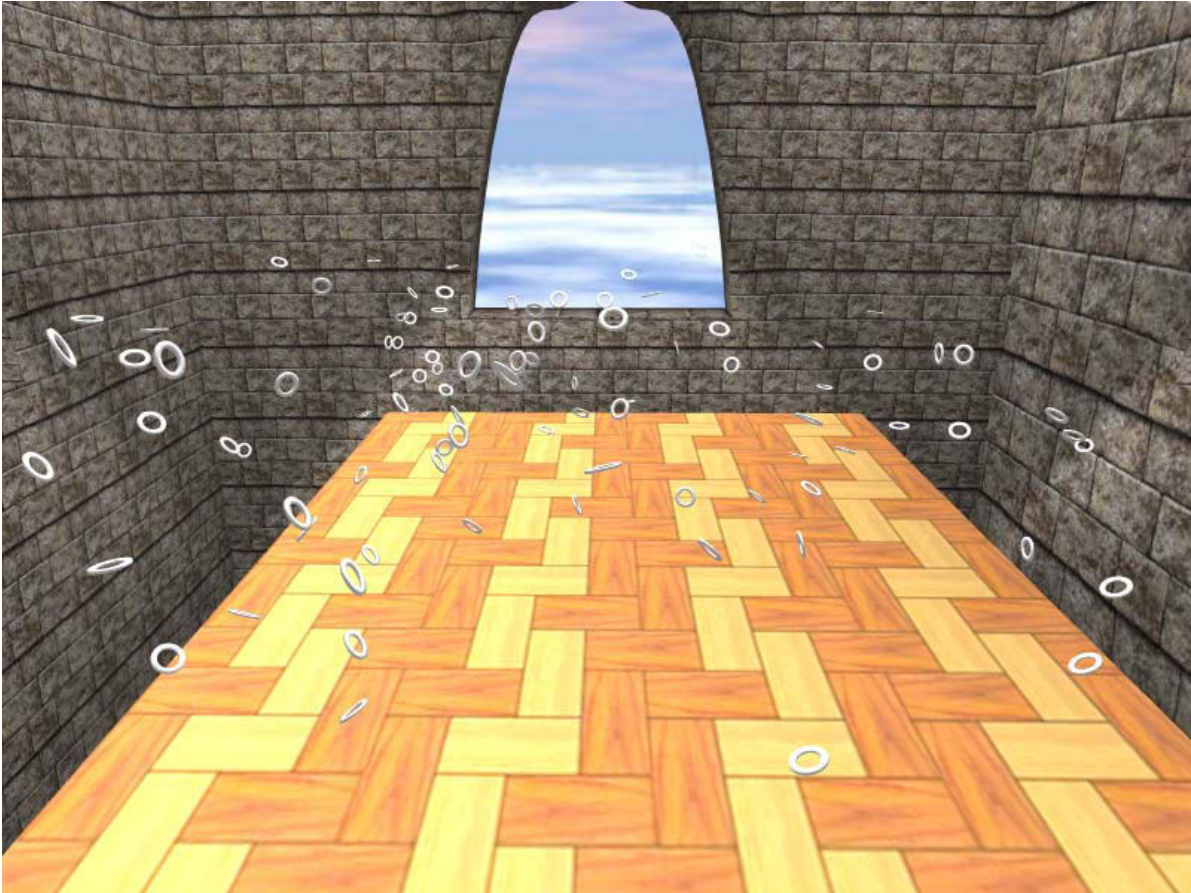


Figure 3.6: More than 100 metallic rings fall onto a wooden table. All the rings and the table are sounding. The audio simulation runs at more than 200 FPS, the application frame rate being 100 FPS. Quality Scaling ensures that the perceived sound quality does not degrade, while ensuring steady frame rates (See Figure 3.7)

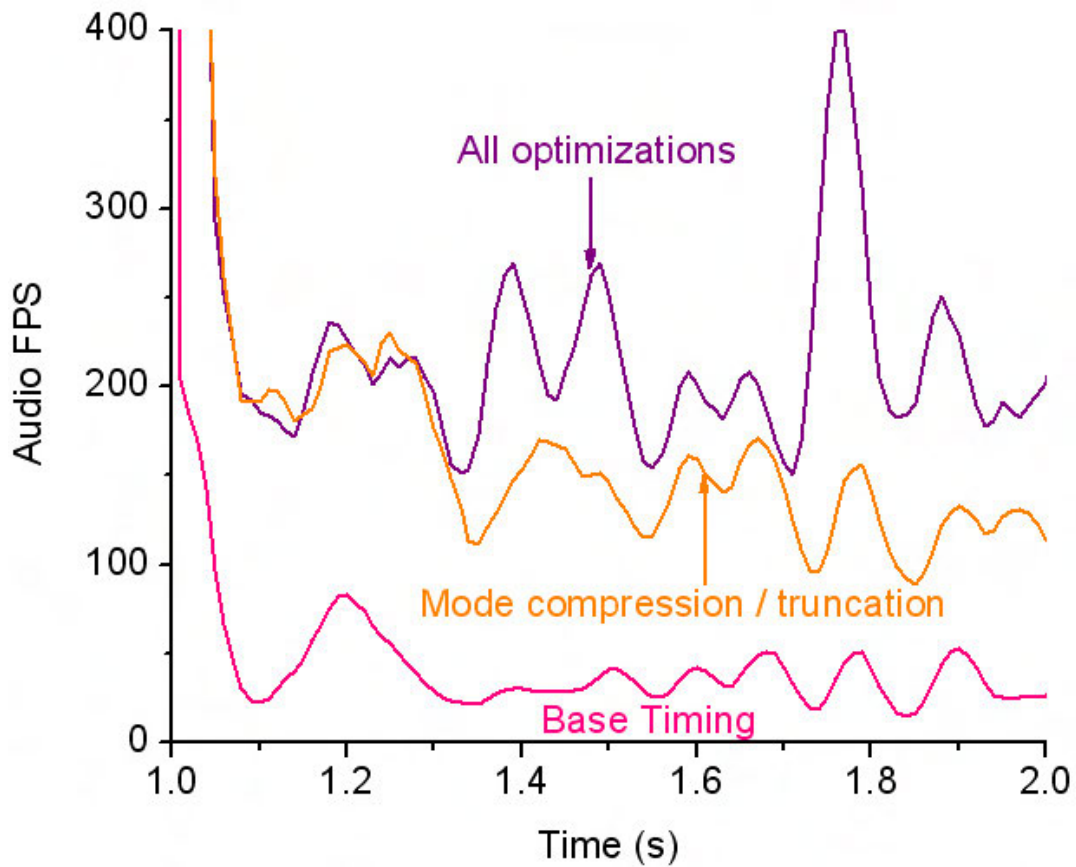


Figure 3.7: This graph shows the audio simulation FPS for the scene shown in Figure 3.6 from time 1s to 2s, during which almost all the collisions take place. The bottom-most plot shows the FPS for an implementation using none of the acceleration techniques. The top-most curve shows the FPS with mode compression, mode truncation and quality scaling. Note how the FPS stays near 200 even when the other two curves dip due to numerous collisions during 1.5-2.0s.

Chapter 4

Efficient Numerical Acoustics

In this chapter, I discuss my work on performing efficient numerical acoustics simulation on large scenes. I begin with a discussion of the mathematical background and describe in some detail, a high-accuracy finite-difference scheme, FDTD (Finite Difference Time Domain). In the next section, I describe my adaptive rectangular decomposition (ARD) approach. Following this, I describe the results obtained with my technique, as well as a discussion of the errors and performance. Finally, I conclude with a summary of my work and a discussion of possible future work in this area.

4.1 Mathematical Background

In this section, I discuss the FDTD method. I do this for two reasons: Firstly, this is the simulator I use as a reference to compare against and its details serve to illustrate the underlying mathematical framework used throughout this chapter. Secondly, this discussion illustrates numerical dispersion errors in FDTD and motivates our technique which uses the analytical solution to the Wave Equation on rectangular domains to remove numerical dispersion errors.

4.1.1 Basic Formulation

The input to an acoustics simulator is a scene in 3D, along with the boundary conditions and the locations of the sound sources and listener. The propagation of sound in a domain is governed by the Acoustic Wave Equation,

$$\frac{\partial^2 p}{\partial t^2} - c^2 \nabla^2 p = F(\mathbf{x}, t), \quad (4.1)$$

This equation captures the complete wave nature of sound, which is treated as a time-varying pressure field $p(\mathbf{x}, t)$ in space. The speed of sound is $c = 340 \text{ms}^{-1}$ and $F(\mathbf{x}, t)$ is the forcing term corresponding to sound sources present in the scene. The operator $\nabla^2 = \frac{\partial^2}{\partial x^2} + \frac{\partial^2}{\partial y^2} + \frac{\partial^2}{\partial z^2}$ is the Laplacian in 3D. The Wave Equation succinctly explains wave phenomena such as interference and diffraction that are observed in reality. I briefly mention a few physical quantities and their relations, which will be used throughout the chapter. For a wave traveling in free space, the frequency, ν and wavelength, λ are related by $c = \nu\lambda$. It is also common to use the angular counterparts of these quantities: angular frequency, $\omega = 2\pi\nu$ and wavenumber, $k = \frac{2\pi}{\lambda}$. Because frequency and wavenumber are directly proportional to each other, I will be using the two terms interchangeably throughout the chapter.

In the next sub-section, I briefly discuss the Finite Difference Time Domain (FDTD) method for numerically solving the Wave Equation. To avoid confusion, I note here that while the term FDTD is sometimes used to specifically refer to the original algorithm proposed by Yee [116] for Electromagnetic simulation, it is common to refer to any Finite Difference-based approach which computes the complete sound field in time domain as an FDTD method. In this chapter, I use the latter definition.

4.1.2 A (2,6) FDTD Scheme

FDTD works on a uniform grid with spacing h . To capture the propagation of a prescribed maximum frequency ν_{max} , the Nyquist theorem requires that $h \leq \frac{\lambda_{max}}{2} = \frac{c}{2\nu_{max}}$. Once the spatial discretization is performed, the continuum Laplacian operator is replaced with a discrete approximation of desired order of accuracy. Throughout this chapter, I consider the sixth order accurate approximation to the Laplacian, which approximates the second order differential in each dimension with the following stencil:

$$\begin{aligned} \frac{d^2 p_i}{dx^2} \approx & \frac{1}{180h^2} (2p_{i-3} - 27p_{i-2} + 270p_{i-1} - 490p_i \\ & + 270p_{i+1} - 27p_{i+2} + 2p_{i+3}) + O(h^6), \end{aligned} \quad (4.2)$$

where p_i is the i^{th} grid cell in the corresponding dimension. Thus, the Laplacian operator at each cell can be represented as a Discrete Laplacian Matrix, K and equation (4.1) becomes,

$$\frac{\partial^2 P}{\partial t^2} - \frac{c^2}{h^2} K P = F(t), \quad (4.3)$$

where P is a long vector listing the pressure values at all the grid cells and F is the forcing term at each cell. Hard-walls may be modeled with the Neumann Boundary Condition $-\frac{\partial p}{\partial \hat{n}} = 0$, where \hat{n} is the normal to the boundary.

The next step is to discretize equation (4.3) in time at some time-step Δt , which is restricted by the CFL condition $\Delta t < \frac{h}{c\sqrt{3}}$. Using the Leapfrog integrator in time, the complete update rule is as follows.

$$P^{n+1} = 2P^n - P^{n-1} + \left(\frac{c\Delta t}{h}\right)^2 K P^n + O(\Delta t^2) + O(h^6).$$

Since the temporal and spatial errors are second and sixth order respectively, this is a (2,6) FDTD scheme. In the next sub-section, I discuss the nature of the numerical errors in FDTD schemes and the resulting performance issues.

4.1.3 Numerical Dispersion in FDTD and Efficiency Considerations

As was previously discussed, the spatial cell size, h for FDTD is chosen depending on the maximum simulated frequency, ν_{max} and is limited by the Nyquist sampling theorem. However, due to numerical errors arising from spatial and temporal discretization, accurate simulation with FDTD typically requires not 2 but 8-10 samples per wavelength [99]. These errors manifest themselves in the form of Numerical Dispersion – Waves with different wavenumbers (or equivalently, different frequencies) do not travel with the same speed in the simulation. This error may be quantified by finding the wavenumber-dependent numerical speed, $c'(k)$, where k is the wavenumber. This speed is then normalized by dividing with the ideal wave speed, c , yielding the dispersion coefficient, $\gamma(k)$. Ideally, the dispersion coefficient should be as close to 1 as possible, for all wavenumbers. Figure 4.1 shows a plot of the dispersion coefficient for FDTD against frequency on a 3D grid and compares the error for different cell sizes. Observe that at 1000 Hz, the dispersion coefficient for FDTD is about $.01c$, while for FDTD running on a $2.5\times$ refined mesh the error is about $.001c$. This is because the spatial sampling increases from 4 samples per wavelength to 10 samples per wavelength.

Consider a short-time signal containing many frequencies, for example, a spoken consonant. Due to Numerical Dispersion, each of the frequencies in the consonant will travel with a slightly different speed. As soon as the phase relations between different frequencies are lost, the signal is effectively destroyed and the result is a muffled sound. From the above values of the dispersion coefficient, it can be shown that with FDTD a signal would have lost phase coherence after traveling just 17m, which is comparable to the diameter of most scenes.

To increase accuracy, the mesh resolution needs to be increased, but that greatly increases the compute and memory requirements of FDTD – Refining the mesh r times implies an increase on memory by a factor of r^3 and the total compute time for a given

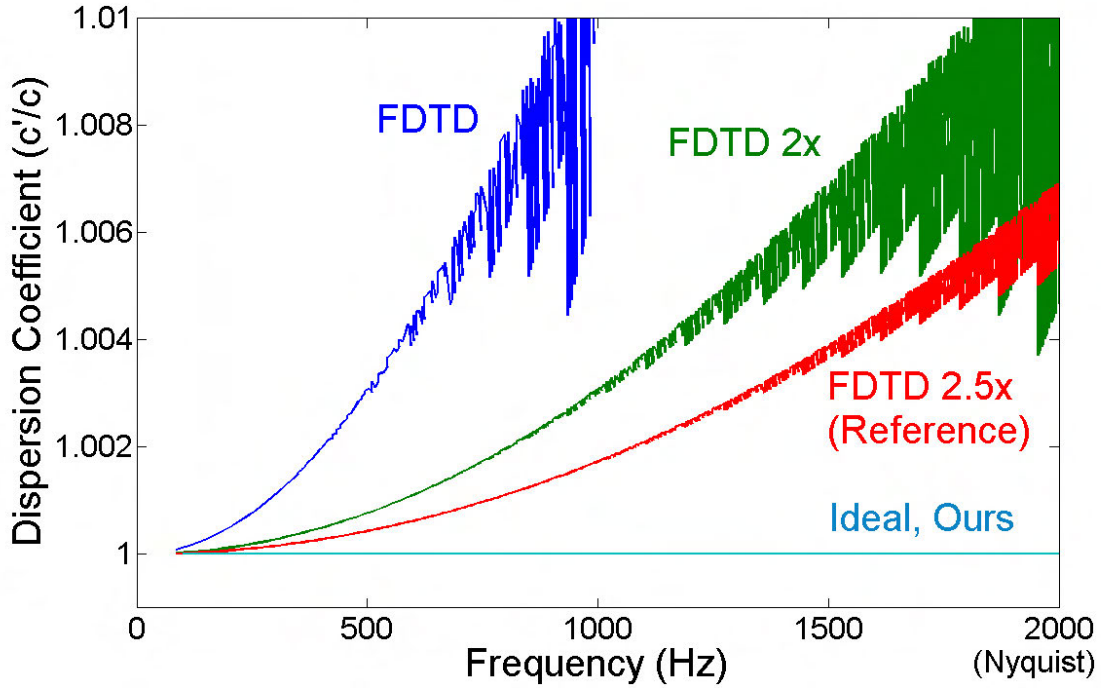


Figure 4.1: Numerical dispersion with a (2,6) FDTD scheme for different mesh resolutions. Increasing the sampling reduces the numerical dispersion errors. Our method suffers from no dispersion errors in the interior of rectangular partitions, while FDTD accumulates errors over each cell a signal propagates across. Reducing these errors with FDTD requires a very fine grid.

interval of time by r^4 . In practice, memory can be a much tighter constraint because if the method runs out of main memory, it will effectively fail to produce *any* results.

4.1.4 Wave Equation on a Rectangular Domain

A lot of work has been done in the field of Spectral/Pseudo-spectral methods [54] to allow for accurate simulations with 2-4 samples per wavelength while still allowing for accurate simulations. Such methods typically represent the whole field in terms of global basis functions, as opposed to local basis functions used in Finite Difference or Finite Element methods. With a suitable choice of the spectral basis (typically Chebyshev polynomials), the differentiation represented by the Laplacian operator can be approximated to a very high degree of accuracy, leading to very accurate simulations. However, spectral methods

still use discrete integration in time which introduces temporal numerical errors. In my work, I use a different approach and instead exploit the well-known analytical solution to the Wave Equation on rectangular domains [51], which enables error-free propagation within the domain. It is important to note here that I am able to achieve this because my technique assumes that the speed of sound is constant in the medium, which is a reasonable assumption for room acoustics and virtual environments.

Consider a rectangular domain in 3D, with its solid diagonal extending from the $(0, 0, 0)$ to (l_x, l_y, l_z) , with perfectly rigid, reflective walls. It can be shown that any pressure field $p(x, y, z, t)$ in this domain may be represented as

$$p(x, y, z, t) = \sum_{i=(i_x, i_y, i_z)} m_i(t) \Phi_i(x, y, z), \quad (4.4)$$

where m_i are the time-varying mode coefficients and Φ_i are the eigenfunctions of the Laplacian for a rectangular domain, given by –

$$\Phi_i(x, y, z) = \cos\left(\frac{\pi i_x}{l_x} x\right) \cos\left(\frac{\pi i_y}{l_y} y\right) \cos\left(\frac{\pi i_z}{l_z} z\right).$$

Given that we want to simulate signals band-limited up to a prescribed smallest wavelength, the above continuum relation may be interpreted on a discrete uniform grid with the highest wavenumber eigenfunctions being spatially sampled at the Nyquist rate. Note that as long as the simulated signal is properly band-limited and all the modes are used in the calculation, this discretization introduces no numerical errors. This is the reason it becomes possible to have very coarse grids with only 2-4 samples per wavelength and still do accurate wave propagation simulations. In the discrete interpretation, equation (4.4) is simply an inverse Discrete Cosine Transform (iDCT) in 3D, with Φ_i being the Cosine basis vectors for the given dimensions. Therefore, we may

efficiently transform from mode coefficients (M) to pressure values (P) as –

$$P(t) = iDCT(M(t)). \quad (4.5)$$

This is the main advantage of choosing a rectangular shape – because the eigenfunctions of a rectangle are Cosines, the transformation matrix corresponds to applying the DCT, which can be performed in $\Theta(n \log n)$ time and $\Theta(n)$ memory using the Fast Fourier Transform algorithm [32], where n is the number of cells in the rectangle, which is proportional to its volume. For general shapes, we would get arbitrary basis functions, and these requirements would increase to $\Theta(n^2)$ in compute and memory, which quickly becomes prohibitive for large scenes, with n ranging in millions. Re-interpreting equation (4.1) in a discrete-space setting, substituting P from the expression above and re-arranging, we get,

$$\begin{aligned} \frac{\partial^2 M_i}{\partial t^2} + c^2 k_i^2 M_i &= DCT(F(t)), \\ k_i^2 &= \pi^2 \left(\frac{i_x^2}{l_x^2} + \frac{i_y^2}{l_y^2} + \frac{i_z^2}{l_z^2} \right). \end{aligned} \quad (4.6)$$

In the absence of any forcing term, the above equation describes a set of independent simple harmonic oscillators, with each one vibrating with its own characteristic frequency, $\omega_i = ck_i$. The above analysis may be equivalently regarded as Modal Analysis applied to a rectangular domain. However, our overall approach is different from Modal Analysis because the latter is typically applied to a domain as a whole, yielding arbitrary basis functions which do not yield to efficient transforms, and extracting all the modes is typically intractable for domains with millions of cells.

Arbitrary forcing functions, for example, due to a volume sound sources, are modeled as follows. Assuming that the forcing function, $F(t)$ is constant over a time-step Δt , it may be transformed to mode-space as –

$$\tilde{F}(t) \equiv DCT(F(t)) \quad (4.7)$$

and one may derive the following update rule –

$$M_i^{n+1} = 2M_i^n \cos(\omega_i \Delta t) - M_i^{n-1} + \frac{2\widetilde{F}^n}{\omega_i^2} (1 - \cos(\omega_i \Delta t)). \quad (4.8)$$

This update rule is obtained by using the closed form solution of a simple harmonic oscillator over a time-step. Since it is a second-order equation, we need to specify one more initial condition, which I choose to be that the function computed over the time-step evaluates correctly to the value at the previous time-step, M^{n-1} . This leads to a time-stepping scheme which has no numerical errors for propagation in the interior of the rectangle, since we are directly using the closed-form solution for a simple harmonic oscillator. The only error introduced is in assuming that the forcing term is constant over a time-step. This is not a problem for input source sounds, as the time-step is necessarily below the sampling rate of the input signal. However, the communication of sound between two rectangular domains is ensured through forcing terms on their interface and this approximation introduces numerical errors at the interface. I discuss these issues in detail in the next section.

4.2 Technique

In the previous section, I discussed the errors and efficiency issues of the FDTD method and discussed a method to carry out numerical solution of the Wave Equation accurately and efficiently on rectangular domains. In this section, I discuss my technique which exploits these observations to perform acoustic simulation on arbitrary domains by decomposing them into rectangular partitions. I end with a discussion of the numerical errors in my approach.

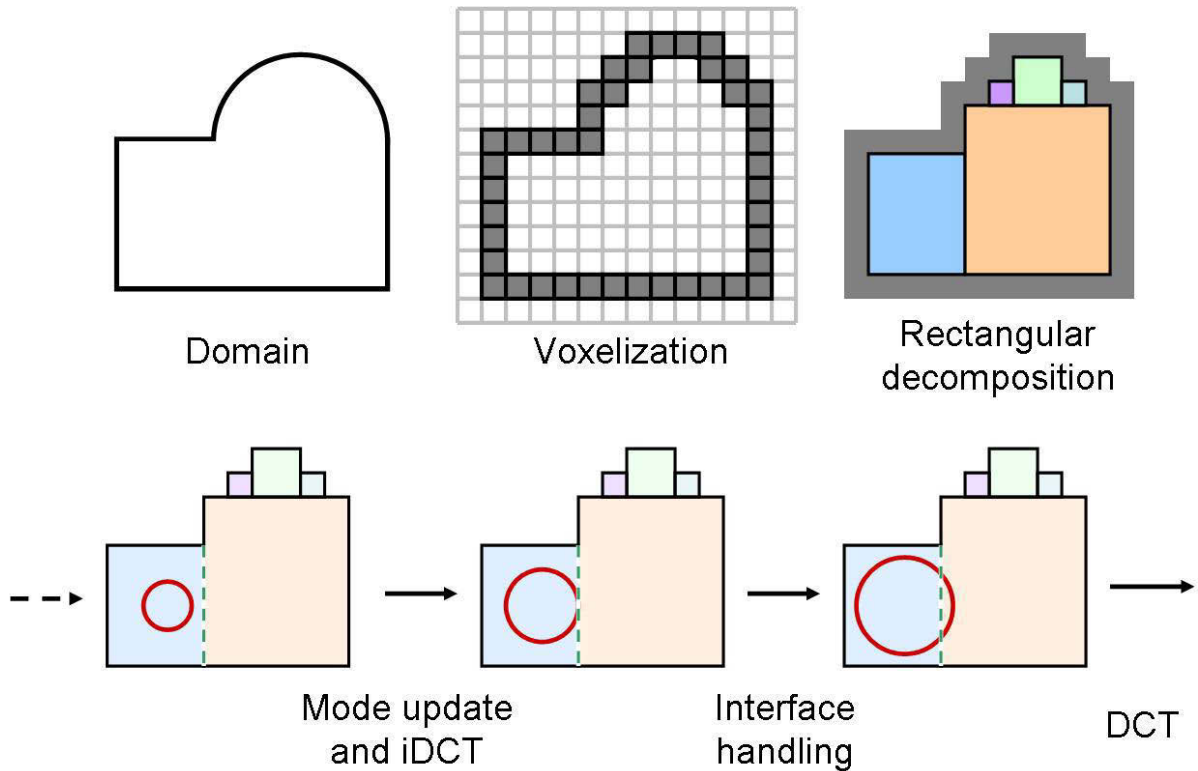


Figure 4.2: Overview of the ARD approach. The scene is first voxelized at a prescribed cell size depending on the highest simulated frequency. A rectangular decomposition is then performed and impulse response calculations then carried out on the resulting partitions. Each step is dominated by DCT and inverse DCT calculations withing partitions, followed by interface handling to communicate sound between partitions.

4.2.1 Adaptive Rectangular Decomposition

Most scenes of interest for the purpose of acoustic simulation necessarily have large empty spaces in their interior. Consider a large scene like, for example, a $30m$ high cathedral in which an impulse is triggered near the floor. With FDTD, this impulse would travel upwards and would accumulate numerical dispersion error at each cell it crosses. Given that the spatial step size is comparable to the wavelength of the impulse, which is typically a few centimeters, the impulse accumulates a lot of error while crossing hundreds to thousands of cells. In the previous section, I discussed that wave propagation on a rectangular domain can be performed very efficiently while introducing no numerical errors. If we fit a rectangle in the scene extending from the bottom to the top, the impulse would have no propagation error. This is the chief motivation for Rectangular Decomposition – Since there are large empty spaces in typical scenes, a decomposition of the space into rectangular partitions would yield many partitions with large volume and exact propagation could be performed in the interior of each.

The rectangular decomposition is performed by first voxelizing the scene. The cell size is chosen based on the maximum frequency to be simulated, as discussed previously. Next, the rectangular decomposition is performed using a greedy heuristic, which tries to find the largest rectangle it can grow from a random seed cell until all free cells are exhausted. I note here that the correctness of our technique does not depend on the optimality of the rectangular decomposition. A slightly sub-optimal partitioning with larger interface area affects the performance only slightly, as the interface area is roughly proportional to the surface area of the domain, while the runtime performance is dominated by the cost of DCT, which is performed on input proportional to the volume of the domain.

4.2.2 Interface Handling

Once the domain of interest has been decomposed into many rectangles, propagation simulation can be carried out inside each rectangle as described in Section 4.1.4. However, since every rectangle is assumed to have perfectly reflecting walls, sound will not propagate across rectangles. I next discuss how this communication is performed using a Finite Difference approximation. Without loss of generality, let's assume that two rectangular partitions share an interface with normal along the X-axis. Recall the discussion of FDTD in Section 4.1.2. Assume for the moment that (2,6) FDTD is running in each rectangular partition, using the stencil given in equation (4.2) to evaluate $\frac{d^2 p_i}{dx^2}$. Further, assume that cell i and $i + 1$ are in different partitions and thus lie on their interface. As mentioned previously, Neumann boundary condition implies even symmetry of the pressure field about the interface and each partition is processed with this assumption. Thus, the Finite Difference stencil may also be thought of as a sum of two parts – The first part assumes that the pressure field has even symmetry about the interface, namely, $p_i = p_{i+1}, p_{i-1} = p_{i+2}$ and $p_{i-2} = p_{i+3}$, and this enforces Neumann boundary conditions. The residual part of the stencil accounts for deviations from this symmetry, caused by the pressure in the neighboring partition. Symbolically, representing the Finite Difference stencil in equation (4.2) as S –

$$S_i = S_i^0 + S'_i, \text{ where}$$

$$S_i^0 = \frac{1}{180h^2} (2p_{i-3} - 25p_{i-2} + 243p_{i-1} - 220p_i)$$

$$S'_i = \frac{1}{180h^2} (-2p_{i-2} + 27p_{i-1} - 270p_i + 270p_{i+1} - 27p_{i+2} + 2p_{i+3}).$$

Since S'_i is a residual term not accounted for while evaluating the LHS of equation (4.3), it is transferred to the RHS and suitably accounted for in the forcing term, thus yielding,

$$F_i = c^2 S'_i. \tag{4.9}$$

Similar relations for the forcing term may be derived for all cells near the partition boundary which index cells in neighboring partitions. If I was actually using (2,6) FDTD in each partition, this forcing term would be exact, with the same numerical errors due to spatial and temporal approximations appearing in the interior as well as the interface. However, because an exact solution is being used in the interior, the interface handling described above introduces numerical errors on the interface. I will discuss these errors in more detail shortly. I would like to note here that a sixth-order scheme was chosen as it gives sufficiently low interface errors, while being reasonably efficient. Lower (second/fourth) order schemes would be more efficient and much easier to implement, but as I have experimented, they result in much higher errors, which results in undesirable, audible high frequency noise. One may use an even higher order scheme if more accuracy is required for a particular application, at the expense of computation and implementation effort. An interesting point to note at this point is that the interface handling doesn't need to know how the field inside each partition is being updated. Therefore, it is easy to mix different techniques for wave propagation in different parts of the domain, if so required.

4.2.3 Domain Decomposition Method and ARD

I now discuss my work in context of the Domain Decomposition Method (DDM). This serves to illuminate the choices in ARD, its novel aspects, the main source of error, and ways to address it. Interestingly, the main motivation of the DDM when it was conceptualized more than a century ago was very similar in spirit to my approach – divide the domain into simpler-shaped partitions which could be analyzed more easily [22]. However, since then, in nearly all DDM approaches for wave propagation the principal goal has been to divide and parallelize the workload across multiple processors. Therefore, the chief requirement in such cases is that the partitions be of near-equal size and have minimal interface area, since such decomposition corresponds to balancing the

computation and minimizing the communication cost between processors.

The motivation of ARD for partitioning the domain is different – it is done to ensure that the partitions have a particular *rectangular shape* even if that implies partitions with highly varying sizes. This is because the rectangular shape yields to analytical solution, which in turn means reduced computation without compromising numerical accuracy for propagation within the partitions. This holds *independently* of any parallelization considerations, which have been the main focus of prior work on wave-solvers in high-performance computing. However, by virtue of having performed a decomposition, parallelism is still present to be exploited in ARD. I have pursued this direction to some extent by off-loading the computed-intensive per-partition FFTs to the GPU, as will be described later in this chapter. It is possible to parallelize my approach further by allocating the partitions to different cores or machines, and doing interface handling between them, and would be the way to scale ARD to very large scenes with billions of cells, just as with other DDM approaches. I am part of current work in this direction [57] which has already shown promising speedups of nearly ten times compared to the results I present in this thesis. Thus, decomposing the domain into partitions and performing interface handling between them are very well-known techniques that are applicable to ARD, but are not the novel contribution of this work – which is the restriction of the partition shape to rectangles and exploitation of analytical solutions.

Another interesting question is whether the existing principles of DDM can be applied directly for performing the interface handling between partitions. Most DDM approaches have been designed for elliptic equations and require a global iterative solution where each partition is updated multiple times before reaching the final, globally-consistent solution. The time-domain wave equation, on the other hand, is hyperbolic. It turns out that using an explicit time-stepping scheme with the wave equation eliminates the need for global iteration. Thus, in order to ensure global consistency at each time-step with explicit wave equation solvers, including ARD, it is sufficient to apply

interface operators between partitions, without any need for such iterations, such as the Schwarz alternating method. The mathematical reason for this is that as long as the discrete spatial derivative operator reads its input values from the correct places, whether these values exist locally or not is immaterial. Domain decomposition in the context of explicit schemes takes a very simple form – the spatial derivative operator near the boundary is split additively into two parts – one local to the partition and the other non-local, potentially indexing anywhere, which is the interface operator. The local part is calculated on all processors in parallel, but the interface operator requires communication between processors. There are no errors introduced due to domain partitioning, no matter how the derivative operator is split additively into the two parts – the result is mathematically identical to the global solution, owing to the linearity of the numerical derivative operator.

The interface errors that result in ARD are because the above-mentioned decomposition of the discrete derivative operator isn't perfect – because of using a spectral approximation (in the Cosine basis), the spatial derivative operators are global in nature, extending all over the domain. In other words, they are not compact, unlike finite-difference techniques. This is the price to pay for the great increase in accuracy. Thus, the *perfect* interface operator is not compact, making it computationally expensive to evaluate. The difference between the ideal global operator and the compact sixth-order finite difference operator actually used results in the erroneous reflections. These errors can thus be decreased by increasing the support of the interface operator and reducing the difference between the ideal operator and the approximate one, preferably while looking at the Fourier transform of the error, which corresponds to the frequency response of the artificial interface. Thus, the interface errors in ARD can be reduced without bound by optimizing the frequency response as discussed above, at the cost of increased computation. In particular, there is no need for global iteration between partitions.

4.2.4 Absorbing Boundary Condition

Our discussion till this point has assumed that all scene boundaries are perfectly reflecting. For modeling real scenes, this is an unrealistic assumption. Moreover, since the computation is carried out on a volumetric grid, it is necessary to truncate the domain and model emission into free space. It is necessary to have absorbing boundaries for this purpose. For this work, I have implemented the Perfectly Matched Layer (PML) absorber [77], which is commonly employed in most numerical wave propagation simulations due to its high absorption efficiency. PML works by applying an absorbing layer which uses coordinate stretching to model wave propagation in an unphysical medium with very high absorption, while ensuring that the impedance of the medium matches that of air at the interface to avoid reflection errors. The interfacing between the PML medium and a partition in our method is simple to implement – Since PML explicitly maintains a pressure field in the absorbing medium, the PML medium can also be treated as a partition and the same technique described above can be applied for the coupling between PML and other partitions. Variable reflectivity can be easily obtained by multiplying the forcing term calculated for interface handling by a number between 0 and 1, 0 corresponding to full reflectivity and 1 corresponding to full absorption.

PML is very well-suited for modeling full absorption at openings in the scene, such as doors or windows. However, because ARD employs PML for modeling partial reflections at scene boundaries as well, it is not able to model frequency-dependent absorption. It is entirely possible to use different boundary-handling schemes in much the same way as it is done for FDTD. Specifically, future investigations into using techniques such as digital impedance filters [49, 90] with ARD will allow for modeling boundary impedance more accurately. Such integration might also offer the additional benefit of reduced computation in boundary handling, since PML is known to be quite computationally expensive. Therefore, I do not expect that the speedups presented in this thesis will not be decreased by such an integration.

4.2.5 Putting everything together

In this subsection, I give a step-by-step description of all the steps involved in our technique. Figure 4.2 shows a schematic diagram of the different steps in my approach, which are as follows –

1. Pre-processing

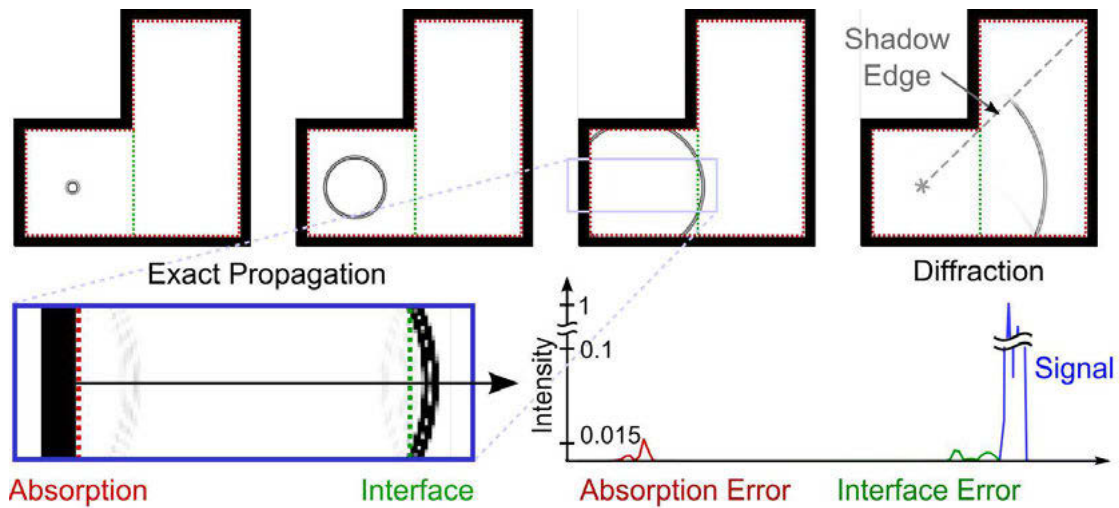
- (a) Voxelize the scene. The cell-size is fixed by the minimum simulated wavelength and the required number of spatial samples per wavelength (typically 2-4)
- (b) Perform a rectangular decomposition on the resulting voxelization, as described in Section 4.2.1.
- (c) Perform any necessary pre-computation for the DCTs to be performed at runtime. Compute all interfaces and the partitions that share them.

2. Simulation Loop

- (a) Update modes within each partition using equation (4.8)
- (b) Transform all modes to pressure values by applying an iDCT as given in equation (4.5)
- (c) Compute and accumulate forcing terms for each cell. For cells on the interface, use equation (4.9), and for cells with point sources, use the sample value.
- (d) Transform forcing terms back to modal space using a DCT as given in equation (4.7).

4.2.6 Numerical Errors

Numerical errors in our method are introduced mainly through two sources – boundary approximation and interface errors. Since I employ a rectangular decomposition to



Frequency	Interface error	Absorption error
250 Hz	-54 dB	-21 dB
500 Hz	-42 dB	-26 dB
750 Hz	-36 dB	-26 dB
1000 Hz	-28 dB	-32 dB

Figure 4.3: Measurements of numerical error due to interface handling and PML absorbing boundary conditions. The interface handling errors stays near -40 dB for most of the frequency spectrum, which is not perceptible. The absorption error stays around -25 dB which introduces very small errors in the reflectivity of different materials.

approximate the simulation domain, there are stair-casing errors near the boundary (see Figure 4.6). These stair-casing errors are identical to those in FDTD because my technique does a rectangular decomposition of a uniform Cartesian grid – there is no additional geometry-approximation error due to using rectangular partitions. In most room acoustic software, it is common practice to approximate the geometry to varying degrees [94]. The reason for doing this is that we are not as sensitive to acoustic detail as much as we are to visual detail. Geometric features comparable or smaller than the wavelength of sound (34 cm at 1kHz) lead to very small variations in the overall acoustics of the scene due to the presence of diffraction. In contrast, in light simulation, all geometric details are visible because of the ultra-small wavelength of light and thus stair-casing is a much more important problem.

The net effect of stair-casing error for numerical simulators is that for frequencies with wavelengths comparable to the cell size (1kHz), the walls act as diffuse instead of specular reflectors. For frequencies with large wavelengths (500 Hz and below), the roughness of the surface is effectively ‘invisible’ to the wave, and the boundary errors are small with near-specular reflections. Therefore, the perceptual impact of boundary approximation is lesser in acoustic simulation.

However, if very high boundary accuracy is critical for a certain scene, this can be achieved by coupling our approach with a high-resolution grid near the boundary, running FDTD at a smaller time-step. As I had mentioned earlier, as long as the pressure values in neighboring cells are available, it is easy to couple the simulation in the rectangular partitions with another simulator running in some other part of the domain. Of course, this would create extra computational overhead, so its an efficiency-accuracy tradeoff.

As I discussed theoretically in Section 4.1.4 and also demonstrate with experiments in the next section, my technique is able to nearly eliminate numerical dispersion errors. However, because the inter-partition interface handling is based on a less accurate (2,6)

FDTD scheme, the coupling is not perfect, which leads to erroneous reflections at the interface. Figure 4.3 shows the interface error for a simple scene. The Nyquist frequency on the mesh is 2000Hz. The table at the bottom of the figure shows the interface reflection errors for different frequencies, in terms of sound intensity. Although the interface errors increase with increasing frequency, it stays $\sim -40dB$ for most of the spectrum. Roughly, that is the difference in sound intensity between normal conversation and a large orchestra.

Since most scenes of practical interest have large empty spaces in their interior, the number of partition interfaces encountered by a wave traveling the diameter of the scene is quite low. For example, refer to Figure 4.6 – a wave traveling the 20 m distance from the source location to the dome at the top encounters only about 10 interfaces. Also, it is important to note that this is a worst-case scenario for our approach, since many rectangles are needed to fit the curved dome at the top. This is the chief advantage of our approach – numerical dispersion is removed for traveling this distance and it is traded off for very small reflection errors which are imperceptible. Please hear the accompanying video (link given in Section 4.3) for examples of audio rendered on complex scenes with numerous interfaces.

Figure 4.3 also shows the absorption errors for the PML Absorbing Boundary Condition. The absorption errors range from -20 to -30dB, which works well for most scenes, since this only causes a slight deviation from the actual reflectivity of the material being modeled. However, if higher accuracy absorption is required, one might increase the PML thickness. I have used a 10-cell thick PML in all the simulations shown.

4.2.7 ARD and FDTD: efficiency comparison

A direct theoretical comparison of performance of FDTD vs ARD for the same amount of error is difficult since both techniques introduce different kinds of errors. Since the final goal in room acoustics is to auralize the sounds to a human listener, it is natural

to set these error tolerances based on their auditory perceivability. However, this is complicated by the absence of systematic listening tests for perceivable errors with both, FDTD and ARD. It is possible to compare them by assuming *conservatively low* errors with both the techniques. I briefly discuss how the parameters in both techniques were set, for keeping the errors conservatively low and then present a theoretical comparison to motivate why ARD is more compute-efficient than FDTD.

In recent work, Sakamoto et al. [83] show that FDTD calculations of room-acoustic impulse responses on a grid with samples per wavelength, $s = 6 - 10$, agree well with measured values on a real hall in terms of room acoustic parameters such as reverberation time. This mesh resolution is also commonly used with the finite difference method applied to electromagnetic wave propagation [99] to control phase errors resulting from numerical dispersion. Motivated from these applications, I have set the mesh resolution conservatively at $s = 10$ points per wavelength for FDTD, assuming that this safely ensures that numerical dispersion errors are inaudible in auralizations, serving as a good reference simulation.

ARD results in fictitious reflections errors at the artificial interfaces. As discussed in Section 4.2.6, using $s = 2.6$ with ARD, the fictitious reflection errors can be kept at a low level of $-40dB$ average over the whole usable frequency range by employing a sixth-order finite difference transmission operator. This means that for a complex scene with many interfaces, the global pollution errors stay $40dB$ below the level of the ambient sound field, rendering them imperceptible, as demonstrated in the accompanying video. Therefore, I assume that safely low errors are achieved in ARD with a sampling of $s = 2.6$.

Computational expenditure: Table 4.1 shows a theoretical performance comparison of FDTD and ARD. For illustrative purposes, consider a point source that emits a broadband Gaussian pulse band-limited to a frequency of $\nu = 1kHz$, corresponding to a wavelength of $\lambda = c/\nu = 34cm$. Further assume that the scene has an air vol-

	s	# cells $N = V/h^3$	# steps t/dt	# FLOPS per cell	Total cost (TeraFLOPS)
FDTD	10	254 Million	17000	55	237.5
ARD	2.6	4.5 Million	4500	120	2.4

Table 4.1: FLOPS comparison of FDTD vs ARD on a scene of volume $V = 10,000m^3$ with maximum simulation frequency $v_{max} = 1kHz$ for the duration $t = 1$ sec. Theoretically, ARD which uses samples per wavelength, $s = 2.6$, is nearly hundred times efficient than FDTD ($s = 10$) on account of using a much coarser grid. The value of “FLOPS per cell” is defined as the ratio of the total FLOPS and N , the total number of cells.

ume of $V = 10,000m^3$ and a 1 second long simulation is performed. The number of cells with either technique is given by $N = V/h^3$, where h is the spatial cell size. The simulation time-step is restricted by the CFL condition $dt \leq h/c\sqrt{3}$, smaller cell sizes require proportionally smaller time-steps. The performance thus scales as ν^4 , ν being the maximum simulated frequency.

The update cost for sixth-order accurate FDTD in 3D is about 55 FLOPS per cell (including the cost of boundary treatment (PML), which is the same as for ARD). The total cost for ARD can be broken down as: DCT and IDCT¹ – $4NlgN$, mode update – $9N$, interface handling – $300 \times 6N^{2/3}$ and boundary treatment (PML) – $390 \times 6N^{2/3}$. The $6N^{2/3}$ term approximates the surface area of the scene by that of a cube with equivalent volume. This estimate is optimistic and close to the lower bound of surface area, and was chosen mainly because estimating surface areas in the general case is quite complex and I wanted to retain generality in the analysis. As can be seen from Table 4.1, theoretically ARD is nearly 100 times more efficient than FDTD. This corresponds quite closely to the actual speedups obtained. Also, ARD is highly memory efficient – ten times more so than FDTD – since it requires fewer cells, as shown in col. 3 of Table 4.1. This makes it possible to perform simulations on much larger scenes than FDTD without overflowing main memory.

¹Assuming a DCT and IDCT take $2NlgN$ FLOPS each.

4.3 Results

The resulting auralizations for all the tests described below can be seen in the accompanying video, which is at the website: <http://gamma.cs.unc.edu/propagation>.

4.3.1 Offline Sound Rendering

Before I describe how sound rendering was performed for this part of my work, I would like to emphasize that the focus here is to perform *offline* auralizations from fixed sources. The next chapter describes far more efficient ways for performing the auralization for moving sources while consuming much less memory than the techniques described here, while also performing high-frequency extrapolation in a much more accurate manner. Thus, if the reader is interested in efficient sound rendering rather than learning how the audio results described here were obtained, this sub-section may be safely ignored.

The input to all audio simulations I have performed is a Gaussian-derivative impulse of unit amplitude. Given the maximum frequency to be simulated, ν_{max} , I fix the width of the impulse so that its maxima in frequency domain is at $\frac{\nu_{max}}{2}$, giving a broadband impulse in the frequency range of interest. This impulse is triggered at the source location and simulation performed until the pressure field has dropped off to about -40 dB, which is roughly the numerical error of the simulation. The resulting signal is recorded at the listener position(s). Next, deconvolution is performed using a simple Fourier coefficient division to obtain the Impulse Response (IR), which is used for sound rendering at a given location.

Auralizing the sound at a moving listener location is performed as follows. First, note that running one simulation from a source location yields the pressure variation at all cell centers because we are solving for the complete field on a volumetric grid. For auralizing sound, the IRs at all cells lying close to the listener path are computed. Next,

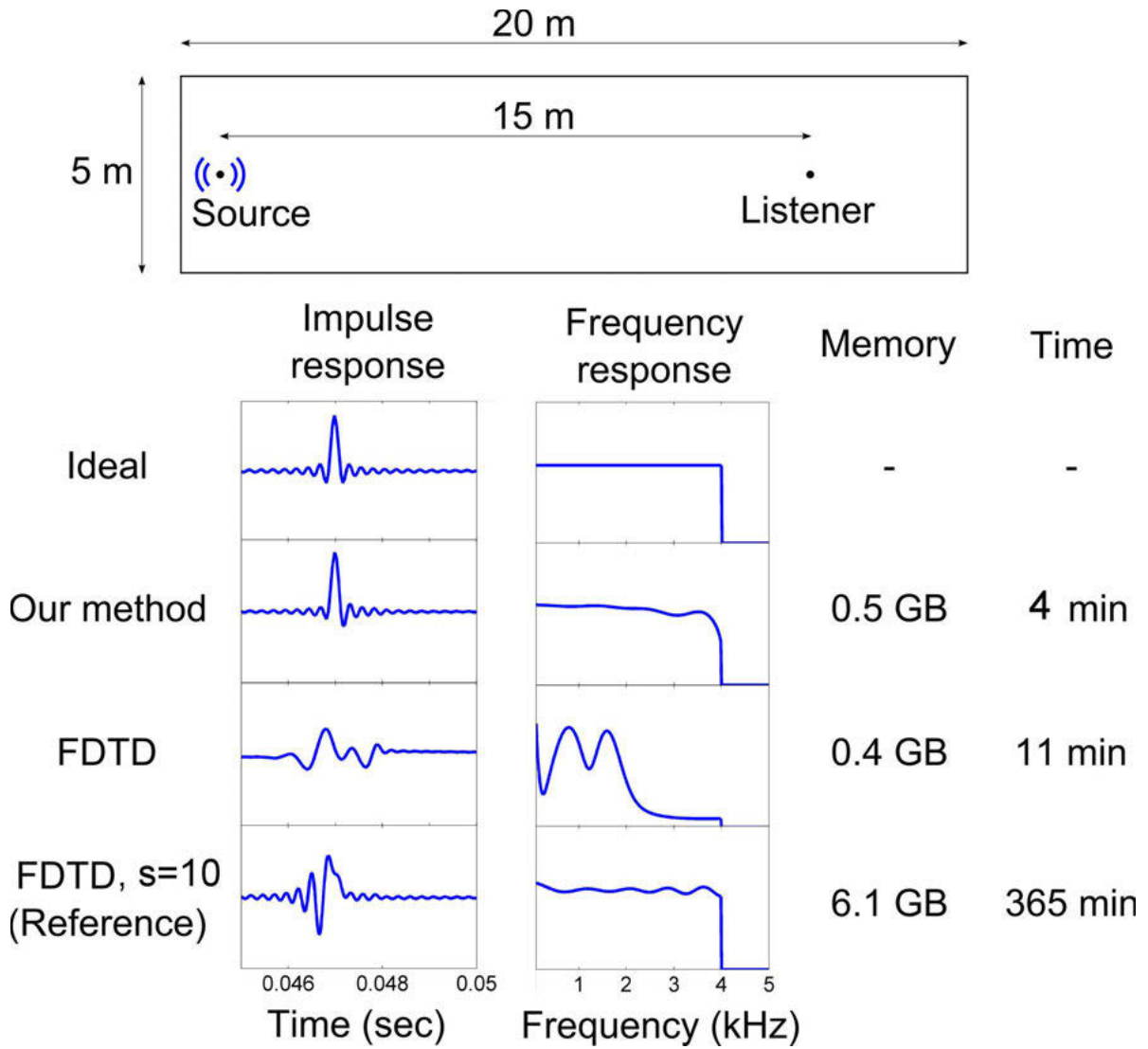


Figure 4.4: Numerical results on the corridor scene, comparing numerical dispersion errors in FDTD and in our method. The reference FDTD solution has a mesh with $s = 10$ samples per wavelength. Note that only the magnitudes of the Fourier coefficients are plotted. Our method suffers from very little numerical dispersion, reproducing the ideal impulse response very closely, while FDTD suffers from large amounts for numerical dispersion. My technique takes an order of magnitude less memory and nearly two orders of magnitude less computation time to produce results with accuracy comparable to the reference solution.

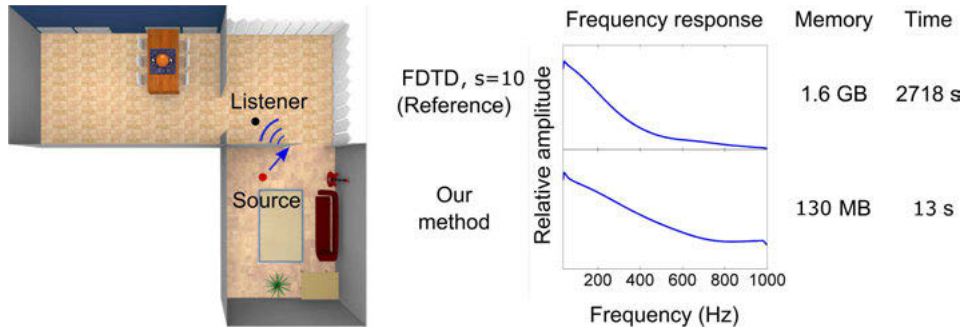


Figure 4.5: The House scene demonstrates diffraction of sound around obstacles. All the scene geometry shown was included in the simulation. Our method is able to reproduce the higher diffraction intensity of sound at lower frequencies, while reducing the memory requirements by about an order of magnitude and the computational requirements by more than two orders of magnitude. The reference solution is computed on a mesh with $s = 10$ samples per wavelength.

the sound at the current position and time is estimated by linearly interpolating the field values at neighboring cell centers. To obtain the field value at a given cell center, a convolution of the IR at the corresponding location and the input sound is performed.

Most of the simulations I have performed are band-limited to 1-2kHz due to computation and memory constraints. However, this is not a big limitation. Although audible sounds go up to 22kHz, it is important to realize that only frequencies up to about 5kHz are perceptually critical [51] for acoustics simulation. Moreover, the frequency perception of humans is logarithmic, which reflects in the frequency doubling between musical octaves. This means that most of the perceptually important frequencies are contained till about 2kHz. For example, the frequency of the fundamental notes of a typical 88-key piano goes from about 30Hz to 4kHz, covering 7 octaves, out of which 6 octaves are below 2kHz. However, even though we don't have accurate perception of higher frequencies, their complete absence leads to perceptual artifacts and therefore, there must be some way of accounting for higher frequencies, even if approximately. One way of doing that would be to combine our technique with a Geometrical Acoustic simulator for the higher frequency range. In my work, I have used a much simpler technique that gives good results in practice.

To auralize sounds in the full audible range up to 22kHz, I first up-sample the IR obtained from the simulation to 44kHz and run a simple peak detector on the IR which works by searching for local maxima/minima. The resulting IR contains peaks with varying amplitudes and delays, corresponding to incoming impulses. This is exactly the kind of IR that geometrical approaches compute by tracing paths for sound and computing the attenuation and delay along different paths. Each path yields a contribution to the IR. The difference here is that numerical simulation does not explicitly trace these paths. Instead, my technique extracts this information from the computed impulse response through peak detection. I use the IR thus computed for higher frequencies. The approximation introduced in this operation is that the diffraction at higher frequencies is approximated since the peak detector doesn't differentiate between reflection and diffraction peaks. Intuitively, this means that high frequencies may also diffract like low frequencies, which is the approximation introduced by this technique. This IR filter is then high-passed at the simulation cutoff frequency to yield a filter to be used exclusively for higher frequencies. As a final step, the exact low-frequency IR and approximate high-frequency IR are combined in frequency domain to yield the required IR to be applied on input signals. I must emphasize here that this technique is applied to obtain an approximate response exclusively in the high-frequency range and it is ensured that numerical accuracy for lower frequencies till 1-2kHz is maintained.

The reference solution for comparing ARD is the (2,6) FDTD method described in Section 4.1.2 running on a fine mesh. Since the main bottleneck of our approach is DCT, which can be performed through an FFT, I used the GPU-based FFT implementation described in [36], to exploit the compute power available on today's high-end graphics cards. Combining optimized transforms with algorithmic improvements described in the previous sections is the reason my technique gains considerable speedups over FDTD. All the simulations were performed on a 2.8GHz Intel Xeon CPU, with 8GB of RAM. The FFTs were performed on an NVIDIA GeForce GTX 280 graphics card.

In the following sub-sections, to clearly demarcate the algorithmic gain of our approach over FDTD and the speedups obtained due to using the GPU implementation of FFT, I provide three timings for each case: the running time for computing the reference solution with FDTD, the time if we use a serial version of FFTW [32] and the time with the GPU implementation of FFT. In general, I obtain a ten-fold performance gain due to algorithmic improvements and another ten-fold due to using GPU FFT. The ten-fold gain in memory usage is of course, purely due to algorithmic improvements.

4.3.2 Numerical Dispersion: Anechoic Corridor

I first demonstrate the near absence of numerical dispersion in my scheme. Refer to Figure 4.4. The scene is a $20m \times 5m \times 5m$ corridor in which the source and listener are located $15m$ apart, as shown in the figure. To measure just the accumulation of numerical dispersion in the direct sound and isolate any errors due to interface or boundary handling, I modeled the scene as a single, fully reflective rectangle. The simulation was band-limited to 4kHz, and the IR was calculated at the listener and only the direct sound part of the impulse response was retained. As Figure 4.4 shows, our method’s impulse response is almost exactly the same as the ideal response. FDTD running on the same mesh undergoes large dispersion errors, while FDTD running on a refined mesh with $s=10$ samples per wavelength, (the reference) gives reasonably good results. Note that since there is only direct transmission from the source to the listener, the magnitude of the ideal frequency response is constant over all frequencies. This is faithfully observed for our method and the reference, but FDTD undergoes large errors, especially for high frequencies. Referring to the video, this is the reason that with FDTD, the sound is ‘muffled’ and dull, while with the reference solution and our technique, the consonants are clear and ‘bright’. Therefore, as clearly demonstrated, our method achieves competitive accuracy with the reference while consuming 12 times less memory. The reference solution takes 365 minutes to compute, our technique with FFTW takes 31 minutes and

our technique with GPU FFT takes about 4 minutes.

4.3.3 House Scene

It is a physically-observed phenomenon that lower frequencies tend to diffract more around an obstacle than higher frequencies. To illustrate that the associated gradual variation in intensity is actually observed with my method, I modeled a House scene, shown in Figure 4.5. Please listen to the accompanying video to listen to the corresponding sound clip. Initially, the listener is at the upper-right corner of the figure shown, and the sound source at the lower-left corner of the scene. The source is placed such that initially, there is no reflected path from the source to the listener. As the listener walks and reaches the door of the living room, the sound intensity grows gradually, instead of undergoing an unrealistic discontinuity as with geometric techniques which don't account explicitly for diffraction. This shows qualitatively that diffraction is captured properly by our simulator.

The dimensions of the House are $17m \times 15m \times 5m$ and the simulation was carried out till 2kHz. The wall reflectivity was set to 50%. The acoustic response was computed for .4 seconds. The total simulation time on this scene for the reference is about 3.5 days, 4.5 hours with our technique using FFTW and about 24 minutes with our technique using GPU FFT. The simulation takes about 700 MB of memory with our technique. This corresponds to speedups of about 18x due to algorithmic improvements and an additional 11x due to using GPU FFT.

To validate the diffraction accuracy of my simulator, the source and listener were placed as shown in Figure 4.5, such that the dominant path from the source to the listener is around the diffracting edge of the door. The middle of the figure shows a comparison of the frequency response (FFT of the Impulse Response) at the listener location, between the reference (FDTD on a fine mesh with $s=10$ samples per wavelength) and our solution. Note that both responses have a similar downward trend. This corroborates with the

physically observed fact that lower frequencies diffract more than higher frequencies. Also, the two responses agree quite well. However, the slight discrepancy at higher frequencies is explained by the fact that there are two partition interfaces right at the diffraction edge and the corresponding interface errors result in the observed difference. Referring to Figure 4.5, observe that our method takes 12x less memory and 200x less computation than the reference to produce reasonably accurate results.

4.3.4 Cathedral Scene

As the largest benchmark, I ran my sound simulator on a Cathedral scene (shown in Figure 1.4) of size $35m \times 26m \times 15m$. The simulation was carried out till 1kHz. The impulse response was computed for 2 seconds with absorptivity set to 10% and 40%, consuming less than 1GB of memory with our technique. I could not run the reference solution for this benchmark because it would take approximately 25GB of memory, which is not available on a desktop systems today, with a projected 2 weeks of computation for this same scene. The running times for this case are: 2 weeks for the reference (projected), 14 hours with our technique using FFTW and 58 minutes with our technique using GPU FFT. This scenario highlights the memory and computational efficiency of our approach, as well as a challenging case that the current approaches cannot handle on desktop workstations. Figure 4.6 shows the rectangular decomposition of this scene. Observe that our heuristic is able to fit very large rectangles in the interior of the domain. The main advantage of our approach in terms of accuracy is that propagation over large distances within these rectangles is error-free, while an FDTD implementation would accumulate dispersion errors over all cells a signal has to cross. The bottom of the figure shows the impulse response of the two simulations with low and high absorptivity in dB. Note that in both cases, the sound field decays exponentially with time, which is as expected physically. Also, with 40% absorption, the response decays much faster as compared to 10% absorption, decaying to -60 dB in 0.5 seconds. Therefore in the

corresponding video, with low absorption, the sound is less coherent and individual notes are hard to discern, because strong reverberations from the walls interfere with the direct sound. This is similar to what is observed in cathedrals in reality.

Also note that my technique is able to capture high order reflections, corresponding to about 30 reflections in this scene. This *late reverberation* phase captures the echoic trail-off of sound in an environment. Geometric techniques typically have considerable degradation in performance with the order of reflections and are therefore usually limited to a few reflections. My technique is able to capture such high order reflections because of two reasons: Firstly, because it is a numerical solver which works directly with the volumetric sound field and is thus insensitive to the number of reflections. Secondly, as discussed in Section 4.3.2, our technique has very low numerical dispersion and thus preserves the signal well over long distances. For 30 reflections in the Cathedral, the signal must travel about 600 meters without much dispersion. As discussed earlier, with FDTD running on the same mesh, the signal would be destroyed in about 20 meters.

4.4 Conclusion and Future Work

I have presented a computation- and memory-efficient technique (ARD) for performing accurate numerical acoustic simulations on complex domains with millions of cells, for sounds in the kHz range. My method exploits the analytical solution to the Wave Equation in rectangular domains and is at least an order of magnitude more efficient, both in terms of memory and computation, compared to a reference (2,6) FDTD scheme. Consequently, my technique is able to perform physically accurate sound simulation, which yields perceptually convincing results containing physical effects such as diffraction. My technique is capable of performing numerical sound simulations on large, complex 3D scenes, which, to the best of our knowledge, was not previously possible on a desktop computer.

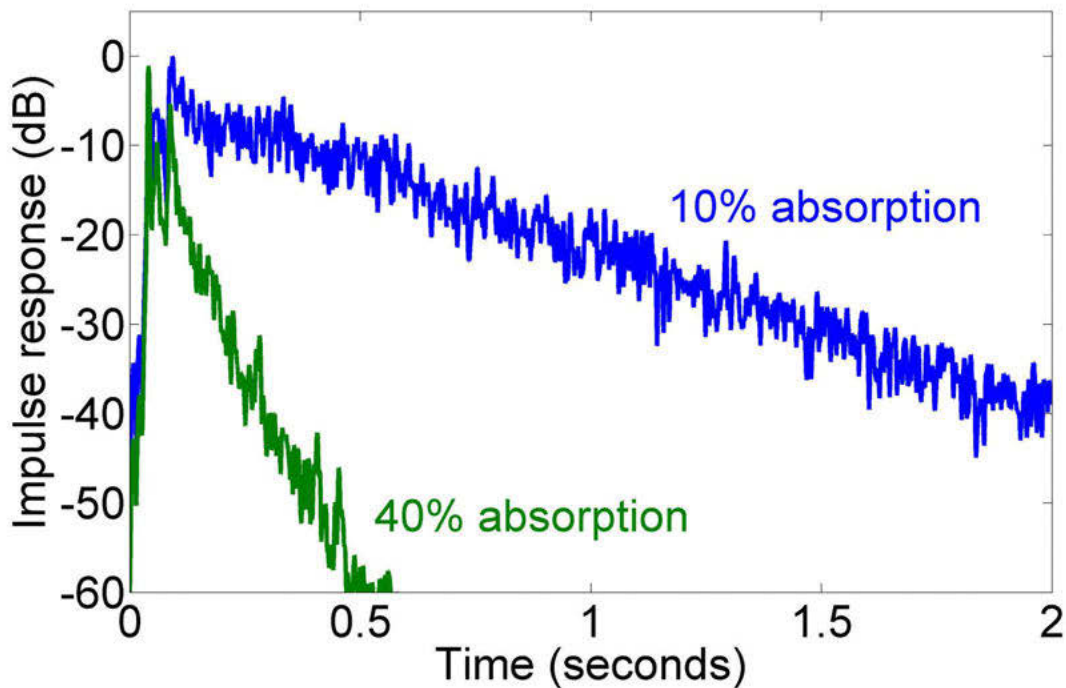
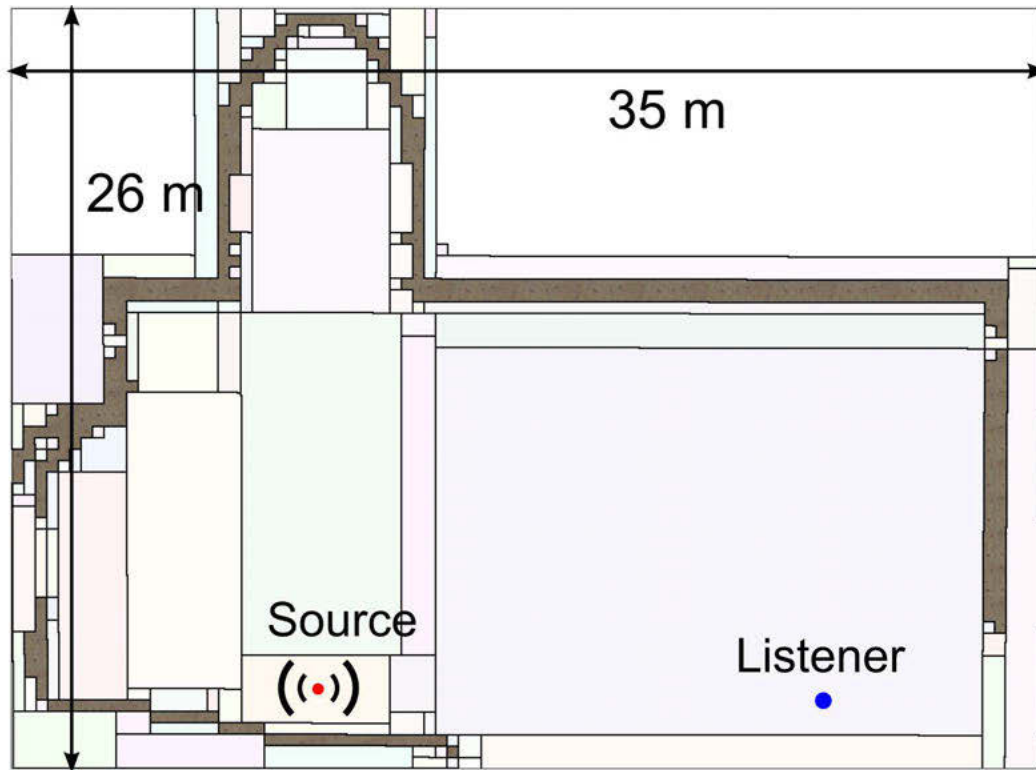


Figure 4.6: The voxelization and rectangular decomposition of the Cathedral scene. Varying the absorptivity of the Cathedral walls directly affects the reverberation time. Note that my technique is able to capture all reflections in the scene, including late reverberation. The impulse responses shown above correspond to high order reflections, in the range of 30 reflections, which would be prohibitively expensive to compute accurately for geometric approaches.

One of the areas where this implementation may be improved is to add a fine-grid simulation, possibly based on FDTD, near the boundary to reduce boundary reflection errors. Another important improvement would be the addition of support for frequency-dependent absorption at the scene boundary, which is quite important acoustically. It might be possible to address both these problems at once by utilizing the recent work by Savioja et. al. [90]. This technique uses the interpolated wideband FDTD (IWB-FDTD) scheme [49] to control numerical dispersion. It is shown that digital impedance filters [49] can be integrated with this technique, making it capable of handling frequency-dependent absorption. Thus, one can imagine ARD running strictly in the interior of the domain on a coarse grid, while the IWB-FDTD technique is used on a fine grid near the boundary. Such an integration would retain computational efficiency, since the fine grid is confined to a region proportional to the surface area of the scene, while resulting in simulations with much more accurate boundary treatment – the finer grid would ensure reduced stair-casing errors and digital impedance filters would capture frequency-dependent reflections.

For the foreseeable future it seems that even after the increase in computational and memory efficiency with the ARD approach, numerical approaches will not be feasible for large 3D scenes for the full audible range till 22kHz. It is interesting to note in this context that geometric and numerical approaches are complimentary with regard to the range of frequencies they can simulate efficiently – with geometric approaches it is hard to simulate low-frequency wave phenomena like diffraction because they assume that sound travels in straight lines like light, while with numerical approaches, simulating high frequencies above a few kilohertz becomes prohibitive due to the excessively fine volume mesh that must be created. Thus, a hybridization of the two techniques, once numerical techniques can be stretched to work till roughly 4kHz, seems like the best alternative. Above 4kHz, diffraction won't be a concern for most scenes and ray-tracing based geometric techniques would work very well. This goal of 4kHz for numerical

approaches seems to be in reach within a few years for scenes with dimensions similar to typical concert halls. ARD is already capable of working till about 1kHz on such scenes. For handling sounds till 4kHz, $(4kHz/1kHz)^4 = 256$ times the computation is needed. This can be achieved by a combination of improving ARD's numerical characteristics to work for even coarser meshes. However, this would offer limited advantage because ARD already operates quite close to the Nyquist limit. Another promising direction would be by exploiting the computational power of Graphics Processing Units (GPUs) and move all stages of the ARD pipeline to GPUs. I am currently part of such an exploration and promising speedups of nearly ten times have already been reported [57].

Chapter 5

Interactive Sound Propagation

The previous chapter focused on an efficient technique I have developed to perform band-limited wave-based acoustic simulations on realistic spaces. The amount of data generated by a typical numerical simulation is very large, typically ranging in tens of gigabytes, for simulation from a single source location. Allowing for moving sources requires sampling from hundreds or thousands such source locations, which clearly makes the memory requirements intractable. The aim of this chapter is to describe a technique and associated system I have developed that can use these numerical simulations as a pre-processing step to allow interactive auralizations with moving sources and listener in an arbitrary 3D environment. This capability requires efficient techniques that exploit human auditory perception such that the runtime memory usage and performance are affordable for interactive applications. Also, it also achieves the desirable goal that the pre-processing time is usually limited to a few hours on today's desktop systems, which could otherwise range into days with standard finite-difference time-domain techniques. The chapter is organized as follows: First I discuss the perceptual properties of reverberant spaces. This is intricately related to research in the area of room acoustics which is a vast area in itself. My focus is only on the parts that are directly relevant to my work. In Section [5.2](#), I give a detailed description of my technique that extensively uses these perceptual observations to post-process and store the results of numerical simulations

in an intuitive and compact representation. In Section 5.3, I describe the interactive sound rendering system I have developed and the underlying techniques for utilizing acoustic data stored in this compact representation for realizing realistic auralizations allowing multiple moving sources and listener. Finally, in Section 5.4, I describe the results obtained with my technique.

5.1 Perception in Acoustic Spaces

Sound propagation in an arbitrary acoustic space from a source location, p_s , to a receiver location, p_r , is completely characterized by the corresponding acoustic *impulse response* (IR), defined as the sound received at p_r due to an ideal Dirac-delta impulse emitted at p_s . The propagated result of an *arbitrary* source sound is then found by convolving it with this IR. Simulating and storing IRs at all possible sample pairs, p_s and p_r , is prohibitively expensive. I attack this problem by exploiting human perception, based on established ideas in room acoustics [51]. This analysis breaks IRs down into two distinct time phases: early reflections (ER) followed by late reverberation (LR). I briefly discuss each below.

Note that the propagated sound received by a human listener depends both on the scene’s IR and on the original sound emitted at the source. A listener does not perceive the acoustic IR directly. Nevertheless, a specific IR usually leads to perceptible characteristics when applied to a wide variety of source sounds, prompting the shorthand “The IR sounds like this.” The more impulsive the source sound, the more it generally reveals about the scene’s acoustic response, but the perceptual effect of even a continuous source sound like music is substantially changed by propagation.

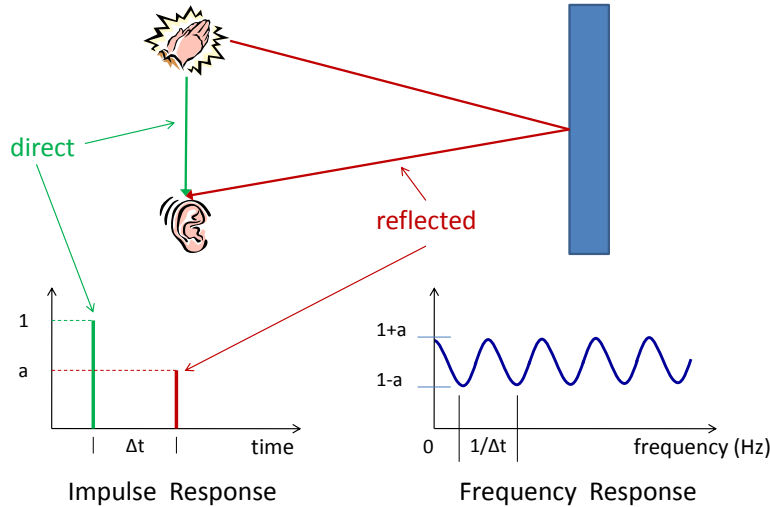


Figure 5.1: **Impulse response (IR)** and corresponding **frequency response (FR)** for a simple scene with one reflection.

5.1.1 Early Reflections (ER)

The ER phase is characterized by a sparse set of high-amplitude pressure peaks, and captures position-dependent variation in loudness, spectral coloration and echoes. Consider the scene shown in Figure 5.1. The scene’s propagated response can be examined in two ways: in the time domain, as the impulse response shown on the bottom-left in Figure 5.1, and equivalently, in the frequency domain, as the complex *frequency response* (FR) whose magnitude is shown on the bottom-right. The IR is a set of two impulse peaks, separated in time by Δt . Assuming the amplitudes of the peaks to be 1 and a , the FR is a comb-filter that oscillates between $1 + a$ and $1 - a$ with “between-teeth” bandwidth of $1/\Delta t$.

When Δt is above 60-70ms, known as the “echo threshold” [53], we perceive a distinct echo, especially for impulsive sources. If the delay is much smaller, the peaks fuse in our perception resulting in no distinct echo. However, the corresponding FR’s between-teeth bandwidth, which is equal to $1/\Delta t$, increases as Δt is reduced, and our auditory system is able to extract the resulting selective attenuation of frequencies. The result is perceived as a comb-filtered, “colored” sound. The most dramatic example this phenomenon of

coloration is in small spaces with smooth reflective surfaces, such as an office corridor or shower.

Following [51, p. 203], if the delay is larger than 20-25ms (FR between-teeth bandwidth less than 50Hz), coloration becomes inaudible due to our auditory system’s limited frequency discrimination [40]. I thus assume that errors in peak delays and amplitudes are tolerable as long as they preserve FR features up to a resolution of 50Hz. Between these thresholds (25ms-60ms), our perception transitions from coloration to echoes, leading to “rough” sounds.

ERs in real scenes are determined by numerous interactions with the boundary. In an empty room, the ER has low temporal density and audible coloration. In a furnished room, sound is scattered more highly, yielding an ER with dense, smaller peaks and leading to a warmer sound. The ER also depends on occlusion, as the sound field diffracts around obstacles leading to spatial variation in its loudness and frequency response.

5.1.2 Late Reverberation (LR)

After undergoing many boundary interactions, the sound field enters the LR phase, becoming dense and chaotic in time and space. The LR between any source and receiver consists of numerous small-amplitude peaks. These peaks are not individually perceived, only their overall decay envelope, which causes reverberations to fade out over time. The decay curve stays largely constant within a room [51, p. 209] and depends on its global geometry.

An important feature of my approach is that it directly simulates the LR, and so captures its decay curve automatically from scene geometry. This is possible because numerical simulation scales linearly in simulated time duration and is insensitive to the order of boundary interactions. Computing the LR from scene geometry also ensures that the ER and LR match, preserving realism. The LR is characterized by peak density:

1000 peaks per second indicate a fully-developed LR phase [34]. I use a value of 500 peaks per second as the LR’s onset.

5.2 Acoustic Precomputation

The precomputation begins by running an *LR probe* simulation, which places a source at the centroid of each room in the scene as described in Section 5.2.2. These LR simulations determine the time at which the ER phase transitions to the LR phase, denoted T_{ER} . T_{ER} depends on the room size. Larger spaces require more time for the sound field to become stochastic; i.e., to reach the required peak density. This is detected automatically by processing on the LR probe data and taking the maximum over all rooms in the scene. For the scenes I have experimented with, values of 50-200ms are obtained.

In many applications, the listener’s position is more constrained than the sources’. This can be exploited to reduce memory and preprocessing time. Uniform samples are placed over a region representing possible locations of the listener at runtime, but are considered as sources in the precomputed simulation. The principle of acoustic reciprocity means that we can reverse the simulated sense of source and listener at runtime. Simulations are then run over multiple source positions, p_s , for time length T_{ER} , to record the spatially-varying ER impulse response (ERIR). For each source, the resulting time-varying field is recorded at samples, p_r , uniformly distributed over the entire 3D scene volume. Each source and receiver sample generates a time-varying sound signal, $s(t)$, which is then processed as described in Section 5.2.3 to extract its relevant content and yield a compact result.

5.2.1 Numerical Simulation

I utilize the ARD numerical acoustic simulator I have developed. It is fast yet still able to propagate an input signal over long distances and many reflections without distorting the waveform due to numerical dispersion errors that arise in finite difference approaches. This is crucial in subsequent processing – dispersion introduces artificial ringing and leads to the detection of spurious peaks during the peak detection phase, which I will describe later. Such spurious peaks would be interpreted as separate physical reflections, generating errors in the final auralization.

Input to the simulator is the room geometry, absorption parameters (potentially varying per surface triangle), grid resolution, source reference signal, and source location. The simulator then generates the resulting sound at each time-step and at all grid cell centers in 3D. A single run of the simulator thus captures the whole room’s acoustic response at every possible listener location, from a fixed source location. Currently, my simulator models spatially-varying but not frequency-dependent sound absorption. Including frequency-dependent absorption requires modifications to the ARD simulator, as discussed in Section 4.4 and would lead to more realistic auralizations, without affecting the approach presented here.

The reference input signal propagated from the source location is a Gaussian pulse of unit amplitude, given by:

$$G(t) = \exp\left(-\frac{(t - 5\sigma)^2}{\sigma^2}\right), \quad (5.1)$$

where $\sigma = (\pi\eta_f)^{-1}$ and η_f is the simulation’s frequency limit, typically 1000Hz. This function’s Fourier transform is a broadband Gaussian spanning all frequencies from 0 to η_f .

Bandlimited simulation To keep preprocessing time and storage manageable, the simulation frequencies are limited up to η_f . A practical limit used in most of the examples is $\eta_f = 1000\text{Hz}$, with a corresponding grid resolution of about 10cm. Information at higher frequencies must be extrapolated. This limitation of the precomputation becomes less of a problem as computational power increases; the run-time supports the results of higher-frequency simulation without change or additional cost. Frequencies in the range 100Hz to 5000Hz are most important perceptually for room acoustics [51, p. 27]. Though humans can hear higher frequencies, they quickly attenuate in air and are highly absorbed by most surfaces.

The simulation’s frequency gap between 1kHz and 5kHz yields two major types of error. First, it limits the time resolution at which peaks can be separated to $500\mu\text{s}$. Merging a high-amplitude peak with another, which follows closer than this limit eliminates coloration effects. The auralizations thus neglect some high-frequency coloration. Second, diffraction information is unavailable beyond 1kHz. My method for extrapolating the frequency trend in Section 5.2.3 produces a plausible, natural-sounding result in this gap.

Spatial sampling The spatial accuracy at which we perceive sound fields is limited. A human head acts as a diffractive occluder which destroys interference patterns at smaller spatial resolution. I thus speculate that its size ($\sim 10\text{cm}$) is a guide to the smallest sampling resolution required for convincing auralization in typical scenes. To my knowledge the question is an open research problem.

My simulator generates spatial samples for the receiver near this resolution, but I further downsample them by a factor of $8\times$ in each dimension to reduce run-time memory requirements. Typical receiver grid resolution is about 1m. Using the interpolation method proposed in the next section, subsampled IRs still provide perceptually artifact-free results without clicks or gurgling, as demonstrated in the accompanying video (link

given in Section 5.4). The sound field changes convincingly as the sources and listener move around obstructions. Increasing spatial resolution would use more memory but would not significantly affect runtime performance, since the expense is dominated by FFTs rather than spatial interpolation.

5.2.2 LR Processing

The purpose of the LR probe simulation is to compute the duration of the ER phase, T_{ER} , and the LRIR. A peak detector is run on the simulated probe response to generate a set of peak delay/amplitude data, $\{t_i, a_i\}$, sorted on delays, t_i . This is shown in the upper right of Figure 5.2. Simulations bandlimited to 1kHz imply a quantization of peak delays at roughly $500\mu s$. Such quantization can introduce artificial periodicities and lead to audible but false coloration. The peak times are perturbed by a random value in the range -500 to $+500\mu s$. Any periodicities above a few milliseconds, including “fluttering” effects in the LR, are still preserved.

Peak detection A straightforward algorithm is used to for peak detection in my technique. It scans the time-dependent signal for maxima and minima by comparing each value with both its neighbors. Detected signal extrema are recorded in terms of their time and amplitude. Such a simple detector is sensitive to noise and would be inappropriate for physically-measured IRs. It works well however on the results of noise-free bandlimited simulations.

LR duration After peak detection, the LR is conservatively truncated when it has decayed by 90dB. The resulting duration, T_{LR} , is calculated as follows. First, the signal’s decay envelope, $d(t)$, is constructed from the peaks detected previously via

$$d(t) = 10 \times \log(a_i^2), \quad t_i \leq t < t_{i+1} \quad (5.2)$$

This operation converts pressure amplitudes to intensities and fills out spaces between peaks. Then, smoothing in time is performed by applying a moving average filter on $d(t)$ of width 40ms. T_{LR} is given by the smallest t such that $d(0) - d(t) > 90$. Peaks with delays beyond T_{LR} are then removed.

ER duration As explained in Section 5.1, T_{ER} is calculated as the time when peak density reaches 500 peaks per second. Starting from time $t = 0$, all peaks within the range $[t, t + 20ms]$ are considered and only those are counted that are within 20 dB of the highest intensity peak in the interval. If the number of such peaks exceeds 500 per second $\times 0.02$ seconds = 10 peaks, this t is recorded as the ER duration. Otherwise, t is increased by 20ms and this is continued until the criterion is satisfied. Since peak density increases with time, this procedure terminates.

Increasing LR peak density Because the simulator is frequency band-limited, it can detect no more than 1000 peaks per second. While this is sufficient for music and voice, it is not for impulsive sources such as gunshots or footsteps, which require roughly 10,000 peaks per second [34]. Following practice in artificial reverberators, peaks are added stochastically to increase the density by a factor of 10. This is done while preserving the decay envelope, as follows.

First, a *densification factor*, $F(t)$, $T_{ER} \leq t < T_{LR}$ is computed as

$$F(t) = 10 \left(\frac{t - T_{ER}}{T_{LR} - T_{ER}} \right)^2. \quad (5.3)$$

$F(t)$ builds quadratically in time from 0 to a terminal value of 10, based on the expected quadratic growth in peak density in physical scenes [51, p. 98]. Next, for each peak $\{t_i, a_i\}$ in the LR after time T_{ER} , $\lfloor F(t_i) \rfloor$ additional peaks are added with amplitudes $a_i \times \text{rand}(-1, 1)$. This preserves the simulated decay envelope and yields the final LRIR for use at runtime.

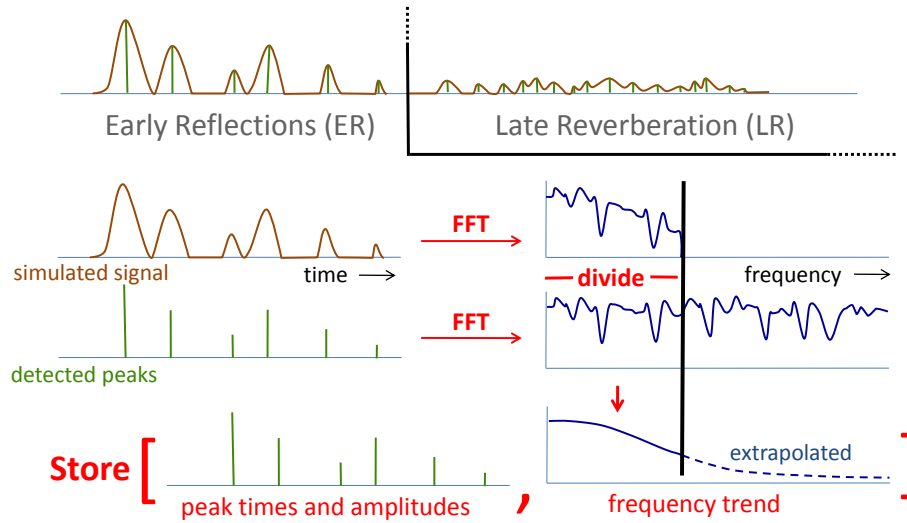


Figure 5.2: **IR encoding.** The late reverberation (LR) filter is stored once per room. The early reflections (ER) filter is represented as a set of peaks and a frequency trend, and stored at each source/listener grid point.

Handling multiple rooms For scenes comprising multiple rooms, LR probe simulations are performed separately and the LRIR stored separately for each room. The user manually marks volumetric scene regions as rooms with enclosing, closed surfaces. An LR probe simulation is run for each of these rooms, as described earlier. ER processing, described in the next section, does not rely on room partitioning but instead operates on the entire scene at once.

5.2.3 ER Processing

At each source and listener location, the simulator produces a propagated signal, $s(t)$, of length T_{ER} . The ERIR can be computed from this signal using straightforward deconvolution. Convolution with input sounds then yields a simple method for runtime auralization. Such a direct approach has three problems: it ignores frequencies above η_f and so muffles sounds, it is difficult to spatially interpolate without producing artifacts, and it uses too much memory. I solve these problems by converting the ERIR to a compact representation having two parts as shown in Figure 5.2: a set of peaks with

associated delays and amplitudes, and a residual frequency response magnitude, called the *frequency trend*. ER peaks capture the main time-domain information such as high-amplitude reflections, as well as coloration effects as described in Section 5.1.1, while the frequency trend accounts for residual frequency-dependent attenuation including low-pass filtering due to diffraction.

Peak information is naturally all-frequency, and so applies to arbitrary inputs without muffling. Only the frequency trend needs to be extrapolated to higher-frequency input signals.

Peak Extraction

A simple method for detecting peaks in the recorded response, $s(t)$, is to run the peak detector introduced in Section 5.2.2. Let's denote this set of peaks as P . First, low-amplitude peaks from P are removed using a threshold of 40dB below the highest-amplitude peak present. Such peaks are masked by the higher energy peaks.

Unfortunately, this method merges peaks separated by less than 1ms, since sums of closely-separated Gaussians have only one extremal point. This can be improved: using results from a simulation bandlimited to 1kHz, it is possible in theory to resolve peaks separated by as little as 0.5ms. The following describes an approach that extracts more information from the simulation in order to preserve coloration effects and simplify later processing to extract the frequency trend. It doesn't guarantee all theoretically-resolvable peaks are detected but provides good results in practice.

The ideal impulse response, $I(t)$, is computed by performing a deconvolution on $s(t)$ with the input signal $G(t)$ given in (5.1). Using \otimes to denote convolution, \odot to denote element-wise complex multiplication, and \hat{x} to denote the Fourier transform of x , the convolution theorem states that

$$s(t) = G(t) \otimes I(t) \Leftrightarrow \hat{s}(f) = \hat{G}(f) \odot \hat{I}(f). \quad (5.4)$$

To solve for the IR I given s and G , deconvolution is performed using a frequency coefficient complex division to obtain

$$\widehat{I}(f) = \frac{\widehat{s}(f)}{\widehat{G}(f)}. \quad (5.5)$$

An inverse FFT on $\widehat{I}(f)$ then yields $I(t)$. Before performing it though, \widehat{I} must be low-pass filtered to eliminate frequencies above η_f , since these are outside the simulator’s range and contain large numerical errors.¹ This can be done by zero-padding the FR vector above η_f up to the target rate of 44.1kHz. It is well-known that such an abrupt zeroing or “brick-wall filtering” leads to ringing artifacts in the time domain and so to fictitious peaks. At the same time, it provides the best possible time resolution for separating peaks.

The problem then is to generate a set of super-resolved peaks P' from $I(t)$ that are guaranteed to be real and not “rings” of earlier peaks, in order to separate high-energy peaks to the fullest possible extent and preserve their audible coloration.

Finding super-resolved peaks P' A bound on ringing error in $I(t)$ can be computed by observing that brick-wall filtering turns an ideal peak into a Sinc function, having a $1/t$ time-decaying amplitude. An error envelope, $e(t)$, can therefore be built against which later peaks in $I(t)$ can be culled to account for “rings” of earlier ones. P' is initialized to contain all peaks detected from the ideal IR, $I(t)$, including rings. Only peaks within 20dB of the highest amplitude one are retained, since we are interested in closely-spaced, high-amplitude peaks that create strong oscillations in the FR.

A ringing envelope, $S(t)$, is then defined as the low-pass filtering result of a unit

¹The reader might wonder why such low-pass filtering was not also applied to the signal $s(t)$ before performing peak detection on it. The reason is that the input source signal $G(t)$ and its response $s(t)$ contain little energy above η_f . It is only when frequency-domain values are divided by each other during deconvolution that a non-negligible result is obtained at higher frequencies, requiring cleanup.

ideal impulse at $t = 0$ to a frequency limit of η_f :

$$S(t) = \begin{cases} 0, & |t| < t_0 \\ |\sin(\omega t)| / \omega t, & t_0 \leq |t| < t_1 \\ 1/\omega t, & |t| \geq t_1 \end{cases} \quad (5.6)$$

where $t_0 = 0.5/\eta_f$, $t_1 = 0.75/\eta_f$, and $\omega = 2\pi\eta_f$. The time t_0 represents the first zero of the Sinc while t_1 represents the following minimum of its negative side lobe. The envelope thus bounds ringing that occurs after a peak's main lobe. If an ideal peak is band-passed, peak detection run on it, and all peaks with absolute amplitudes less than this envelope culled, only the original peak remains.

To build the complete error envelope, $e(t)$, we accumulate these over each peak in $P' = \{a_i, t_i\}$ via

$$e(t) = \sum_i |a_i| S(t - t_i) \quad (5.7)$$

The fact that P' itself contains ringing peaks serves to make the envelope conservative in the sense that in the worst case we may remove a real peak but never fail to remove a ringing peak. Culling is straightforward: a peak (a_i, t_i) is removed if $|a_i| < e(t_i)$.

Supplementing P with P' I use P' to supplement P since multiple peaks in P' may have merged to a single peak in P . This is done by scanning through all peaks in P' and assigning each to the peak in P closest to it in time. Then, each peak in P is replaced with the set of peaks in P' that were assigned to it, yielding the final set of peaks. This automatic procedure generates about $N=20-50$ peaks in all the scenes I have tested.

Frequency Trend Extraction

Peak extraction ignores diffraction and implicitly assumes every peak acts on all frequencies uniformly. Diffraction introduces frequency-dependent filtering not captured by this set of peaks. This residual information is captured by my method of frequency

trend extraction, as illustrated in the middle of Figure 5.2. It compares the simulated FR, $\widehat{I}(f)$, to the FR of the idealized IR composed of the extracted peaks, P , in order to extract any residual low-pass trend due to diffraction. The following description assumes $\eta_f=1\text{kHz}$, the typical frequency limit in this work.

The impulse response corresponding to the extracted ER peaks, I' , is constructed by summing over its peaks via

$$I' = \sum_{i=1}^N a_i \delta(t - t_i) \quad (5.8)$$

where $\delta(t)$ is the discrete analog of the Dirac-delta function – a unit-amplitude pulse of one sample width. Its corresponding FR is denoted \widehat{I}' . The FR of the ideal IR of the original simulation, \widehat{I} , is also constructed, which contains complete information up to frequencies of 1kHz. The overall frequency-dependent diffraction trend for $f \leq 1\text{kHz}$ is obtained via

$$T(f) = \frac{|\widehat{I}(f)|}{|\widehat{I}'(f)|}. \quad (5.9)$$

Before performing this division, both the numerator and denominator are smoothed with a Gaussian of width 50Hz. The unsmoothed $\widehat{I}'(f)$ often has near-zero values; smoothing takes care of this problem and makes the above operation numerically stable. As explained in Section 5.1.1, this has little perceptual impact because we are insensitive to finer details in the magnitude frequency response. $T(f)$ is then smoothed again with the same Gaussian to yield the final frequency trend. Average values of $T(f)$ in each octave band 0-62.5Hz, 62.5-125Hz, ..., 500-1000Hz are then stored.

This trend contains information only up to 1kHz. Fortunately, much of the perceivable diffraction-related occlusion effect in common acoustic spaces manifests itself in frequencies below 1kHz [51]. Sound wavelength for 1kHz is about 34cm, which is comparable to large features such as pillars, doors and windows.

This trend can be plausibly extrapolated to frequencies higher than were simulated.

To do this, $T(f)$ is expressed on a log-log scale, which corresponds to plotting the power at each frequency, in dB, against the frequencies in octaves. These scales better match our loudness and pitch perception. Moreover, the low-pass diffraction trend for physical edges is roughly linear on such a log-log scale for mid-to-high frequencies [98]. A line is then fit to the log-log trend in the frequency range 125-1000Hz. If the slope is negative, indicating a low-pass trend, the line is extrapolated and stored at octave bands higher than 1000Hz up to 22,050Hz. If the slope is positive, extrapolation is not performed; instead the value at the 500-1000Hz octave is just copied into to higher ones.

5.3 Interactive Auralization Runtime

The precomputed, perceptually-encoded information from numerical simulation supports interactive sound propagation from moving sources to a moving listener. My approach performs perceptually-smooth spatial interpolation of the IRs, and then propagates source sounds by convolving them with these IRs. My technique generates realistically dense IRs, and the run-time works in the frequency domain to perform the convolution efficiently. A schematic diagram of my real-time auralization system is shown in Figure 5.3.

5.3.1 Load-time Computation

At load-time, per-room LR filters are loaded and processed. The initial T_{ER} part of the LRIR is zeroed out, to be replaced at run-time with the spatially-varying ERIR. The LRIR's Fourier Transform \widehat{I}_{LR} is then computed and stored, along with its time-domain peaks.

Next, ERIR filters for the whole scene are loaded, yielding a table, $I_{ER}(p_s, p_r)$, where points p_s lie on a 2.5D region of potential listener positions and p_r sample sources over the entire 3D volume of the scene. Note the reversal of sense of source/listener from

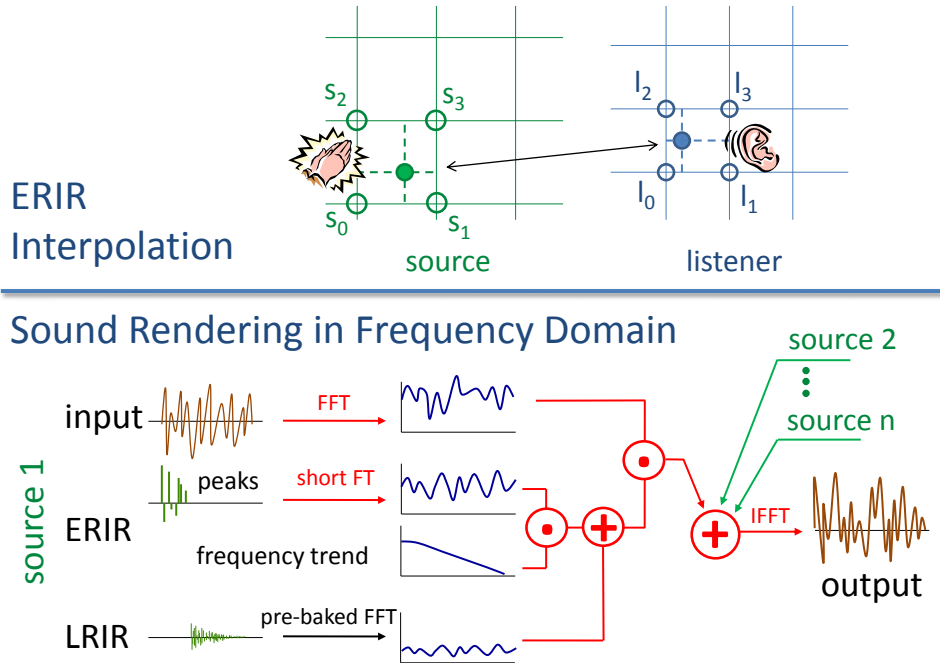


Figure 5.3: **Run-time processing.** Operations computed at run-time are colored red. Processing for only one channel (ear) is shown at figure bottom.

the original simulation, which is justified by acoustic reciprocity. Each sample in the $I_{ER}(p_s, p_r)$ contains a set of peaks with associated delays and amplitudes, and an octave-band frequency trend.

5.3.2 ERIR Interpolation

Spatial interpolation Given the current source and listener locations, p_s and p_r , the ERIR table is indexed and interpolated to reconstruct the ERIR as shown in the top of Figure 5.3. This interpolation is bilinear over p_r and tri-linear over p_s , and so involves 32 point pairs (8 over p_s and 4 over p_r). The result is denoted I_{SL} , and is based on the temporal interpolation described next.

Temporal Interpolation High-quality interpolation of IRs is a challenging problem. Direct linear interpolation (cross-fading) leads to unrealistic oscillations in the sound amplitude and audible “gurgling” artifacts. Each peak represents a wavefront from the

source arriving at the listener. As the listener moves, this peak smoothly translates in time; cross-fading instead generates twin “ghosts” which only modify amplitudes at fixed peak times evaluated at the two spatial samples. Frequency-domain interpolation fails to help because the time and frequency domains are linearly related. Interpolating over the peak delays and amplitudes that are extracted in my technique better matches the physical situation and produces no artifacts in all the experiments performed.

Interpolating between delays and amplitudes of two peaks assumes that they correspond; i.e., belong to the same propagating wavefront. The finite speed of sound dictates that the peaks from the same wavefront at two points in space separated by a distance Δd can be separated in time by no more than

$$\Delta t \leq \frac{\Delta d}{c}, \quad (5.10)$$

where Δd is the spatial sampling distance (1m) and c is the speed of sound in air, 343m/s at 20°C. The following procedure computes correspondences and achieves convincing interpolation.

Denote the peak sets of the two IRs as P_1 and P_2 , and assume both are sorted over peak times t_i . Construct a graph whose edges represent potential correspondence between a peak in P_1 and a peak in P_2 ; in other words, the difference between peak times satisfies (5.10). Edge weight is assigned the absolute value of the peaks’ amplitude difference. The algorithm iterates greedily by selecting the edge of smallest weight currently in the set, finalizing it as a correspondence, and removing all other edges sharing either of the two peaks selected. The operation is commutative in P_1 and P_2 and interpolates associated peak delays and amplitudes, yielding a perceptually smooth auralization for moving sources and listener.

In addition to peaks, the ERIR’s frequency trend must also be interpolated. In this case, straightforward linear interpolation of amplitudes in each octave band works well.



Figure 5.4: Scenes used for auralization tests.

5.3.3 LRIR Scaling

The overall propagation IR combines the interpolated ERIR between the source and listener, I_{SL} , with the room’s LRIR, I_{LR} . My technique currently chooses the LRIR of the room in which the source lies. This approach yields good results in practice but could be extended in future work [96]. Since convolutions are already performed in the frequency domain, chains of IRs from multiple rooms can be computed by element-wise complex multiplication, so such an extension would not incur much run-time cost. To make a natural-sounding transition between ERIR and LRIR (at time T_{ER}), the LRIR must be scaled properly.

The LRIR’s scaling factor is calculated by first computing the RMS peak amplitude of the ERIR during the time interval $[t_0 + 5ms, T_{ER}]$, where t_0 is the time of the first peak in the ERIR. The result, denoted A_{ER} , discards the first (direct) peak and any that closely follow it. Also, the LRIR’s maximum absolute peak amplitude in $[T_{ER}, 2T_{ER}]$ is computed, yielding A_{LR} . Finally, the LRIR’s attenuation from the frequency trend is accounted for; this is done by computing the mean of amplitudes over all the ERIR’s frequency bins, yielding F_{ER} . The final scaling factor is given by

$$\beta_{LR} = \frac{A_{ER} F_{ER}}{A_{LR}}. \quad (5.11)$$

This scaling is then applied to the LRIR’s frequency response, \hat{I}_{LR} computed during load-time, before adding it to the ERIR.

5.3.4 Binaural Processing

Human auditory perception is binaural; that is, based on two ears. This allows us to estimate direction and distance to sound sources, a capability known as *localization* [10]. Ideally, this requires augmenting each peak in the ERIR with information about the corresponding wavefront gradient; i.e., the direction in which the sound is propagating. It may be possible to extract such information from simulation, but its calculation is challenging. This is especially true because my technique exploits reciprocity, which might require tracking simulated wavefronts all the way back to their sources.

Fortunately, a well-known property of localization is the “precedence effect”, also known as the “law of the first wavefront”, which states that our perception of the direction to a source is determined almost exclusively by the first arriving sound. My technique therefore assign to the first peak the direction from source to listener, and the remaining peaks to random directions. Each peak in I_{SL} is processed depending on its assigned direction and two ERIRs generated for the left and right ear respectively, I_{SL}^{left} and I_{SL}^{right} .

Binaural perception is sensitive to the exact geometry of the individual listener’s ears, head and shoulders, which can be encapsulated as his *head-related transfer function* (HRTF). Non-individualized HRTFs can lead to large errors in localization [41]. My system is easily extensible to customized HRTFs and supports them with little additional run-time cost. To avoid the complexity and present results to a general audience, I currently use a simple model [41], based on a spherical head and cardioid directivity function.

5.3.5 ERIR Short Fourier Transform

To perform convolutions, the left/right ERIRs, I_{SL}^{left} and I_{SL}^{right} , are transformed to the frequency domain. This processing is identical for both; I simplify notation by referring to the ERIR as I_{SL} . Denote the number of audio time samples in the ER and LR

phases as N_{ER} and N_{LR} , respectively. $T_{ER} \ll T_{LR}$ and so $N_{ER} \ll N_{LR}$. Because the ERIR and LRIR are later added in the frequency domain before convolving with the source signal, a straightforward approach is to perform an FFT of length N_{LR} on I_{SL} . However, it contains only zeros beyond sample N_{ER} . Zero-padding a signal in the time-domain corresponds to interpolating in the frequency domain, a fact I exploit to reduce computation. A short FFT on I_{SL} of length $4N_{ER}$ is performed and then the resulting frequency coefficients are upsampled by a factor of $N_{LR}/4N_{ER}$. The interpolation filter used is a Sinc truncated at the fifth zero on either side, multiplied by the Lanczos window. These choices of intermediate buffer size ($4N_{ER}$) and windowing function reduce FFT wrap-around effects enough to avoid ghost echoes.

The same idea can be applied to compute the Fourier transform on audio buffers representing each input sound source. Overall, all required per-source FFTs are reduced from length N_{LR} to $4N_{ER}$, a speedup of 2-4 \times compared to the straightforward approach.

5.3.6 Auralization

Audio processing is done in fixed-sized buffers at a constant sampling rate. The size of FFTs is clamped to the longest LR filter over all rooms. For each source, a sample queue is maintained in which buffers are pushed from the front at each audio time step. The input sound signal for the i -th source is denoted $u_i(t)$. Refer to Figure 5.3 for the overall organization of the auralization pipeline.

Processing begins by performing an FFT on the current buffer for the source sound, u_i , yielding the transformed signal \hat{u}_i . Next, the interpolated ERIR, I_{SL} , is computed based on the current source and listener locations as discussed in Section 5.3.2. The LRIR is accessed depending on the room containing the source, and its scaling factor β_{LR} computed as described in Section 5.3.3. Binaural processing from Section 5.3.4 is performed to yield ERIRs for the two ears, I_{SL}^{left} and I_{SL}^{right} . These are transformed to the

frequency domain as described in Section 5.3.5, and the scaled LRIRs added to yield

$$\begin{aligned}\hat{I}^{\text{left}} &= \hat{I}_{SL}^{\text{left}} + \beta_{LR} \hat{I}_{LR}, \\ \hat{I}^{\text{right}} &= \hat{I}_{SL}^{\text{right}} + \beta_{LR} \hat{I}_{LR}.\end{aligned}\tag{5.12}$$

The source signal is then efficiently convolved in the frequency domain, yielding the propagated versions of this sound for each ear:

$$\begin{aligned}\hat{v}_i^{\text{left}} &= \hat{I}^{\text{left}} \odot \hat{u}_i, \\ \hat{v}_i^{\text{right}} &= \hat{I}^{\text{right}} \odot \hat{u}_i.\end{aligned}\tag{5.13}$$

In this way, contributions are accumulated from all sources in the frequency domain, at each ear. The final result is transformed back to the time domain using two inverse FFTs:

$$\begin{aligned}v^{\text{left}} &= \text{FFT}^{-1} \left(\sum_i \hat{v}_i^{\text{left}} \right), \\ v^{\text{right}} &= \text{FFT}^{-1} \left(\sum_i \hat{v}_i^{\text{right}} \right).\end{aligned}\tag{5.14}$$

The first audio buffers for v^{left} and v^{right} are then sent to the sound system for playback. Between consecutive buffers in time, linear interpolation is performed within a small (5%) window of overlap.

5.4 Implementation and Results

My system is implemented in C++ and uses the Intel MKL library for computing FFTs. Vector operations are optimized using SSE3. Performance was measured on a 2.8 GHz Quad-core Intel Xeon processor, with 2.5 GB RAM. I have intentionally ensured that the entire sound engine runs inside one thread on a single core, mirroring the practice

Scene	Dim. (m)	$\eta_f(Hz)$	#ERL	#ERS	#R	ST
walkway	19×19×8	1000	1.5M	100	1	120min
living room	6×8×3	2000	4.9M	129	1	75min
Citadel	28×60×32	1000	1.7M	155	6	350min
train station	36×83×32	500	1.1M	200	3	310min

(a) Precomputation

Scene	Mem.	T_{ER}	T_{LR}	#S	ABT
walkway	600MB	70ms	1100ms	1	1.7ms
living room	1000MB	45ms	250ms	2	1.8ms
Citadel	620MB	80ms	1900ms	8	27.2ms
train station	390MB	200ms	2600ms	~15	60ms

(b) Runtime

Table 5.1: **Performance statistics.** Tables (a) and (b) show performance numbers for precomputation and runtime stages, respectively, for the four different scenes used for auralization tests. Abbreviated column headings are as follows. **Precomputation:** “Dim.” is the scene dimensions. “#ERL” is the simulated number of ER listener probes (before downsampling). “#ERS” is the simulated number of ER source probes. “#R” is the number of rooms in the scene. “ST” is total simulation time, including LR and ER probes. **Runtime:** “Mem.” is the total memory used for all source and receiver positions, including extracted peaks and frequency trend. T_{ER} is the length of the ER phase, and T_{LR} the LR phase, maximized over all rooms in the scene. “#S” is the number of different sources simulated at run-time. “ABT” is the total time needed to process each audio buffer, summed over all run-time sources.

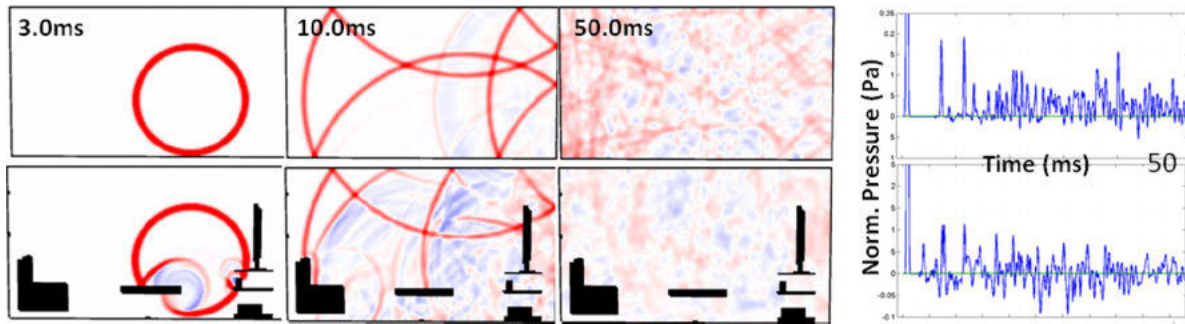


Figure 5.5: **Sound scattering and diffusion in the living room scene.** The top row shows an empty room while the bottom row is fully-furnished. The left three columns show a 2D slice of the sound field generated by a Gaussian impulse emitted near the room’s center, while the right column shows the entire IR at a single receiver point placed at the source location. Red/blue represents positive/negative pressure in the sound field. Black areas represent solid geometry in the scene. Note the large difference in wave propagation in the two scenes because of scattering and diffraction. Refer to the video (link given in Section 5.4) for comparative auralizations.

in interactive applications such as games. Precomputation and run-time statistics are summarized in Table 5.1. In all examples, the preprocessing time is dominated by the numerical simulation; the perceptually-based encoding is comparatively negligible.

The accompanying video shows real-time results collected from my system, and a demonstration of integration with Valve’s Source™ game engine. The video can be found at the following website: <http://gamma.cs.unc.edu/PrecompWaveSim>, or alternatively, in the supplemental material archive at the ACM portal: <http://doi.acm.org/10.1145/1778765.1778805>.

Geometry input to the acoustic simulator is exactly what is shown rendered in each video segment. No manual simplification is performed. Audio buffer length in the system is 4096 samples, representing about 100ms at a sample rate of 44.1kHz. The system takes 1.7-3.5ms per source for every audio buffer, which allows about 30 moving sources and a moving listener in real time. The sound engine utilizes XAudio2 for buffer-level access to the sound-card.

5.4.1 Living room

My technique handles complex scenes like the furnished living room shown in Figure 5.4a. Scattering off furnishings has a noticeable effect on a room’s acoustics. Figure 5.5 compares visualizations of the sound field in a 2D slice of this scene, between the furnished room and an empty version with all interior objects and carpet removed. In the empty room, specular wavefronts dominate the sound field and substantial energy still remains after 50ms. In the furnished room, the greater scattering and larger absorbing surface area more quickly reduce the sound field’s coherence and energy. Refer to the accompanying video to hear the difference. The right column of the figure plots pressure as a function of time at a single receiver location. The empty room’s IR is dominated by high, positive-amplitude peaks, while the furnished room’s contains negative pressure peaks due to diffraction at geometric discontinuities and more closely resembles a real room’s response qualitatively.

5.4.2 Walkway

Figure 5.4b shows an outdoor scene designed to demonstrate various acoustic effects. Scene surfaces are all highly reflective with a pressure reflection coefficient of 0.95. Specular reflections from the walls and lack of scattering yield a fairly long $T_{LR}=1.1s$, with a characteristic hollow reverberation due to the parallel walls and lack of intervening geometry. The walkway’s concave ceiling (blue) focuses sounds, so that they become louder when the source and receiver both move below it. Occlusion effects are also important in this scene because diffraction is the only major source of energy transport behind the walls. The sound loudness changes realistically and smoothly as the listener walks behind a wall separating him from the source, and demonstrates a convincing diffracted shadowing effect. Refer to the video for the auralization.

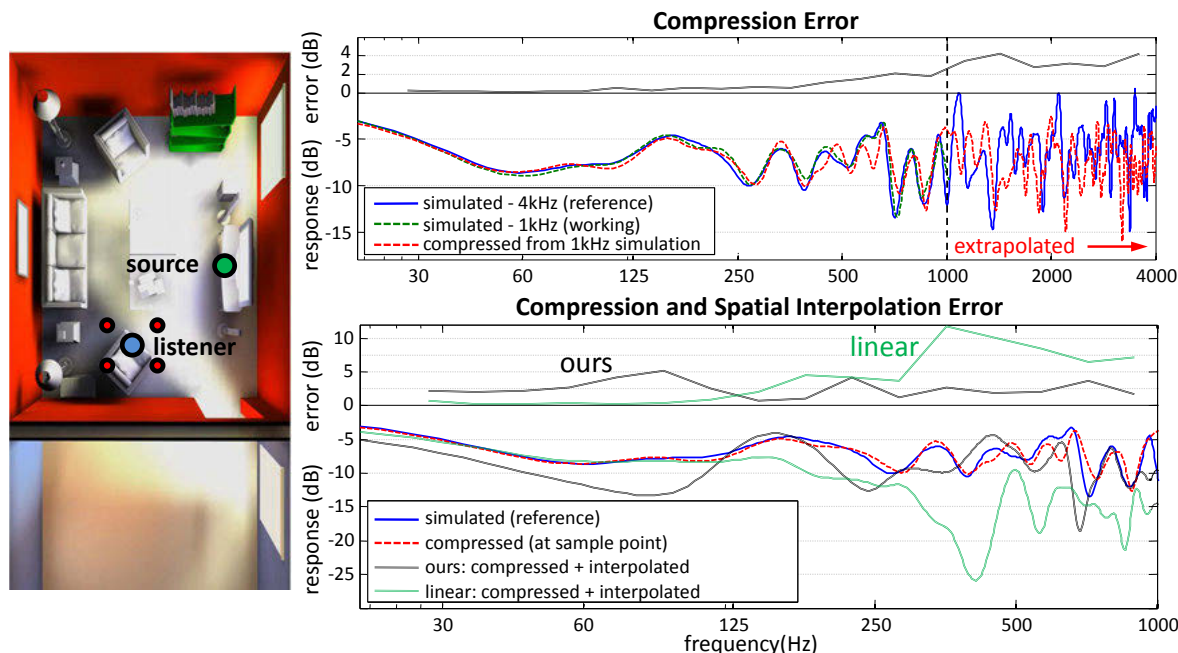


Figure 5.6: **Error analysis of my technique in the living room scene**, at the source/listener points shown on the left. The top graph isolates errors from IR parametrization (peaks and frequency trend) alone, while the bottom graph accounts for interpolation as well, at a point midway between listener samples (red dots on left). The error between the approximated response with my technique and the reference appears in the top part of each plot. The bottom graph also compares linear interpolation (green curve) against my method (black curve). Linear interpolation produces more error overall and incorrectly attenuates higher frequencies.

5.4.3 Citadel

Figure 5.4c shows a larger scene taken from the “Citadel” scene of Half Life 2. Sound sources include a walking narrator, his footsteps, as well as other sources both fixed and moving within the environment. Realistic, spatially-varying acoustic propagation is captured automatically from scene geometry, including a varying LR, and is especially dramatic as the narrator moves from a large room into a narrow corridor. Interesting reverberation is produced in the largest room because of its high ceiling, which causes it to “flutter” especially audible for impulsive sounds.

5.4.4 Train station

Figure 1.5 shows a frame from the game Half-Life 2™, with which I have integrated my sound engine. I have written a game “mod” that broadcasts all in-game sound events over a pipe to my sound engine running in a separate process. Sound events include information about the WAV file played as well as the source/listener locations. The engine then uses this information to propagate sounds in the scene, based on precomputed results over the scene, without requiring any access to the scene geometry at runtime. My system can handle up to 15 sources in real time on this scene, including the game’s ambient sounds as well as main source sounds, such as gunshots, footsteps and voices. Refer to the accompanying video for acoustic results and a comparison of my engine’s sounds with the original game’s with its “sound quality” set to “high”.

5.4.5 Error Analysis

To validate my approach, I have compared it against a reference numerical simulation bandlimited to a higher frequency of 4kHz. This tests the three sources of error in my approach: the simulation’s frequency limit, my perceptually-based parametrization scheme, and spatial interpolation of IRs. The comparison was done on the fully furnished living room. The IR from the numerical simulator was convolved directly with the input sound for producing the reference output. My system’s sound closely matches the reference; refer to the accompanying video for the audio comparison.

Figure 5.6 quantitatively analyzes error in the same scene. Errors are calculated in third-octave bands with respect to a 4kHz reference simulation. Frequency responses for decoded result with my technique based on a bandlimited working simulation (1kHz) are compared to this reference. The top graph shows errors due to compression alone, by placing the listener on a simulation grid point and avoiding interpolation. Below the simulated frequency limit of 1kHz, error with my technique stays within 2 dB of the reference and increases only moderately to 4 dB in the extrapolated range. Including

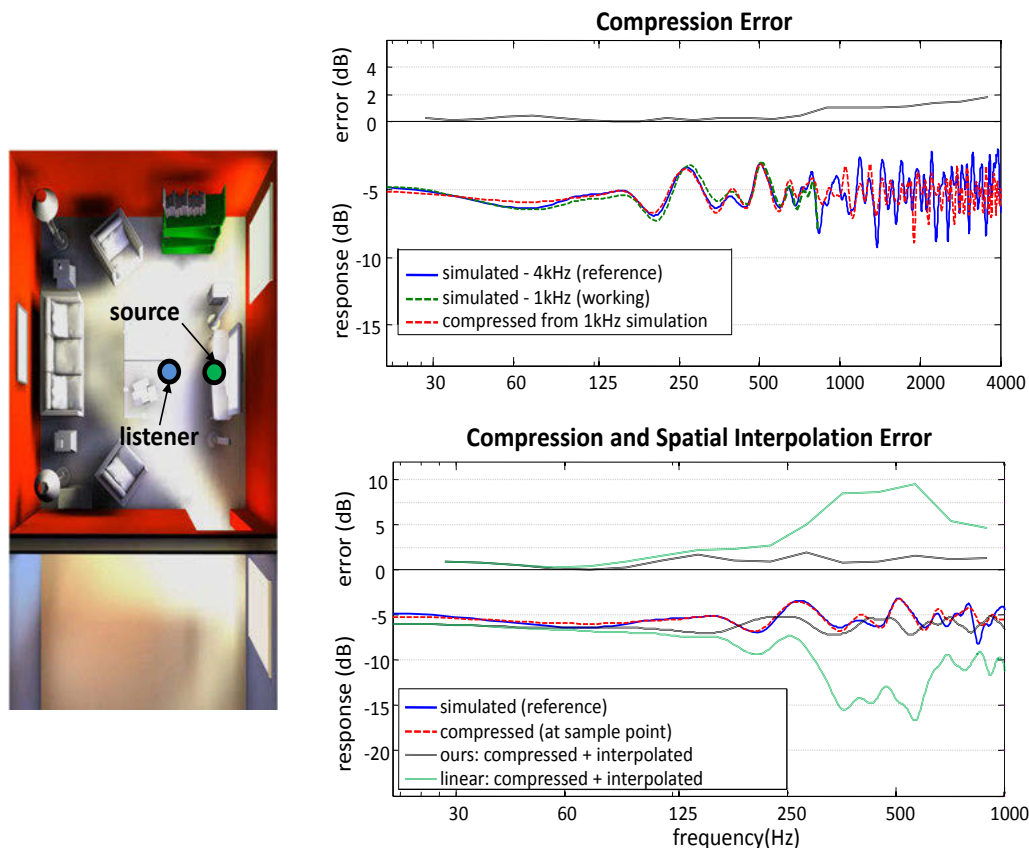


Figure 5.7: **Error analysis compared to broadband numerical simulation: listener close to source.** My method matches the reference solution very closely, while linear interpolation yields substantial errors.

spatial interpolation (bottom graph) increases error to a maximum of 5 dB, with an average of 2-3 dB. These errors may be compared to the human loudness discrimination threshold at roughly 1 dB over all audible frequencies [44].

Figures 5.7, 5.8, and 5.9 analyze error at three more listener locations in the furnished living room scene. Error is shown in two parts: first (top of each figure), from encoding alone using my representation of peak times/amplitudes and a frequency trend, and second (bottom of each figure), from both encoding and interpolation at a listener location midway between the simulated grid points. Errors are computed with respect to a higher-frequency (4kHz) wave-based reference simulation, and so include frequencies beyond the “working” simulation which is bandlimited to 1kHz. Overall, compression

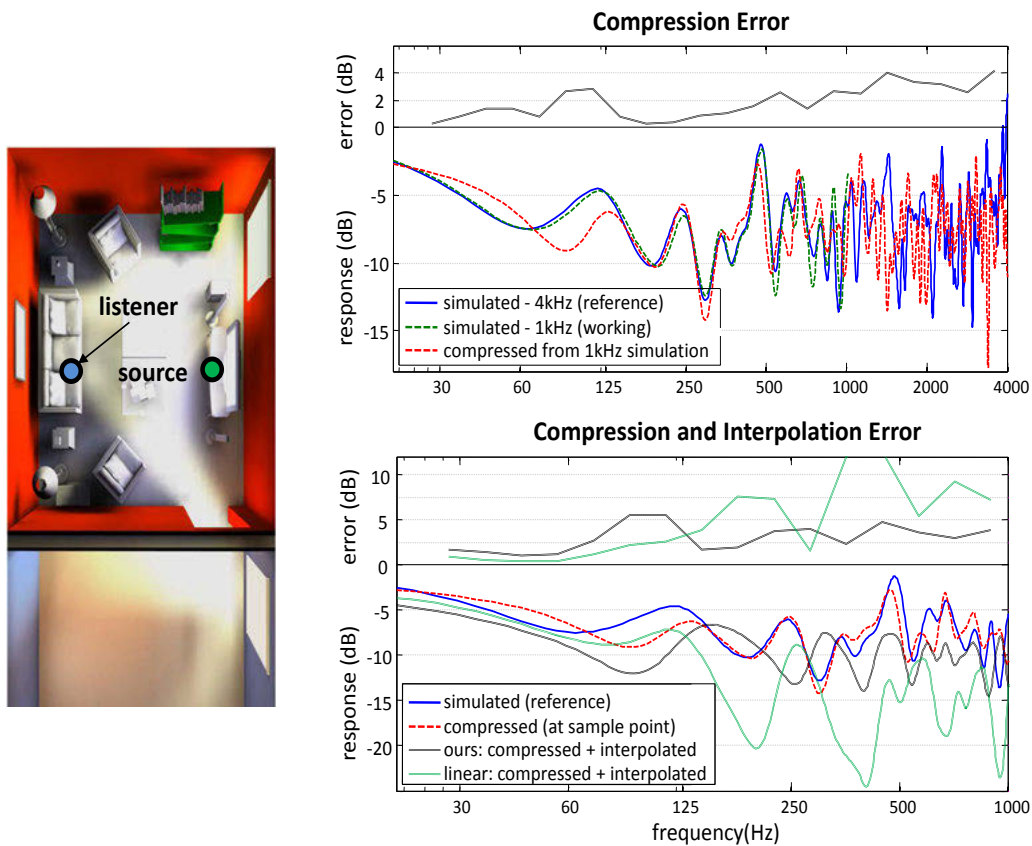


Figure 5.8: **Error analysis compared to broadband numerical simulation: listener on couch.** Compression error stays around 2dB till 1kHz and then increases to 4dB at 4kHz. Linear interpolation produces much more error.

error is low, often near the threshold of audibility, while total error (interpolation + compression) is somewhat higher but still reasonably small. In all cases, my method of interpolating peak times and amplitudes better preserves the high-frequency content of the impulse response than does straightforward linear interpolation of the signals. Not only is the result obtained with my technique more accurate, but it also avoids “gurgling” artifacts from linear interpolation in which high sound frequencies are alternately preserved at the grid points and then attenuated between them, as the listener or sources move.

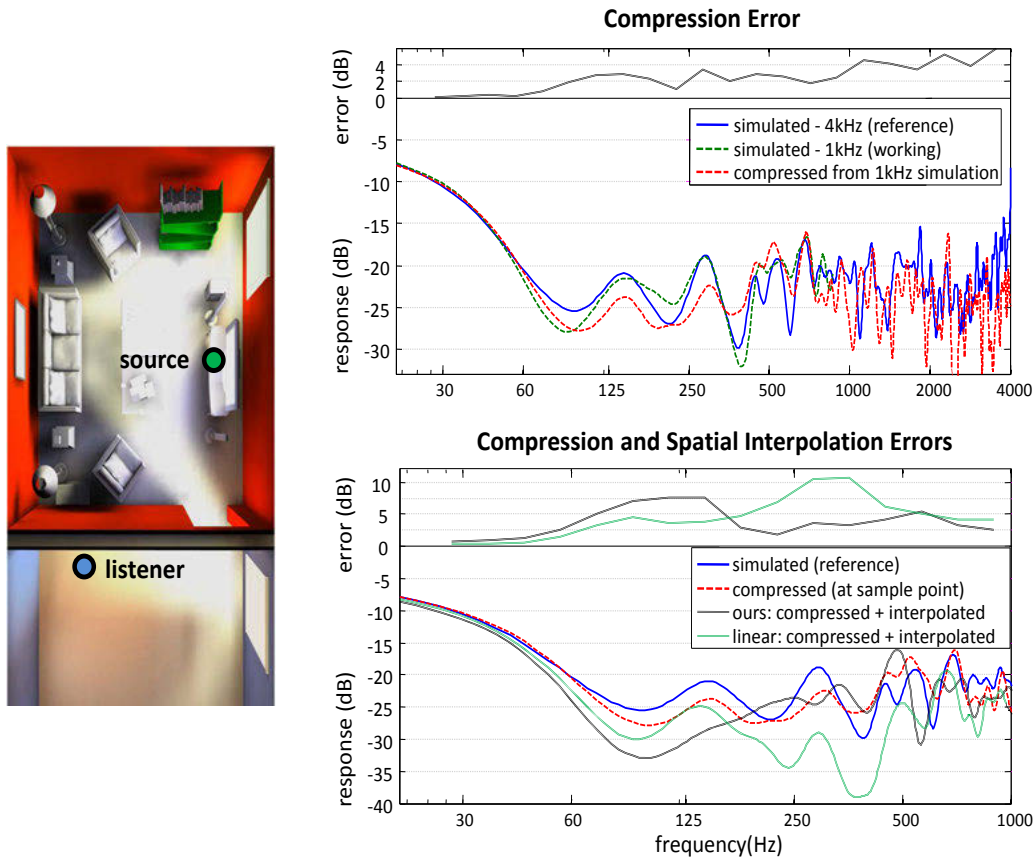


Figure 5.9: **Error analysis compared to broadband numerical simulation: listener outside door.** Sound from the source undergoes multiple scattering in the room, then diffracts around the door to arrive at the listener. Such high-order effects are very hard to model convincingly and a challenging case for current systems. Notice the clear low-pass filtering in the frequency response plotted and audible in the demo. Compression error lies between 2 to 4 dB, which is quite low. Spatial interpolation errors are higher, crossing 5 dB, but my technique produces less error over all frequencies than linear interpolation.

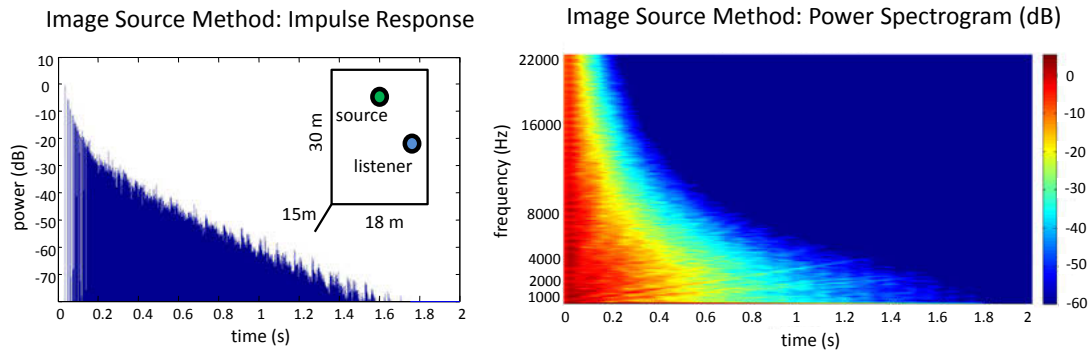


Figure 5.10: **Effect of atmospheric attenuation.** Results for the Image Source method on a simple “shoebox” geometry shown in the upper-right inset are plotted on the left. Impulse responses were calculated assuming a frequency-independent pressure absorption coefficient of 0.15 at the room walls, but with frequency-dependent atmospheric attenuation using the formulae given in ISO 9613-1 assuming an air temperature of 20°C and relative humidity of 40%. The spectrogram on the right shows strong attenuation of frequencies above 5kHz. In particular, a 10kHz sound component decays by nearly 20 dB after just 200 ms of propagation. In a real scene where frequency-dependent material absorption is also accounted for, the attenuation would be even higher.

5.4.6 “Shoebox” Experimental Results

I have implemented the Image Source method as a second reference solution, based on a simple, rectangularly-shaped room. The walls are assumed to be purely specular and without frequency-dependent absorption. Frequency-dependent atmospheric absorption is however taken into account. I mentioned earlier that above 5kHz, frequencies are strongly attenuated when propagating in air. The spectrogram on the right of Figure 5.10 demonstrates this well-known result.

Figure 5.11 compares errors between the frequency response obtained with the Image Source method and the approximation obtained with my technique based on a numerical simulation limited to 1kHz, encoded by peak delays and amplitudes plus a frequency trend, and interpolated spatially. In this simple scene, the Image Source method provides perfect interpolation, yielding the response at any desired point and so serving as a good reference.² My technique’s results agree well with this reference. While the maximum

²The corners of a room do produce diffracted scattering which is captured by my simulator but not

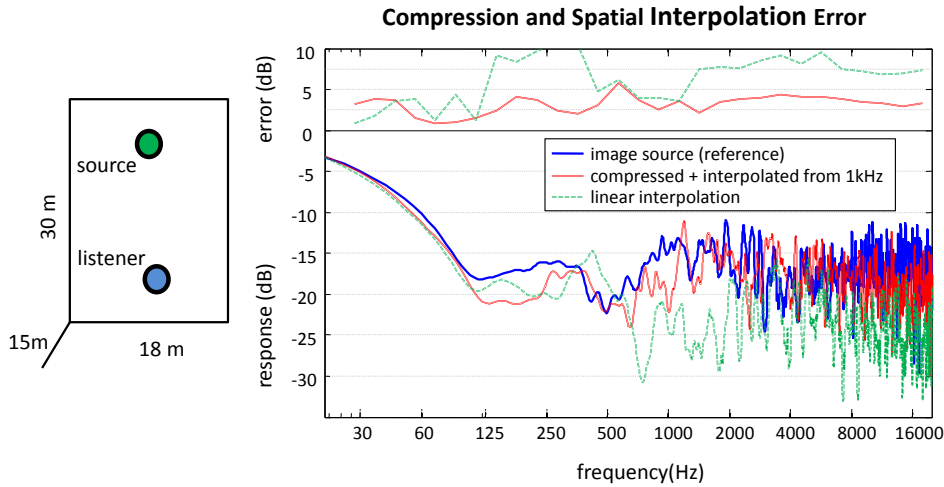


Figure 5.11: **Error analysis compared with Image Source method.** The left image shows the locations of source and listener in a simple “shoebox” room. A reference 200 ms long IR was generated with the Image Source method. The resulting frequency response is compared with my technique’s result based on a wave simulation bandlimited to 1kHz, and including compression and spatial interpolation errors. The result obtained with my technique (red curve) agrees well with the reference solution. In the top error plot, maximum error is about 5 dB while average error over the full frequency range up to 16kHz is 2-3 dB. Linear interpolation (green curve) yields larger errors and incorrectly attenuates higher frequencies.

error is around 5 dB, the average error is roughly 2-3 dB over the whole spectrum up to 16kHz. These errors very closely match those obtained when comparing with the wave-based reference simulation. Linear interpolation performs far worse, underestimating energy in all octaves above 2kHz by about 7-10 dB.

5.5 Conclusion, Limitations and Future Work

My approach for interactive auralization is the first real-time method for wave-based acoustic propagation from multiple moving sources to a moving listener. It exploits human auditory perception to express the precomputed, spatially-varying impulse response

the Image Source method. This can be safely disregarded by choosing high wall reflectivity and keeping the source and listener far from the corners, as I have done in this experiment.

of a complex but static scene in a compact form. My run-time technique convolves in the frequency-domain, allowing arbitrarily dense impulse responses. Overall, my system captures realistic acoustic effects including late reverberation, diffuse reflections, reverberation coloration, sound focusing, and diffraction low-pass filtering around obstructions.

Some limitations of my approach are due to the high computational cost of wave simulators on today’s desktops – the simulation’s frequency limit and restricted volume. Others arise from precomputation – the restriction to static scenes and high runtime memory use (hundreds of MBs) even with fairly low spatial sampling. Memory use could be reduced by extracting an even more compact set of ERIR perceptual parameters such as loudness, clarity, etc. Finding a “perceptually complete” set is an open research problem, as is determining spatial sampling requirements for perceptually accurate auralization. My technique might be practically extended to dynamic scenes by simulating low-dimensional parameterized scenes, such as an opera house at various degrees of seating occupation. It could also benefit from approximations to handle dynamic objects, perhaps by separately precomputing frequency-dependent occlusion factors and then applying them on the fly.

Chapter 6

Conclusion and Future Work

The contributions of my dissertation lie in the three inter-connected sub-problems of Physically-based Sound Simulation – Interactive Sound Synthesis, Numerical Acoustics Simulation and Interactive Sound Propagation. In the area of Interactive Sound Synthesis, I have presented techniques that exploit human auditory perception, such as its limited frequency resolution, to deliver large gains in performance. The system I have developed has been integrated with existing physics engines such as ODE and NVIDIA PhysX, to enable interactive applications with hundreds of sounding objects undergoing impacts and rolling, resulting in richly interactive applications with realistic sound. The second part of my work is on performing fast numerical acoustic simulations that are hundred times faster than a high-order finite difference technique. This is achieved by exploiting known analytical solutions for the Wave Equation and decomposing the simulation domain into rectangular partitions. This enables acoustic prediction on large scenes that were intractable earlier on a desktop computer – simulations that would have taken days on a small cluster of processors can be performed in minutes with the simulator I have developed.

Lastly, I have developed the first interactive auralization system to utilize wave-based acoustics for arbitrary static scenes with complex geometry and be able to handle moving sound sources and listener. My system is capable of automatically handling

commonly perceivable acoustic effects such sound focusing, low-pass filtering due to occlusion/obstruction, realistic reverberation, and diffuse reflections. Prior techniques relying on geometric methods have difficulty handling diffraction and high-order reflections. The key idea behind this technique is a compact representation that captures the perceptually salient aspects of acoustics responses. This representation allows a reduction of memory usage by a factor of up to thousand times compared to a simple, direct storage scheme. In addition to this, I have developed an auralization system that performs perceptually realistic interpolation of impulse responses stored in this compact representation, and performs fast convolutions in frequency domain to render the acoustics in real time.

The Future: Over the past few decades, the area of computer graphics has seen a synergistic development of computational techniques, perceptual approximations, and computational power, that has enabled the stunning visual realism of interactive applications today. Based on my experience working on this thesis and the increasing amount of concurrent work in this area, I believe that interactive sound simulation is following the same trend. The development of graphics processors has largely removed the burden of graphics computations from the CPU. In addition, graphics processors offer massive parallelism, that can be helpful for accelerating precomputation for sound simulation, as I have shown for the ARD technique. Furthermore, there is an increasing trend towards multi-core processors – the Xbox 360 gaming console released in 2005 already had three cores and high-end, quad-core desktop system are easily available today. Therefore, the amount of computation available for audio is increasing consistently over time. What is needed is continued development of fast algorithms and approximations based on our current (and improving) understanding of psycho-acoustics to design ever more efficient algorithms to translate this available computational power into a compelling overall aural experience, at interactive speeds.

There are many interesting areas for future research in interactive sound simulation. Perhaps the most general theme to be explored is a systematic study of the limits of auditory perception in the context of interactive applications and human error tolerances while approximating different aural phenomena, whether in the context of sound synthesis, or propagation. Existing wisdom from other areas of research, such as room acoustics, speech synthesis and musical synthesis would surely inform such work, as is the case for this thesis. However, I am quite certain that new studies specific to interactive applications will be required, since some questions arise that are very specific to this area. As an example, it would be very useful to study the tolerable errors in sound propagation for moving sources and listener, as this would give valuable insights into approximations that work for acoustic responses in such cases.

The first and foremost requirement for such systematic studies seems to be finding a “perceptually complete” set of parameters and their associated error tolerance values for humans. In addition to traditionally used quantities, such as loudness, I am sure such a list would also contain far more detailed quantities relating to the spectral content and its time-varying nature. This would prove invaluable for research in this area, serving as an essential guideline for designing perceptually realistic interactive techniques for sound simulation, and informing any such technique about the ultimate limits of efficiency gains from perceptually-based approximations. I am sure that this would be a very rewarding direction, and might even contribute to research in psychoacoustics as well – interactive virtual environments can potentially be a very useful tool for psychoacoustic studies.

There are many future directions possible in the area of sound synthesis. Interactive sound synthesis is a very nascent area, and there is a large variety of sounds that have seen limited exploration (or none at all), that can possibly yield to interactive synthesis through an understanding of their underlying physics, as well as perception. To give a non-exhaustive list here – cloth sounds, efficient sliding and rolling sounds, explosions,

creaking, liquids, footsteps, fracture and engine sounds. Simulating all of these sounds would add a new layer of immersion to existing interactive applications.

In the area of acoustics, my work has shown that significant compression can be achieved for storing the results of wave simulation. However, I am sure that a lot more compression can still be achieved. The first step would be to find a perceptually sufficient set of perceptually important acoustic parameters. The acoustic responses would then be stored as lists of these parameters alone. Such development, coupled with the development of scalable, fast, and memory-efficient acoustic techniques that can handle indoor and outdoor scenes with equal ease, would allow interactive applications to make a large step in terms of the realism achieved. However, the challenge of designing such techniques is quite similar to what global illumination research in graphics has faced over the years. I am sure that this challenge can be met by a combination of increasing computational power and improved numerical techniques that rely on physics as well as perception.

The impact of such sound synthesis and propagation techniques would extend beyond just game or movie studios – we are seeing the rise of massively multi-player immersive worlds that let the players collaboratively build environments and objects of their own. What if you make a “virtual” wooden bowl and it automatically sounds like one? What if you build a house and its acoustics automatically corresponds to what would be expected in reality? How does it sound if you drop the bowl in your house’s kitchen? Obviously, this problem is quite impractical with pre-recorded sounds and filters mainly because the scene doesn’t exist in reality and thus recording the information might not even be possible. Moreover, the process of applying such prerecorded information is very unintuitive – in real life you don’t make an object and then cast a magic spell to assign some sound to it. The same should apply for the virtual world – by virtue of designing an object, it should have visual as well as aural properties automatically. What I have described can be potentially achieved in the future, and my work has served as a step in

this direction. But as I have conveyed, a large number of very interesting and challenging research problems still need to be solved. There are many possible improvements to the techniques I have described in this thesis, which I have discussed individually. The hope is that in the future we will be seeing more and more virtual worlds which will integrate realistic physically-based sounds, and combined with ever-improving graphics, give us a visceral feeling – “I am here”.

Bibliography

- [1] Domain decomposition method. <http://www.ddm.org>. 60
- [2] The havok physics engine. <http://www.havok.com/>. 25
- [3] The nvidia physx physics engine. http://www.nvidia.com/object/physx_new.html. 25
- [4] The open dynamics engine. <http://www.ode.org/>. 25
- [5] Soundscapes in half-life 2, valve corporation. <http://developer.valvesoftware.com/wiki/Soundscapes>, 2008. 30
- [6] J. B. Allen and D. A. Berkley. Image method for efficiently simulating small-room acoustics. *J. Acoust. Soc. Am*, 65(4):943–950, 1979. 52
- [7] F. Antonacci, M. Foco, A. Sarti, and S. Tubaro. Real time modeling of acoustic propagation in complex environments. *Proceedings of 7th International Conference on Digital Audio Effects*, pages 274–279, 2004. 52
- [8] M. Bertram, E. Deines, J. Mohring, J. Jegorovs, and H. Hagen. Phonon tracing for auralization and visualization of sound. In *IEEE Visualization 2005*, pages 151–158, 2005. 52
- [9] Stefan Bilbao. *Wave and Scattering Methods for Numerical Simulation*. Wiley, July 2004. 58
- [10] J. Blauert. An introduction to binaural technology. In R. Gilkey and T. R. Anderson, editors, *Binaural and Spatial Hearing in Real and Virtual Environments*. Lawrence Erlbaum, USA, 1997. 11, 139
- [11] Nicolas Bonneel, George Drettakis, Nicolas Tsingos, Isabelle V. Delmon, and Doug James. Fast modal sounds with scalable frequency-domain synthesis. *ACM Transactions on Graphics (SIGGRAPH Conference Proceedings)*, 27(3), 2008. 47
- [12] D. Botteldooren. Acoustical finite-difference time-domain simulation in a quasi-cartesian grid. *The Journal of the Acoustical Society of America*, 95(5):2313–2319, 1994. 58

- [13] D. Botteldooren. Finite-difference time-domain simulation of low-frequency room acoustic problems. *Acoustical Society of America Journal*, 98:3302–3308, December 1995. [58](#)
- [14] John P. Boyd. *Chebyshev and Fourier Spectral Methods: Second Revised Edition*. Dover Publications, 2 revised edition, December 2001. [60](#)
- [15] Paul Calamia. *Advances in Edge-Diffraction Modeling for Virtual-Acoustic Simulations*. PhD thesis, Princeton University, June 2009. [36](#), [52](#), [53](#), [62](#)
- [16] Jeffrey N. Chadwick, Steven S. An, and Doug L. James. Harmonic shells: a practical nonlinear sound model for near-rigid thin shells. In *SIGGRAPH Asia '09: ACM SIGGRAPH Asia 2009 papers*, pages 1–10, New York, NY, USA, 2009. ACM. [48](#)
- [17] A. Chaigne and V. Doutaut. Numerical simulations of xylophones. i. time domain modeling of the vibrating bars. *J. Acoust. Soc. Am.*, 101(1):539–557, 1997. [26](#), [45](#), [86](#)
- [18] Anish Chandak, Christian Lauterbach, Micah Taylor, Zhimin Ren, and Dinesh Manocha. Ad-frustum: Adaptive frustum tracing for interactive sound propagation. *IEEE Transactions on Visualization and Computer Graphics*, 14(6):1707–1722, 2008. [36](#), [52](#), [62](#)
- [19] A. Cheng and D. Cheng. Heritage and early history of the boundary element method. *Engineering Analysis with Boundary Elements*, 29(3):268–302, March 2005. [56](#)
- [20] J. Y. Chung, J.W.S Liu, and K. J. Lin. Scheduling real-time, periodic jobs using imprecise results. In *Proc. IEEE RTS*, 1987. [47](#)
- [21] Perry R. Cook. *Real Sound Synthesis for Interactive Applications (Book & CD-ROM)*. AK Peters, Ltd., 1st edition, 2002. [45](#)
- [22] Carlos A. de Moura. Parallel numerical methods for differential equations - a survey. [59](#), [100](#)
- [23] Yoshinori Dobashi, Tsuyoshi Yamamoto, and Tomoyuki Nishita. Real-time rendering of aerodynamic sound using sound textures based on computational fluid

- dynamics. *ACM Trans. Graph.*, 22(3):732–740, July 2003. [48](#)
- [24] Yoshinori Dobashi, Tsuyoshi Yamamoto, and Tomoyuki Nishita. Synthesizing sound from turbulent field using sound textures for interactive fluid simulation. *Computer Graphics Forum (Proc. EUROGRAPHICS 2004)*, 23(3):539–546, 2004. [48](#)
- [25] Jack Dongarra. Performance of various computers using standard linear equations software. Technical report, Electrical Engineering and Computer Science Department, University of Tennessee, Knoxville, TN 37996-1301, 2008. [73](#)
- [26] Durlach. Virtual reality scientific and technological challenges. Technical report, National Research Council, 1995. [14](#)
- [27] M. David Egan. *Architectural Acoustics (J. Ross Publishing Classics)*. J. Ross Publishing, January 2007. [4](#), [49](#)
- [28] M. Emerit, J. Faure, A. Guerin, R. Nicol, G. Pallone, P. Philippe, and D. Virette. Efficient binaural filtering in QMF domain for BRIR. In *AES 122th Convention*, May 2007. [65](#)
- [29] Thomas Ertl, Ken Joy, Beatriz S. Editors, E. Deines, F. Michel, M. Bertram, H. Hagen, and G. M. Nielson. Visualizing the phonon map. In *IEEE-VGTC Symposium on Visualization*, 2006. [52](#)
- [30] J. L. Florens and C. Cadoz. The physical model: modeling and simulating the instrumental universe. In G. D. Poli, A. Piccialli, and C. Roads, editors, *Representations of Musical Signals*, pages 227–268. MIT Press, Cambridge, MA, USA, 1991. [45](#)
- [31] H. Fouad, J. Ballas, and J. Hahn. Perceptually based scheduling algorithms for real-time synthesis of complex sonic environments. In *Proc. Int. Conf. Auditory Display*, 1997. [47](#)
- [32] M. Frigo and S. G. Johnson. The design and implementation of fftw3. *Proc. IEEE*, 93(2):216–231, 2005. [95](#), [114](#)
- [33] Thomas Funkhouser, Nicolas Tsingos, Ingrid Carlbom, Gary Elko, Mohan Sondhi, James E. West, Gopal Pingali, Patrick Min, and Addy Ngan. A beam tracing

- method for interactive architectural acoustics. *The Journal of the Acoustical Society of America*, 115(2):739–756, 2004. [36](#), [52](#), [62](#)
- [34] W. G. Gardner. Reverberation algorithms. In M. Kahrs and K. Brandenburg, editors, *Applications of Digital Signal Processing to Audio and Acoustics (The Springer International Series in Engineering and Computer Science)*, pages 85–131. Springer, 1 edition, 1998. [64](#), [125](#), [129](#)
- [35] Carolyn Gordon, David L. Webb, and Scott Wolpert. One cannot hear the shape of a drum. *Bulletin of the American Mathematical Society (N.S.)*, 27(1):134–138, 1992. [11](#)
- [36] Naga K. Govindaraju, Brandon Lloyd, Yuri Dotsenko, Burton Smith, and John Manferdelli. High performance discrete fourier transforms on graphics processors. In *SC '08: Proceedings of the 2008 ACM/IEEE conference on Supercomputing*, pages 1–12, Piscataway, NJ, USA, 2008. IEEE Press. [32](#), [113](#)
- [37] Eran Guendelman, Robert Bridson, and Ronald Fedkiw. Nonconvex rigid bodies with stacking. *ACM Trans. Graph.*, 22(3):871–878, July 2003. [81](#)
- [38] Nail A. Gumerov and Ramani Duraiswami. Fast multipole methods on graphics processors. *J. Comput. Phys.*, 227(18):8290–8313, September 2008. [56](#), [57](#)
- [39] Nail A. Gumerov and Ramani Duraiswami. A broadband fast multipole accelerated boundary element method for the three dimensional helmholtz equation. *The Journal of the Acoustical Society of America*, 125(1):191–205, 2009. [56](#)
- [40] Tor Halmrast. Coloration due to reflections. further investigations. In *International Congress on Acoustics*, September 2007. [124](#)
- [41] W. M. Hartmann and A. Wittenberg. On the externalization of sound images. *The Journal of the Acoustical Society of America*, 99(6):3678–3688, June 1996. [139](#)
- [42] Murray Hodgson and Eva M. Nosal. Experimental evaluation of radiosity for room sound-field prediction. *The Journal of the Acoustical Society of America*, 120(2):808–819, 2006. [52](#)
- [43] Doug L. James, Jernej Barbic, and Dinesh K. Pai. Precomputed acoustic transfer:

- output-sensitive, accurate sound generation for geometrically complex vibration sources. *ACM Transactions on Graphics*, 25(3):987–995, July 2006. [63](#)
- [44] Walt Jesteadt, Craig C. Wier, and David M. Green. Intensity discrimination as a function of frequency and sensation level. *The Journal of the Acoustical Society of America*, 61(1):169–177, 1977. [147](#)
- [45] Matti Karjalainen and Cumhur Erku. Digital waveguides versus finite difference structures: equivalence and mixed modeling. *EURASIP J. Appl. Signal Process.*, 2004(1):978–989, January 2004. [55](#), [57](#), [58](#)
- [46] Young J. Kim, Ming C. Lin, and Dinesh Manocha. Deep: Dual-space expansion for estimating penetration depth between convex polytopes. In *IEEE International Conference on Robotics and Automation*, May 2002. [81](#)
- [47] Lawrence E. Kinsler, Austin R. Frey, Alan B. Coppens, and James V. Sanders. *Fundamentals of acoustics*. Wiley, 4 edition, December 2000. [29](#), [49](#)
- [48] Mendel Kleiner, Bengt-Inge Dalenbäck, and Peter Svensson. Auralization - an overview. *JAES*, 41:861–875, 1993. [55](#)
- [49] K. Kowalczyk and M. van Walstijn. Room acoustics simulation using 3-d compact explicit fdtd schemes. *IEEE Transactions on Audio, Speech and Language Processing*, 2010. [58](#), [103](#), [119](#)
- [50] A. Krokstad, S. Strom, and S. Sorsdal. Calculating the acoustical room response by the use of a ray tracing technique. *Journal of Sound and Vibration*, 8(1):118–125, July 1968. [52](#)
- [51] Heinri Kuttruff. *Room Acoustics*. Taylor & Francis, October 2000. [31](#), [35](#), [37](#), [49](#), [94](#), [112](#), [122](#), [124](#), [127](#), [129](#), [134](#)
- [52] Tobias Lentz, Dirk Schröder, Michael Vorländer, and Ingo Assenmacher. Virtual reality system with integrated sound field simulation and reproduction. *EURASIP J. Appl. Signal Process.*, 2007(1):187, 2007. [61](#)
- [53] Ruth Y. Litovsky, Steven H. Colburn, William A. Yost, and Sandra J. Guzman. The precedence effect. *The Journal of the Acoustical Society of America*, 106(4):1633–1654, 1999. [123](#)

- [54] Qing H. Liu. The pstd algorithm: A time-domain method combining the pseudospectral technique and perfectly matched layers. *The Journal of the Acoustical Society of America*, 101(5):3182, 1997. [60](#), [93](#)
- [55] T. Lokki. *Physically-based Auralization*. PhD thesis, Helsinki University of Technology, 2002. [61](#)
- [56] C. Masterson, G. Kearney, and F. Boland. Acoustic impulse response interpolation for multichannel systems using dynamic time warping. In *35th AES Conference on Audio for Games*, 2009. [65](#)
- [57] Ravish Mehra, Nikunj Raghuvanshi, Ming Lin, and Dinesh Manocha. Efficient gpu-based solver for acoustic wave equation. Technical report, Department of Computer Science, UNC Chapel Hill, USA, 2010. [101](#), [120](#)
- [58] P. Min and T. Funkhouser. Priority-driven acoustic modeling for virtual environments. *Computer Graphics Forum*, pages 179–188, September 2000. [64](#)
- [59] Brian Mirtich and John Canny. Impulse-based simulation of rigid bodies. In *I3D '95: Proceedings of the 1995 symposium on Interactive 3D graphics*, New York, NY, USA, 1995. ACM. [81](#)
- [60] James Moody and Paul Dexter. *Concert Lighting, Third Edition: Techniques, Art and Business*. Focal Press, 3 edition, September 2009. [1](#)
- [61] William Moss, Hengchin Yeh, Jeong-Mo Hong, Ming C. Lin, and Dinesh Manocha. Sounding liquids: Automatic sound synthesis from fluid simulation. *ACM Transactions on Graphics (proceedings of SIGGRAPH 2010)*, 29(3), July 2010. [48](#)
- [62] D. Murphy, A. Kelloniemi, J. Mullen, and S. Shelley. Acoustic modeling using the digital waveguide mesh. *Signal Processing Magazine, IEEE*, 24(2):55–66, 2007. [57](#), [58](#)
- [63] James F. O’Brien, Perry R. Cook, and Georg Essl. Synthesizing sounds from physically based motion. In *SIGGRAPH '01: Proceedings of the 28th annual conference on Computer graphics and interactive techniques*, pages 529–536, New York, NY, USA, 2001. ACM Press. [26](#), [45](#)
- [64] James F. O’Brien, Chen Shen, and Christine M. Gatchalian. Synthesizing sounds

- from rigid-body simulations. In *The ACM SIGGRAPH 2002 Symposium on Computer Animation*, pages 175–181. ACM Press, July 2002. [26](#), [46](#), [69](#), [72](#)
- [65] R. Petrausch and S. Rabenstein. Simulation of room acoustics via block-based physical modeling with the functional transformation method. *Applications of Signal Processing to Audio and Acoustics, 2005. IEEE Workshop on*, pages 195–198, 16-19 Oct. 2005. [60](#)
- [66] Jackson Pope, David Creasey, and Alan Chalmers. Realtime room acoustics using ambisonics. In *The Proceedings of the AES 16th International Conference on Spatial Sound Reproduction*, pages 427–435. Audio Engineering Society, April 1999. [64](#)
- [67] Alfio Quarteroni and Alberto Valli. *Domain Decomposition Methods for Partial Differential Equations (Numerical Mathematics and Scientific Computation)*. Oxford University Press, USA, July 1999. [60](#)
- [68] R. Rabenstein, S. Petrausch, A. Sarti, G. De Sanctis, C. Erkut, and M. Karjalainen. Block-based physical modeling for digital sound synthesis. *Signal Processing Magazine, IEEE*, 24(2):42–54, 2007. [60](#)
- [69] Nikunj Raghuvanshi, Nico Galoppo, and Ming C. Lin. Accelerated wave-based acoustics simulation. In *SPM '08: Proceedings of the 2008 ACM symposium on Solid and physical modeling*, pages 91–102, New York, NY, USA, 2008. ACM. [33](#)
- [70] Nikunj Raghuvanshi, Christian Lauterbach, Anish Chandak, Dinesh Manocha, and Ming C. Lin. Real-time sound synthesis and propagation for games. *Commun. ACM*, 50(7):66–73, July 2007. [27](#)
- [71] Nikunj Raghuvanshi and Ming C. Lin. Interactive sound synthesis for large scale environments. In *SI3D '06: Proceedings of the 2006 symposium on Interactive 3D graphics and games*, pages 101–108, New York, NY, USA, 2006. ACM Press. [27](#)
- [72] Nikunj Raghuvanshi and Ming C. Lin. Physically based sound synthesis for large-scale virtual environments. *IEEE Computer Graphics and Applications*, 27(1):14–18, 2007. [27](#)
- [73] Nikunj Raghuvanshi, Brandon Lloyd, Naga K. Govindaraju, and Ming C. Lin. Efficient numerical acoustic simulation on graphics processors using adaptive rect-

- angular decomposition. In *EAA Symposium on Auralization*, June 2009. 33
- [74] Nikunj Raghuvanshi, Rahul Narain, and Ming C. Lin. Efficient and accurate sound propagation using adaptive rectangular decomposition. *IEEE Transactions on Visualization and Computer Graphics*, 15(5):789–801, 2009. 33
- [75] Nikunj Raghuvanshi, John Snyder, Ravish Mehra, Ming C. Lin, and Naga K. Govindaraju. Precomputed wave simulation for real-time sound propagation of dynamic sources in complex scenes. *ACM Transactions on Graphics (proceedings of SIGGRAPH 2010)*, 29(3), July 2010. 41
- [76] Zhimin Ren, Hengchin Yeh, and Ming C. Lin. Synthesizing contact sounds between textured models. In *2010 IEEE Virtual Reality Conference (VR)*, pages 139–146. IEEE, March 2010. 48
- [77] Y. S. Rickard, N. K. Georgieva, and Wei-Ping Huang. Application and optimization of pml abc for the 3-d wave equation in the time domain. *Antennas and Propagation, IEEE Transactions on*, 51(2):286–295, 2003. 103
- [78] J. H. Rindel. The use of computer modeling in room acoustics. *Journal of Vibro-engineering*, 3(4):219–224, 2000. 52
- [79] D. Rizos and S. Zhou. An advanced direct time domain bem for 3-d wave propagation in acoustic media. *Journal of Sound and Vibration*, 293(1-2):196–212, May 2006. 56
- [80] Ton Roosendaal. The blender foundation. <http://www.blender.org>. 49
- [81] H. Sabine. Room acoustics. *Audio, Transactions of the IRE Professional Group on*, 1(4):4–12, 1953. 49
- [82] S. Sakamoto, T. Yokota, and H. Tachibana. Numerical sound field analysis in halls using the finite difference time domain method. In *RADS 2004*, Awaji, Japan, 2004. 58
- [83] Shinichi Sakamoto, Hiroshi Nagatomo, Ayumi Ushiyama, and Hideki Tachibana. Calculation of impulse responses and acoustic parameters in a hall by the finite-difference time-domain method. *Acoustical Science and Technology*, 29(4), 2008. 108

- [84] Shinichi Sakamoto, Takuma Seimiya, and Hideki Tachibana. Visualization of sound reflection and diffraction using finite difference time domain method. *Acoustical Science and Technology*, 23(1):34–39, 2002. [58](#)
- [85] Shinichi Sakamoto, Ayumi Ushiyama, and Hiroshi Nagatomo. Numerical analysis of sound propagation in rooms using the finite difference time domain method. *The Journal of the Acoustical Society of America*, 120(5):3008, 2006. [58](#)
- [86] L. Savioja. *Modeling Techniques for Virtual Acoustics*. Doctoral thesis, Helsinki University of Technology, Telecommunications Software and Multimedia Laboratory, Report TML-A3, 1999. [51](#), [57](#), [61](#)
- [87] L. Savioja, J. Backman, A. Järvinen, and T. Takala. Waveguide mesh method for low-frequency simulation of room acoustics. In *15th International Congress on Acoustics (ICA'95)*, volume 2, pages 637–640, Trondheim, Norway, June 1995. [57](#)
- [88] L. Savioja, T. Rinne, and T. Takala. Simulation of room acoustics with a 3-d finite difference mesh. In *Proceedings of the International Computer Music Conference*, pages 463–466, 1994. [58](#)
- [89] L. Savioja and V. Valimaki. Interpolated 3-d digital waveguide mesh with frequency warping. In *ICASSP '01: Proceedings of the Acoustics, Speech, and Signal Processing, 2001. on IEEE International Conference*, pages 3345–3348, Washington, DC, USA, 2001. IEEE Computer Society. [58](#)
- [90] Lauri Savioja. Real-time 3d finite-difference time-domain simulation of mid-frequency room acoustics. In *13th International Conference on Digital Audio Effects (DAFx-10)*, September 2010. [58](#), [59](#), [103](#), [119](#)
- [91] Lauri Savioja, Jyri Huopaniemi, Tapio Lokki, and Ritta Väänänen. Creating interactive virtual acoustic environments. *Journal of the Audio Engineering Society (JAES)*, 47(9):675–705, September 1999. [61](#)
- [92] A. Sek and B. C. Moore. Frequency discrimination as a function of frequency, measured in several ways. *J. Acoust. Soc. Am.*, 97(4):2479–2486, April 1995. [47](#), [73](#)
- [93] K. L. Shlager and J. B. Schneider. A selective survey of the finite-difference time-domain literature. *Antennas and Propagation Magazine, IEEE*, 37(4):39–57, 1995.

- [94] Samuel Siltanen. Geometry reduction in room acoustics modeling. Master's thesis, Helsinki University of Technology, 2005. [36](#), [51](#), [106](#)
- [95] Julius O. Smith. *Physical Audio Signal Processing*. <http://ccrma.stanford.edu/~jos/pasp>, 2010. [45](#)
- [96] Efstathios Stavrakis, Nicolas Tsingos, and Paul Calamia. Topological sound propagation with reverberation graphs. *Acta Acustica/Acustica - the Journal of the European Acoustics Association (EAA)*, 2008. [65](#), [138](#)
- [97] C. Stoelinga and A. Chaigne. Time-domain modeling and simulation of rolling objects. *Acustica united with Acta Acustica*, 93(2):290–304, 2007. [48](#)
- [98] U. Peter Svensson, Paul Calamia, and Shinsuke Nakanishi. Frequency-domain edge diffraction for finite and infinite edges. In *Acta Acustica/Acustica 95*, pages 568–572, 2009. [135](#)
- [99] Allen Taflove and Susan C. Hagness. *Computational Electrodynamics: The Finite-Difference Time-Domain Method, Third Edition*. Artech House Publishers, 3 edition, June 2005. [44](#), [58](#), [60](#), [92](#), [108](#)
- [100] Tapio Takala and James Hahn. Sound rendering. *SIGGRAPH Comput. Graph.*, 26(2):211–220, July 1992. [13](#), [15](#)
- [101] Micah T. Taylor, Anish Chandak, Lakulish Antani, and Dinesh Manocha. Re-sound: interactive sound rendering for dynamic virtual environments. In *MM '09: Proceedings of the seventeen ACM international conference on Multimedia*, pages 271–280, New York, NY, USA, 2009. ACM. [52](#), [62](#)
- [102] Lonny L. Thompson. A review of finite-element methods for time-harmonic acoustics. *The Journal of the Acoustical Society of America*, 119(3):1315–1330, 2006. [55](#)
- [103] Rendell R. Torres, U. Peter Svensson, and Mendel Kleiner. Computation of edge diffraction for more accurate room acoustics auralization. *The Journal of the Acoustical Society of America*, 109(2):600–610, 2001. [62](#)
- [104] Andrea Toselli and Olof B. Widlund. *Domain decomposition methods—algorithms*

- and theory*. Springer series in computational mathematics, 34. Springer, 1 edition, November 2005. [60](#)
- [105] Nicolas Tsingos. *Simulating High Quality Dynamic Virtual Sound Fields For Interactive Graphics Applications*. PhD thesis, Universite Joseph Fourier Grenoble I, December 1998. [52](#)
- [106] Nicolas Tsingos. Pre-computing geometry-based reverberation effects for games. In *35th AES Conference on Audio for Games*, 2009. [64](#), [65](#)
- [107] Nicolas Tsingos, Carsten Dachsbacher, Sylvain Lefebvre, and Matteo Dellepiane. Instant sound scattering. In *Rendering Techniques (Proceedings of the Eurographics Symposium on Rendering)*, 2007. [63](#)
- [108] Nicolas Tsingos, Thomas Funkhouser, Addy Ngan, and Ingrid Carlbom. Modeling acoustics in virtual environments using the uniform theory of diffraction. In *SIGGRAPH '01: Proceedings of the 28th annual conference on Computer graphics and interactive techniques*, pages 545–552, New York, NY, USA, 2001. ACM. [52](#), [53](#)
- [109] K. van den Doel and D. K. Pai. Synthesis of shape dependent sounds with physical modeling. In *Proceedings of the International Conference on Auditory Displays*, 1996. [46](#)
- [110] K. van den Doel and D. K. Pai. The sounds of physical shapes. *Presence*, 7(4):382–395, 1998. [46](#)
- [111] Kees van den Doel. Physically based models for liquid sounds. *ACM Trans. Appl. Percept.*, 2(4):534–546, October 2005. [48](#)
- [112] Kees van den Doel, Dave Knott, and Dinesh K. Pai. Interactive simulation of complex audiovisual scenes. *Presence: Teleoper. Virtual Environ.*, 13(1):99–111, 2004. [47](#)
- [113] Kees van den Doel, Paul G. Kry, and Dinesh K. Pai. Foleyautomatic: physically-based sound effects for interactive simulation and animation. In *SIGGRAPH '01: Proceedings of the 28th annual conference on Computer graphics and interactive techniques*, pages 537–544, New York, NY, USA, 2001. ACM Press. [46](#)

- [114] S. Van Duyne and J. O. Smith. The 2-d digital waveguide mesh. In *IEEE Workshop on Applications of Signal Processing to Audio and Acoustics*, pages 177–180, 1993. [57](#)
- [115] Michael Vorländer. *Auralization: Fundamentals of Acoustics, Modelling, Simulation, Algorithms and Acoustic Virtual Reality (RWTHedition)*. Springer, 1 edition, November 2007. [61](#)
- [116] Kane Yee. Numerical solution of initial boundary value problems involving maxwell’s equations in isotropic media. *IEEE Transactions on Antennas and Propagation*, 14(3):302–307, May 1966. [58](#), [90](#)
- [117] Changxi Zheng and Doug L. James. Harmonic fluids. In *SIGGRAPH ’09: ACM SIGGRAPH 2009 papers*, pages 1–12, New York, NY, USA, 2009. ACM. [48](#)
- [118] Changxi Zheng and Doug L. James. Fracture sound with precomputed soundbanks. *ACM Transactions on Graphics (SIGGRAPH 2010)*, 29(3), July 2010. [48](#)
- [119] Eberhard Zwicker and Hugo Fastl. *Psychoacoustics: Facts and Models (Springer Series in Information Sciences) (v. 22)*. Springer, 2nd updated ed. edition, April 1999. [73](#)